Computers and Mathematics with Applications 70 (2015) 507–547

Contents lists available at ScienceDirect

Computers and Mathematics with Applications

journal homepage: www.elsevier.com/locate/camwa

The cumulant lattice Boltzmann equation in three dimensions: Theory and validation

Martin Geier*, Martin Schönherr, Andrea Pasquali, Manfred Krafczyk

TU Braunschweig, Institute for Computational Modeling in Civil Engineering (iRMB), Braunschweig, Germany

ARTICLE INFO

Article history:
Received 4 September 2014
Received in revised form 13 March 2015
Accepted 3 May 2015
Available online 18 June 2015

Keywords:
Lattice Boltzmann
Cumulants
Multiple relaxation time
Galilean invariance
Orthogonalization

ABSTRACT

We propose, analyze, and validate a lattice Boltzmann model with a cumulant collision operator. The new model is analytically and numerically shown to poses smaller errors than a moment based Multiple Relaxation Time lattice Boltzmann model. We demonstrate the usability of the cumulant lattice Boltzmann model by simulations of flow around a sphere for Reynolds numbers from 200 to 10^5.

1. Introduction

The lattice Boltzmann equation (LBE) [1,2] is a discrete model used to solve various partial differential equations, most notably the Navier–Stokes equation. The basic components of the lattice Boltzmann equation are a discrete local distribution function f in momentum space, a uniform discrete distribution of lattice nodes in space, an advection rule that moves the distributions according to their momenta from node to node, and a local collision rule that permutes the distributions on the nodes in momentum space.

In this paper we derive a lattice Boltzmann method based on a cumulant collision operator. Our motivation to do this arises from several limitations we found with the established lattice Boltzmann methods in particular when flow at higher Reynolds number is considered. Cumulants [3] are observable quantities of a distribution that successively encode the deviation of the distribution from a Gaussian equilibrium distribution. Unlike in the case of usual moments a cumulant of order n encodes only information that is not already encoded in cumulants of order lower than n. Cumulants are therefor natural candidates for mutually independent observable quantities. We demonstrate below that cumulants help us to ensure Galilean invariance and the decoupling between independent degrees of freedom to a higher extent than moments do. This is also the case when all other aspects of the model, like the velocity set, the equilibrium function, and the relaxation rates are strictly the same for the cumulant and moment models. The primary focus of the paper is on the collision operator but we also discuss two other aspects of the lattice Boltzmann method, the velocity set, and the equilibrium function since we make some decisions which are not standard.

The choice of the velocity set is a compromise between efficiency and accuracy. For solving the incompressible Navier–Stokes equation sets with 15 or 19 speeds in three dimensions are popular. Recently evidence has been accumulated

* Correspondence to: iRMB Pockelsstr. 3, 38106 Braunschweig, Germany. Tel.: +49 531 391 94518; fax: +49 531 391 94511.
E-mail address: geier@irmb.tu-bs.de (M. Geier).

http://dx.doi.org/10.1016/j.camwa.2015.05.001

that the 19 speed model is not able to provide axisymmetric solutions for axisymmetric problems at moderate or high Reynolds number [4–7]. A particularly alarming observation is that the anisotropy of the solution appears to persist under grid-refinement [4]. These results put the consistency of the 19 speed model with the Navier–Stokes equation into question. The same studies showed that a 27 speed model can recover axisymmetric solutions. Here we restrict ourselves to the 27 speed velocity set.

The equilibrium in the lattice Boltzmann equation is a fixed-point for the relaxation of the momentum distribution function. It is usually of polynomial type and designed to fulfill the minimal requirements of the Navier–Stokes equation. Terms beyond $\mathcal{O}(Ma^2)$ are usually disregarded. In this paper we follow our previous philosophy to obtain the equilibrium directly from the Maxwellian distribution and consider all terms in Mach number Ma that are supported by the velocity set [8].

The design of the collision operator is the primary topic of this paper. Almost all lattice Boltzmann models use the relaxation time approximation. The pre-collision distribution is relaxed towards the equilibrium to obtain a post-collision distribution. Models differ in whether they apply a single relaxation rate or multiple relaxation rates for different hydrodynamic quantities. Another distinction can be made on whether the relaxation rate(s) are constant or dependent on observable quantities. The latter is the case in various techniques supposed to model sub-grid-scales like the Smagorinsky model [9] or entropic limiters [10]. These techniques have physical motivations but are primarily used to run simulations at high Reynolds number without losing stability by locally increasing viscosity. Changing the relaxation rates locally usually results in non-constant transport coefficients unless the change is imposed to compensate for numerical defects (e.g. [11]).

The usage of multiple relaxation times (MRT) was introduced to maximize the number of adjustable parameters of the model in order to tune both stability and accuracy [12]. Many of the available parameters do not influence the solution of the LBE to leading order and their exact influence on stability and accuracy might depend on the problem under consideration. Using the free parameters MRT can be both more accurate and stable than a single relaxation time (BGK) LBE or less so. The set of relaxation rates presented in [12] is sometimes considered to be the "official" MRT method. However, the rates presented there were derived only for a specific viscosity and a specific velocity set. Another common choice is to optimize the relaxation rates for better accuracy of certain boundary conditions [13,14]. In this case the relaxation rates of third order moments become functions of viscosity. It is noted in [13] that the exact relationship between the parameters is only known for Poiseuille-flow and that the optimal choice for other cases depends on the problem at hand. The parameters can be optimized for higher linear stability from a linearized LBE [15]. It is also possible to optimize the parameters for higher accuracy in the bulk [16]. Further, it has been proposed to scale the relaxation rates of fourth order moments together with the viscosity in order to prevent the MRT method from diverging for small Mach numbers [17]. Finally, it is possible to disregard the search for optimal rates altogether and make the simple choice of setting all moments without first order contribution to the solution to their equilibrium values. This popular choice can be used to accelerate the computation [18]. The obvious disadvantage of this large number of problem specific possibilities to chose the free relaxation parameters is that an optimal choice suiting any simulation task is unknown.

While the optimal choice of the relaxation rates has been addressed from various standpoints another obvious question regarding the LBE with multiple relaxation times has received astonishingly little attention: which set of observable quantities should be used? The original MRT method transforms the local distribution function into a set of raw moments by means of a linear transformation. Each non-conserved moment is an observable quantity orthogonal to all the others and is allowed to relax with its own rate. Taking moments in a static frame of reference and relaxing them with different rates introduces violations of Galilean invariance not present in a single relaxation time model with the same velocity set and the same equilibrium function. This problem is solved with the cascaded LBE [8,19] that uses a non-linear transformation of the distribution function to central moments in the frame of the moving fluid. However, mutual linear independence or even orthogonality of the observable quantities is not sufficient to isolate their evolution. Observable quantities can also be coupled on the level of their equivalent partial differential equations. By relaxing different quantities with different rates we implicitly postulate that they evolve due to different processes. This implicit assumption was found to lead to inaccurate results when relaxation rates of different moments were not optimally chosen. An *ad hoc* solution to this problem was proposed with the Factorized Central Moment LBE [20,21]. The Factorized Central Moment LBE is also used in the commercial flow solver XFlow [22]. The same problem was solved in a mathematically more concise way using cumulants instead of central moments as observable quantities [23]. Seeger et al. analyzed the Boltzmann equation in cumulant space, derived equations of motion and boundary conditions for the cumulants and solved these equations numerically using the Lax method [24–26]. In [24] Seeger et al. show that their cumulant ansatz and Grad's moment expansion from [27] are equivalent. Seeger considers the cumulant expansion in one and two dimensions and observes a difference to the moment expansion at order six. The work of Seeger et al. differs from ours in that they solved the equations of motions for the cumulants while we use cumulants only in the collision step and solve the advection problem using a discrete distribution function and exact shift.

The LBE is often first considered in one or two dimensions and the results are later extended to three dimensions. We find this procedure problematic as the Navier–Stokes equations degenerate in lower dimensions. It is not *a priori* known that conclusions drawn from one- or two-dimensional models apply also to three-dimensional problems. It would, in fact, be more plausible to infer on lower dimensions from higher dimensions. For this reason we present our approach in three dimensions.

2. Cumulant lattice Boltzmann equation

We define the lattice Boltzmann equation in three dimensions as:

$$f_{ijk(x+ic\Delta t)(y+jc\Delta t)(z+kc\Delta t)(t+\Delta t)} = f_{ijkxyzt} + \Omega_{ijkxyzt} = f^*_{ijkxyzt}. \tag{1}$$

Here ic, jc, and kc refer to the variables in momentum space with c being the velocity quantum and $i, j, k \in \mathbb{Z}$, x, y, and z are the variables in space and t is the time variable. The lattice Boltzmann equation traces the evolution of the discrete momentum distribution function $f \in \mathbb{R}+$ in time, space, and momentum. The evolution proceeds by linear advection (streaming) and local collision with collision operator Ω. In order to solve the lattice Boltzmann equation we have to specify a discrete momentum distribution and a corresponding collision operator. The momentum distribution is chosen so that the exact shift by the velocities ic, jc, and kc moves the distribution from one lattice node to another one on a Cartesian grid. Further we restrict our considerations to so-called tensor product lattices, specific to the set $\{-c, 0, c\} \bigotimes \{-c, 0, c\} \bigotimes \{-c, 0, c\}$ where $c\Delta t = \Delta x$, Δx being the lattice spacing. This velocity set is further referred to as the D3Q27 lattice [28].

The discrete momentum distribution function f is interpreted as the probability to find a particle in a certain state in momentum space. The momentum space representation is advantageous for the description of streaming as streaming is linear in the particle velocity. The momentum state representation is disadvantageous for describing particle collisions since this involves the complete momentum distribution function in an *a priori* unknown way. This is an obstacle for the separation of different degrees of freedom involved in the collision process.

In order to make the distribution function independent from the frame of reference we apply a two-sided Laplace transform to the distribution in momentum space. We denote by $\vec{\xi} = \{\xi, \upsilon, \zeta\}$ the microscopic velocities and by $\vec{u}_0 = \{u_0, v_0, w_0\}$ an arbitrary velocity that shifts the distribution into another frame of reference. The Laplace-transform of an arbitrary function $g(\vec{\xi} + \vec{u}_0)$ is:

$$\mathcal{L}\{g(\vec{\xi} + \vec{u}_0)\} = \int_{-\infty}^{\infty} g(\vec{\xi} + \vec{u}_0) e^{-\vec{\Xi}\cdot\vec{\xi}} d\vec{\xi} \tag{2}$$

$$= \int_{-\infty}^{\infty} g(\vec{\xi}) e^{-\vec{\Xi}\cdot(\vec{\xi}-\vec{u}_0)} d\vec{\xi} \tag{3}$$

$$= e^{\vec{\Xi}\cdot\vec{u}_0} \int_{-\infty}^{\infty} g(\vec{\xi}) e^{-\vec{\Xi}\cdot\vec{\xi}} d\vec{\xi} \tag{4}$$

$$= e^{\vec{\Xi}\cdot\vec{u}_0} \mathcal{L}\{g(\vec{\xi})\}. \tag{5}$$

In the Laplace-transformed momentum space denoted by the velocity–frequency variable $\vec{\Xi}$ the frame of reference enters the distribution only as a known factor. In order to make the remainder independent of velocity it is always possible to shift the frame of reference such that the local velocity is zero. In the following we consider the momentum distribution function in its Laplace-transformed form as to eliminate any frame dependencies of the observable quantities during collision.

Collisions have the tendency to randomize the momentum distribution function. Randomization means that the distribution function is randomly rearranged while the constraints (such like mass and mean) are preserved. In the lattice Boltzmann model we consider the ensemble over many collisions such that randomization leads to the state of maximal likelihood constraint by the conservation laws. This state is called the equilibrium. Due to the condition that all degrees of freedom must be statistically independent it must be possible to write the joint probability for all degrees of freedom in equilibrium as a product of the independent degrees of freedom:

$$F^{eq} = \prod_a \mathrm{C}_a \prod_b \mathrm{F}_b. \tag{6}$$

Here C_a are the constraints that usually arise from conservation laws. For example, if mass, three components of momentum, and energy are the conserved quantities under consideration then there are five independent constraints to the equilibrium. Each constraint is a function of only one conserved quantity and the equilibrium is a function of the product of the five constraints. The degrees of freedom F_b are mutually uncorrelated in equilibrium and they are uncorrelated with the constraints by definition. Since they do not depend on anything they must all be constant. Since the integral of the distribution is also a constraint (conservation of mass) the product needs to be unity in order not to influence the mass of the distribution. The equilibrium must hence be a product of the constraints alone:

$$F^{eq} = \prod_a \mathrm{C}_a. \tag{7}$$

The relaxation time approximation, on which the collision operator is based, assumes a frequent occurrence of events that destroy information about the distribution of the particles in momentum space. The pre-collision distribution function describes the probability of a particle to enter a time and space window in a certain state in momentum space. Consequently, the post-collision distribution gives the joint probability of a particle entering a time and space window and to undergo an

event that destroys the information that it carries. The relaxation time is tied to the frequency of these events and not to the information that is being destroyed. In the lattice Boltzmann equation we have to assign the relaxation rate to a specific observable quantity that loses its memory by a decay of its non-equilibrium part. For the algorithm we are able to choose these observable quantities in any arbitrary way. In reality, different observable quantities can only change by different rates if they are influenced by different events that have different probabilities to occur. In contrast to previous work we demand that the observable quantities that are chosen to decay with different rates must also be driven by different random events. Consequently, the observable quantities that we choose should be the probabilities for a certain event to occur. It is self-evident that two events that occur with different frequencies must occur statistically independently (i.e. if two changes in observable quantities do not occur at the same time or with the same frequency, then they were not caused by the same event). Since they occur statistically independently, their joint probability must be the product of their individual probabilities. The mathematical supposition is hence that there exist observable quantities c_α such that the momentum distribution function can be written as a product of the constraints and probabilities of the different observable quantities in a Galilean invariant format.

Since a factorization in the space $\{\xi, \upsilon, \zeta\}$ is not Galilean invariant we transform the distribution function into frequency space $\vec{\Xi} = \{\Xi, \Upsilon, \mathrm{Z}\}$. This also helps in measuring the distance of each observable quantity to its equilibrium state. In frequency space the equilibrium and the local distribution function are both smooth and can be expanded into Taylor series.

We start by rewriting the discrete probability density function in continuous form using the microscopic velocity variables ξ, υ, and ζ and the Dirac delta function:

$$f(\vec{\xi}) = f(\xi, \upsilon, \zeta) = \sum_{i,j,k} f_{ijk}\delta(ic - \xi)\delta(jc - \upsilon)\delta(kc - \zeta). \tag{8}$$

Next we take the two-sided Laplace transform of this distribution:

$$\begin{aligned} F(\vec{\Xi}) &= \mathcal{L}\{f(\vec{\xi})\} = \int_{-\infty}^{\infty} f(\vec{\xi}) e^{-\vec{\Xi}\cdot\vec{\xi}} d\vec{\xi} \\ &= \sum_{i,j,k} f_{ijk} e^{-\Xi ic} e^{-\Upsilon jc} e^{-\mathrm{Z}kc}. \end{aligned} \tag{9}$$

The Laplace transformed probability distribution function $F = \mathcal{L}\{f(\vec{\xi})\}$ with $f_{ijk} \in \mathbb{R}+$ is continuous and smooth in the momentum wave number $\{\Xi, \Upsilon, \mathrm{Z}\}$. Fortunately, the Maxwellian equilibrium which is a Gaussian function in the space $\{\xi, \upsilon, \zeta\}$ is also smooth in $\{\Xi, \Upsilon, \mathrm{Z}\}$.

For the statistically independent and Galilean invariant observable quantities c_α the joint probability density must be written like:

$$F(\Xi, \Upsilon, \mathrm{Z}) = \prod_\alpha F_\alpha(c_\alpha). \tag{10}$$

If we want to write this equation in Taylor series form we have to transform the product into a sum using the Logarithm of F:

$$\ln(F(\Xi, \Upsilon, \mathrm{Z})) = \sum_\alpha \ln(F_\alpha(c_\alpha)). \tag{11}$$

We now define the coefficients of the series as countable cumulants $c_{\alpha\beta\gamma}$ [3]:

$$c_{\alpha\beta\gamma} = c^{-\alpha-\beta-\gamma} \frac{\partial^\alpha \partial^\beta \partial^\gamma}{\partial \Xi^\alpha \partial \Upsilon^\beta \partial \mathrm{Z}^\gamma} \ln(F(\Xi, \Upsilon, \mathrm{Z}))\Big|_{\Xi=\Upsilon=\mathrm{Z}=0}. \tag{12}$$

Cumulants fulfill the supposition of statistical independence between different degrees of freedom and frame invariance by construction. The countable cumulants can be combined in various additive ways in order to separate observable quantities by their rotational properties, for example to isolate shear from bulk viscosity. The order of a cumulant defines its metric (in our case in powers of c) such that only cumulants of the same order can be added together in a metric preserving way. The order of a countable cumulant is the sum of its indices $\alpha + \beta + \gamma$. Here, however, we define the cumulants in a dimensionless way by dividing by $c^{\alpha+\beta+\gamma}$. This is done to facilitate the analysis of the method. In this non-dimensional form the velocity is measured relative to the lattice velocity c rather than relative to an absolute measure. This is important when the lattice velocities are scaled in order to assess the asymptotic behavior of the method. In the practical implementation c is usually assumed to be unity. Each decay process can be modeled by an individual rate equation:

$$c^*_{\alpha\beta\gamma} = c^{eq}_{\alpha\beta\gamma}\omega_{\alpha\beta\gamma} + (1 - \omega_{\alpha\beta\gamma})c_{\alpha\beta\gamma}. \tag{13}$$

The asterisk $(*)$ indicates the post-collision cumulant, $c^{eq}_{\alpha\beta\gamma}$ is the equilibrium value of the cumulant and $\omega_{\alpha\beta\gamma}$ is the relaxation frequency.

The Maxwellian equilibrium can be easily written in the appropriate form as:

$$\ln(F^{eq}(\Xi, \Upsilon, \mathrm{Z})) = \ln(\rho/\rho_0) - \Xi u - \Upsilon v - \mathrm{Z}w + \frac{c^2\theta}{2}(\Xi^2 + \Upsilon^2 + \mathrm{Z}^2). \tag{14}$$

The velocities u, v, and w are given in lattice units $\Delta x/\Delta t$ and $c\theta^{1/2}$ is a parameter that can be identified as the speed of sound in lattice units. The constant ρ_0 defines a density metric for dimensional consistency. Since the logarithm of the Laplace transformed equilibrium is a polynomial it has a finite Taylor expansion and since the coefficients of the Taylor expansion are the cumulants it is seen that the equilibrium has only a finite number of non-zero cumulants.

In summary we propose a lattice Boltzmann collision operator with multiple relaxation rates for observable quantities that are both Galilean invariant and statistically independent of each other. This proposal is based on the following assumptions:

- The two sided Laplace transform F of f exists and is smooth such that its Taylor expansion exists.
- The logarithm of F is also smooth such that its Taylor expansion exists.
- The Laplace transformed distribution F can be written as a product of the constraints from conservation laws and the observable quantities that are allowed to relax with different rates.
- Each multiplicand in this product is an observable quantity independent of all other multiplicands in the product.

3. Relation to other lattice Boltzmann models

The lattice Boltzmann equation considering several different relaxation rates is classically not derived using cumulants but moments. The observable quantities in the classical Multiple Relaxation Time (MRT) approach are derived from raw moments. We define countable raw moments as:

$$m_{\alpha\beta\gamma} = c^{-\alpha-\beta-\gamma}\frac{\partial^\alpha\partial^\beta\partial^\gamma}{\partial\Xi^\alpha\partial\Upsilon^\beta\partial\mathrm{Z}^\gamma}F(\Xi, \Upsilon, \mathrm{Z})\Big|_{\Xi=\Upsilon=\mathrm{Z}=0} = \sum_{i,j,k} i^\alpha j^\beta k^\gamma f_{ijk}. \tag{15}$$

3.1. Orthogonality of moments

The classical MRT method is obtained by orthogonalizing the base vectors of the transformation matrix used to transform the distributions into moments. Unfortunately orthogonalization of the basis vectors might mean two different things. Consider vectors q_i and p_i that extract the moments M_q and M_p from the distributions f_i:

$$M_q = \sum_i q_i f_i, \tag{16}$$

$$M_p = \sum_i p_i f_i. \tag{17}$$

Here we use only one index i for the distribution since this is the standard nomenclature in the MRT literature. Some authors [15,29,12,30,16,31,32] consider two moments M_q and M_p to be orthogonal if their *unweighted* product is zero:

$$\sum_i q_i p_i = 0. \tag{18}$$

Dellar [33] and Asinari [34] consider two moments to be orthogonal if their *weighted* product is zero:

$$\sum_i w_i q_i p_i = 0. \tag{19}$$

Here w_i is the weighting factor usually used in the BGK lattice Boltzmann method. To distinguish the two methods we will call the first one unweighted orthogonalization and the second one weighted orthogonalization. We emphasize here that the classical work on the MRT method [15,12] used unweighted orthogonalization. We will call the MRT method with unweighted orthogonalization the classical MRT method since it is the method that was originally named MRT method. Whenever we write "orthogonal" without further specification we mean unweighted orthogonal.

A convincing justification for the application of the unweighted orthogonalization is not known to the authors. Unweighted orthogonalization can be used to separate isotropic parts from non-isotropic parts of certain tensors. This is in particular important for the separation of shear and bulk viscosity but it is hardly a justification for the unweighted orthogonalization since this separation is usually applied before orthogonalization [16] (i.e. the non-orthogonal basis would offer the same property).

For the D3Q27 model an unweighted orthogonal basis was derived in [16], analyzed in [35] and is given here in Appendix B. The orthogonal raw moments are also assumed to decay exponentially to a local equilibrium with individual rates. However, the probability densities for the individual processes do not fulfill the condition for statistical independence:

The joint probability density in frequency space is not the product of the individual probabilities. This is true for non-orthogonal as well as for weighted and unweighted orthogonal raw moments. It is also true for the cascaded lattice Boltzmann equation that uses non-orthogonal central moments as observable quantities that are derived from a centered distribution function:

$$\tilde{F} = \mathcal{L}\{f(\xi - u, \upsilon - v, \zeta - w)\} = e^{-u\Xi - v\Upsilon - w\mathrm{Z}} F(\Xi, \Upsilon, \mathrm{Z}), \tag{20}$$

were u, v, and w are the components of the local velocity vector. The central moments are:

$$\kappa_{\alpha\beta\gamma} = c^{-\alpha-\beta-\gamma} \frac{\partial^\alpha \partial^\beta \partial^\gamma}{\partial \Xi^\alpha \partial \Upsilon^\beta \partial \mathrm{Z}^\gamma} \tilde{F}(\Xi, \Upsilon, \mathrm{Z})\Big|_{\Xi=\Upsilon=\mathrm{Z}=0} = \sum_{i,j,k} (i - u/c)^\alpha (j - v/c)^\beta (k - w/c)^\gamma f_{ijk}. \tag{21}$$

The MRT method with orthogonal or non-orthogonal raw moments and the cascaded LBE provide solutions that are asymptotically consistent with the Navier–Stokes equation to second order in diffusive scaling (scaling the Mach number proportional to the grid spacing). From an asymptotic point of view we would not expect an improvement from the usage of cumulants as opposed to moments. However, asymptotic analysis to leading order does not take into account that dissipation at higher asymptotic order might not be Galilean invariant or might go along with a very large damping coefficient.

3.2. Galilean invariance

Let us first consider the Galilean invariance issue by comparison of the equivalent partial differential equations for third order moments versus the equivalent partial differential equations for cumulants: Considering the asymptotic analysis of the third order raw non-orthogonal moment $m_{120+102} = m_{120} + m_{102}$ assumed to evolve with rate ω_3 leads to (details on asymptotic analysis are given in Appendix G):

$$\begin{aligned}\bar{m}^{(3)}_{120+102} = {} & \frac{2}{3}(\rho^{(0)}u^{(3)} + \rho^{(2)}u^{(1)}) + u^{(1)}\rho^{(0)}(v^{(1)2} + w^{(1)2}) - \frac{2\rho^{(0)}}{3}\left(\frac{1}{\omega_3} - \frac{1}{2}\right)\Big\{v^{(1)}(\partial_x v^{(1)} + \partial_y u^{(1)}) \\ & + w^{(1)}(\partial_x w^{(1)} + \partial_z u^{(1)}) + u^{(1)}(\partial_y v^{(1)} + \partial_z w^{(1)}) \\ & - \frac{1}{3}\left(\frac{1}{\omega_1} - \frac{1}{2}\right)(\partial_{yy}u^{(1)} + \partial_{zz}u^{(1)} + 2\partial_{xy}v^{(1)} + 2\partial_{xz}w^{(1)})\Big\}.\end{aligned} \tag{22}$$

Here we used the shorthand $\bar{m}_{120} = (m_{120} + m^*_{120})/2$. This equation appears at the leading order of the error with respect to the Navier–Stokes equation. It does not influence the actual solution but the asymptotic behavior of the error. The decaying non-equilibrium part (in $\{\cdot\}$) of this moment depends on the absolute value of the velocity. This is obviously not Galilean invariant as the rate of change in this moment due to collision depends on the frame of reference. Since the third order moment governs the viscous stress we expect a defect in the Galilean invariance of viscosity to originate from this violation. Orthogonalization has no effect on this problem. This is seen by considering the corresponding unweighted orthogonal raw moment as defined in Appendix B:

$$M_{10} = -4m_{100} + 3(m_{102} + m_{120}). \tag{23}$$

The equivalent partial differential equation of M_{10} is:

$$\begin{aligned}\bar{M}^{(3)}_{10} = {} & -2(\rho^{(0)}u^{(3)} + \rho^{(2)}u^{(1)}) + 3u^{(1)}\rho^{(0)}(v^{(1)2} + w^{(1)2}) - 2\rho^{(0)}\left(\frac{1}{s_{10}} - \frac{1}{2}\right)\Big\{v^{(1)}(\partial_x v^{(1)} + \partial_y u^{(1)}) \\ & + w^{(1)}(\partial_x w^{(1)} + \partial_z u^{(1)}) + u^{(1)}(\partial_y v^{(1)} + \partial_z w^{(1)}) \\ & - \frac{1}{3}\left(\frac{1}{s_\nu} - \frac{1}{2}\right)(\partial_{yy}u^{(1)} + \partial_{zz}u^{(1)} + 2\partial_{xy}v^{(1)} + 2\partial_{xz}w^{(1)})\Big\}.\end{aligned} \tag{24}$$

The non-equilibrium part of the unweighted orthogonal raw moment differs only by a constant factor from the non-orthogonal raw moment. Both violate Galilean invariance in exactly the same way. The weighted orthogonal MRT method would also produce the same defect. The problem is absent when we relax central moments instead:

$$\bar{\kappa}^{(3)}_{120+102} = \frac{2\rho^{(0)}}{9}\left(\frac{1}{\omega_3} - \frac{1}{2}\right)\left(\frac{1}{\omega_1} - \frac{1}{2}\right)(\partial_{yy}u^{(1)} + \partial_{zz}u^{(1)} + 2\partial_{xy}v^{(1)} + 2\partial_{xz}w^{(1)}). \tag{25}$$

Orthogonalization was not used here and would be as irrelevant as in the case of raw moments. Cumulants of third order are identical to central moments at third order. Thus, we expect to see smaller errors in the Galilean invariance of viscosity in both the cascaded LBE as well as in the cumulant LBE as opposed to the MRT LBE. We do not expect any influence of orthogonalization on Galilean invariance at this order.

3.3. Hyper-viscosity

The equivalence between central moments and cumulants is lost at order four and higher. Moments of order four can have a significant influence on the accuracy of the method as they control error terms containing fourth derivatives of velocity. The spurious dissipation from the fourth order moments can be significantly larger than the physical dissipation at sufficiently short wave lengths. One such problem arises, for example, from the moment m_{211} or the corresponding central moment κ_{211}. Deriving the equivalent partial differential equation by Taylor expansion and diffusive scaling yields to second order in diffusive scaling:

$$\bar{m}^{(2)}_{211} = \frac{\rho^{(0)}}{3} v^{(1)} w^{(1)} - \frac{\rho^{(0)}}{9} \left(\frac{1}{\omega_8} - \frac{1}{2} \right) (\partial_y w^{(1)} + \partial_z v^{(1)}), \tag{26}$$

$$\bar{\kappa}^{(2)}_{211} = -\frac{\rho^{(0)}}{9} \left(\frac{1}{\omega_8} - \frac{1}{2} \right) (\partial_y w^{(1)} + \partial_z v^{(1)}). \tag{27}$$

Here (26) is the equation solved for non-orthogonal raw moments and (27) is the equation solved in the cascaded LBE. Even though the two methods are not completely equivalent they are equivalent at second order even for fourth order moments (see Appendix I). The problem with (26) and (27) is that they are not independent of moments of lower order, m_{011} and κ_{011} specifically:

$$\bar{m}^{(2)}_{011} = \rho^{(0)} v^{(1)} w^{(1)} - \frac{\rho^{(0)}}{3} \left(\frac{1}{\omega_1} - \frac{1}{2} \right) (\partial_y w^{(1)} + \partial_z v^{(1)}), \tag{28}$$

$$\bar{\kappa}^{(2)}_{011} = -\frac{\rho^{(0)}}{3} \left(\frac{1}{\omega_1} - \frac{1}{2} \right) (\partial_y w^{(1)} + \partial_z v^{(1)}). \tag{29}$$

Eqs. (28) and (29) are almost identical to (26) and (27) but they come with a different relaxation rate. The relaxation rate ω_1 is easily shown to govern shear viscosity while ω_8 governs a hyper-viscosity which is formally two orders smaller in wave number than the usual viscosity and therefore usually assumed to be asymptotically small. It is, however, a typical requirement in industrial applications to study flow at large Reynolds numbers such that the viscosity defined by ω_1 is very small while the relaxation rate for the non-hydrodynamic moments is kept high for stability reasons, thus we typically have:

$$\left(\frac{1}{\omega_8} - \frac{1}{2} \right) \gg \left(\frac{1}{\omega_1} - \frac{1}{2} \right). \tag{30}$$

For the simulation of turbulent flows the difference between the hyper-viscosity (*lhs*) and shear viscosity (*rhs*) can easily grow to several orders of magnitude where the hyper-viscosity can no longer be neglected even if it is formally higher order. The simplest and obvious solution is to couple the two relaxation rates ω_8 and ω_1 to have proportional values. This is undesirable for two reasons. First, lowering the hyper-viscosity would result in no damping of the non-hydrodynamic observable quantities and would therefore limit the stability of the method. Second, we presented the moment m_{211} only as an example and similar conditions hold for other moments, too. If we tried to solve this problem by coupling of relaxation rates we had to choose the same relaxation rate for all moments. The result would be a return to the single relaxation time method. Basing the collision operator on cumulants instead of moments solves the problem at any combination of relaxation rates. In fact for cumulants we have:

$$\bar{C}^{(2)}_{011} = -\frac{\rho^{(0)}}{3} \left(\frac{1}{\omega_1} - \frac{1}{2} \right) (\partial_y w^{(1)} + \partial_z v^{(1)}), \tag{31}$$

$$\bar{C}^{(2)}_{211} = 0. \tag{32}$$

The capital C indicates a cumulant times density $C_{211} = c_{211}\rho$ which is used to simplify the analysis. For the cumulant C_{211} the second order non-equilibrium part vanishes altogether. Any dissipation exerted to this cumulant appears at least two orders in wave number higher in the solution than in the case of the corresponding moments. The ability to dampen non-hydrodynamic observable quantities is not accompanied by a leading order hyper-viscosity in the case of the cumulant lattice Boltzmann method.

Next we test whether orthogonalization of the raw moments has any effect on the problem. For this we consider the unweighted orthogonal raw moments $M_8 = m_{011}$ and $M_{21} = 3m_{211} - 2m_{011}$. Relaxing orthogonal raw moments leads to the equivalent partial differential equations at the leading order of the error:

$$\bar{M}^{(2)}_{8} = \rho^{(0)} v^{(1)} w^{(1)} - \frac{\rho^{(0)}}{3} \left(\frac{1}{s_\nu} - \frac{1}{2} \right) (\partial_y w^{(1)} + \partial_z v^{(1)}), \tag{33}$$

$$\bar{M}^{(2)}_{21} = -\rho^{(0)} v^{(1)} w^{(1)} + \frac{\rho^{(0)}}{3} \left(\frac{1}{s_{21}} - \frac{1}{2} \right) (\partial_y w^{(1)} + \partial_z v^{(1)}). \tag{34}$$

The orthogonalization of the base vectors is seen to be ineffective for the separation of the partial differential equation of different degrees of freedom. Eqs. (33) and (34) imply:

$$\bar{M}_{21}^{(2)} = -\rho^{(0)} v^{(1)} w^{(1)} - \frac{\left(\frac{1}{s_{21}} - \frac{1}{2}\right)}{\left(\frac{1}{s_\nu} - \frac{1}{2}\right)} (\bar{M}_8^{(2)} - \rho^{(0)} v^{(1)} w^{(1)}). \tag{35}$$

Since cumulants successfully separate the degrees of freedom it is instructive to ask whether or not cumulants produce an orthogonal basis when written in terms of a transformation matrix. This question is not easy to answer in general since the corresponding transformation matrix is not constant. Therefore we consider the limiting case of zero velocity and equilibrium. In this limiting case the cumulants reduce to:

$$C_{011} \to m_{011}, \tag{36}$$

$$C_{211} \to m_{211} - m_{011}/3. \tag{37}$$

Writing these moments in terms of distributions gives (using the Miller indices with $\bar{1} \equiv -1$):

$$m_{011} = f_{\bar{1}\bar{1}\bar{1}} + f_{1\bar{1}\bar{1}} + f_{\bar{1}11} + f_{111} - f_{\bar{1}1\bar{1}} - f_{11\bar{1}} - f_{\bar{1}\bar{1}1} - f_{1\bar{1}1} + f_{0\bar{1}\bar{1}} + f_{011} - f_{01\bar{1}} - f_{0\bar{1}1}, \tag{38}$$

$$m_{211} - m_{011}/3 = 2/3(f_{\bar{1}\bar{1}\bar{1}} + f_{1\bar{1}\bar{1}} + f_{\bar{1}11} + f_{111} - f_{\bar{1}1\bar{1}} - f_{11\bar{1}} - f_{\bar{1}\bar{1}1} - f_{1\bar{1}1}) - 1/3(f_{0\bar{1}\bar{1}} + f_{011} - f_{01\bar{1}} - f_{0\bar{1}1}). \tag{39}$$

Rewriting this in form of lattice vectors of unit length and taking the unweighted dot product according to Eq. (18) between the vectors $\vec{m}_{011}$ and $\vec{m}_{211} - \vec{m}_{011}/3$ does not give zero and the base vectors of the cumulant method are hence seen to be non-orthogonal (in the unweighted sense) even in equilibrium and at velocity zero. It has to be concluded that unweighted orthogonalization of the base vectors does not decouple the observable quantities in their equivalent partial differential equations. Decoupling the equivalent partial differential equations of the observable quantities by factorization does not result in an orthogonal transformation basis in the unweighted sense. The two methods to obtain independence of the observable quantities, factorization and unweighted orthogonalization, are hence seen to be mutually incompatible. However, if we use the weighted orthogonalization considering the weights $w_{000} = 8/27$, $w_{001} = 2/27$, $w_{011} = 1/54$, and $w_{111} = 1/216$ and compute the weighted scalar product according to Eq. (19) we obtain zero. The weighted orthogonalization is hence seen to agree with the cumulant method. However, this correspondence only holds in equilibrium and at zero velocity. The weighted orthogonality breaks Galilean invariance the same way as the unweighted orthogonality does.

3.4. Summary

The analytical investigation above already confirms that unweighted orthogonalization fails in decoupling the degrees of freedom while factorization succeeds. The consequences of this disagreement are further investigated numerically in Section 5 of this paper. The consequences of unweighted orthogonalization for stability and a detailed comparison of the quantities M_{21}, m_{211}, κ_{211}, and C_{211} is given in Appendix I.

The cumulant LBE is very similar to the Factorized Central Moment LBE introduced by us in [20], adopted in [21], and successfully commercialized in the fluid solver XFlow [22]. The Factorized Central Moment LBE does not suffer from the hyper-viscosity arising from (27). The factorized quasi-equilibrium of that method was introduced exactly for the purpose to eliminate this artifact. A detailed comparison between the factorized quasi-equilibrium and cumulants shows that differences exist only at orders beyond the formal truncation error of the LBE. The factorized quasi-equilibrium can be obtained from cumulants by dropping out higher order terms. Our derivation of the cumulant LBE is hence also a justification of the established Factorized Central Moment LBE. While the original derivation in [20] was somewhat *ad hoc* and required the construction of quasi-equilibria that depended on non-conserved quantities the derivation from cumulants is solely based on first principles.

The hyper-viscosity arising from (27) is a three-dimensional effect that cannot be anticipated from a two-dimensional model with nine speeds, the projection of the 27 speeds lattice into two dimensions. It is, in fact, difficult to appreciate the difference between weighted and unweighted orthogonality in two dimensions as the moments for which orthogonality matters (for example κ_{112}) do not exist in two dimensions. In two dimensions there would only be one moment of fourth order that differed from its counterpart in terms of cumulants.

Considering the equivalent partial differential equation for the moment $\bar{m}_{220}$ in the non-orthogonal raw moment method reveals the critical difference between two and three dimensions:

$$\bar{m}_{220}^{(2)} = \frac{\rho^{(0)}}{3}\left(\frac{1}{3} + u^{(1)2} + v^{(1)2}\right) - \frac{1}{3}\left(\frac{1}{\omega_6} - \frac{1}{2}\right)\left\{\partial_x u^{(1)} + \partial_y v^{(1)}\right\}. \tag{40}$$

Due to the incompressibility condition that holds to second order in diffusive scaling this can be recast as:

$$\bar{m}_{220}^{(2)} = \frac{\rho^{(0)}}{3}\left(\frac{1}{3} + u^{(1)2} + v^{(1)2}\right) + \frac{1}{3}\left(\frac{1}{\omega_6} - \frac{1}{2}\right)\partial_z w^{(1)}. \tag{41}$$

The velocity gradient $\partial_z w^{(1)}$ is zero in two dimensions but it is not zero in three dimensions. The non-equilibrium part of the moment m_{220} is $\mathcal{O}(\epsilon^4)$ in diffusive scaling in two dimensions while it is $\mathcal{O}(\epsilon^2)$ in three dimensions. Consequently, fourth order moments and the question whether they have been properly orthogonalized to other observable quantities have nearly no influence on the accuracy and the stability in two dimensions while it has a significant influence in three dimensions. This example highlights how important it is not to draw conclusion on three-dimensional behavior from two-dimensional analysis. In fact, up to a few negligible terms of higher order the cumulant method reduces to the cascaded lattice Boltzmann model when considered in two dimensions.

4. Implementation of a cumulant LBM kernel

In this section we list the complete implementation of the D3Q27 cumulant collision operator for the reader to implement. Our description here does not cover other aspects of the LBE like the streaming step or the implementation of boundary conditions. Also, we describe only the classical compressible version where a non-zero background pressure is assumed and density is calculated from summing up the distributions. A well conditioned implementation subtracts the background pressure from the distribution in order to reduce round-off errors. The well conditioned implementation is discussed in Appendix J. An incompressible formulation is possible but not considered here since it would introduce some additional violations of Galilean invariance [11].

4.1. Forward central moment transformation

The density is computed from the zeroth moment $\rho = m_{000}$. The velocity is computed from the first moments by dividing by the zero moment:

$$u = \frac{m_{100} + F_x/2}{m_{000}}, \qquad v = \frac{m_{010} + F_y/2}{m_{000}}, \qquad w = \frac{m_{001} + F_z/2}{m_{000}}. \tag{42}$$

Here F_x, F_y, and F_z denote the components of a forcing term if applicable.

Cumulants can be computed directly from the definition in Eq. (12). However, since cumulants are not simple functions this direct computation is extremely expensive. Therefore we propose to transform the original distribution function f_{ijk} to cumulants using several steps. Cumulants can be computed relatively efficiently from central moments which we defined in Eq. (21).

Unlike the computation of cumulants the computation of central moments can be split easily among the three different directions:

$$\kappa_{ij|\gamma} = \sum_k f_{ijk}(k - w/c)^\gamma, \tag{43}$$

$$\kappa_{i|\beta\gamma} = \sum_j \kappa_{ij|\gamma}(j - v/c)^\beta, \tag{44}$$

$$\kappa_{\alpha\beta\gamma} = \sum_i \kappa_{i|\beta\gamma}(i - u/c)^\alpha. \tag{45}$$

The split up version requires only one third of the operations compared to the direct version using Eq. (21).

4.2. Forward cumulant transformation

The non-conserved cumulants are computed from the central moments. Since the equilibrium of most cumulants is zero the normalization is omitted in the following and we define:

$$C_{abc} = c_{abc}\rho. \tag{46}$$

In what follows we omit equations for cumulants which can be obtained by permuting indices in the listed equations. The first few cumulants are seen to be identical to the first few central moments:

$$C_{110} = \kappa_{110}, \tag{47}$$

$$C_{200} = \kappa_{200}, \tag{48}$$

$$C_{120} = \kappa_{120}, \tag{49}$$

$$C_{111} = \kappa_{111}. \tag{50}$$

Equations for C_{101} and C_{011} and so on are obtained by permuting the indices in the above. Differences from central moments start at order four:

$$C_{211} = \kappa_{211} - (\kappa_{200}\kappa_{011} + 2\kappa_{110}\kappa_{101})/\rho, \tag{51}$$

$$C_{220} = \kappa_{220} - (\kappa_{200}\kappa_{020} + 2\kappa_{110}^2)/\rho, \tag{52}$$

$$C_{122} = \kappa_{122} - (\kappa_{002}\kappa_{120} + \kappa_{020}\kappa_{102} + 4\kappa_{011}\kappa_{111} + 2(\kappa_{101}\kappa_{021} + \kappa_{110}\kappa_{012}))/\rho, \tag{53}$$

$$\begin{aligned} C_{222} \;=\; & \kappa_{222} - (4\kappa_{111}^2 + \kappa_{200}\kappa_{022} + \kappa_{020}\kappa_{202} + \kappa_{002}\kappa_{220} + 4(\kappa_{011}\kappa_{211} + \kappa_{101}\kappa_{121} + \kappa_{110}\kappa_{112}) \\ & + 2(\kappa_{120}\kappa_{102} + \kappa_{210}\kappa_{012} + \kappa_{201}\kappa_{021}))/\rho \\ & + (16\kappa_{110}\kappa_{101}\kappa_{011} + 4(\kappa_{101}^2\kappa_{020} + \kappa_{011}^2\kappa_{200} + \kappa_{110}^2\kappa_{002}) + 2\kappa_{200}\kappa_{020}\kappa_{002})/\rho^2. \end{aligned} \tag{54}$$

and so on by permuting indices.

4.3. Collision

As in the case of moments rotational invariance requires to rearrange some cumulants and to choose some relaxation rates to be the same [36]. The collision reads explicitly (now listing all cases):

$$C_{110}^* = (1-\omega_1)C_{110}, \tag{55}$$

$$C_{101}^* = (1-\omega_1)C_{101}, \tag{56}$$

$$C_{011}^* = (1-\omega_1)C_{011}. \tag{57}$$

The following three cumulants are modified from their standard equilibrium in order to lessen the aliasing artifacts originating from the absence of the cumulants C_{300}, C_{030}, and C_{003}. Details are given in Appendix H. We first determine the required velocity gradients using asymptotic analysis. The variables $D_x u$, $D_y v$, and $D_z w$ denote approximate first derivatives which are computed from the cumulants as:

$$D_x u = -\frac{\omega_1}{2\rho}(2C_{200} - C_{020} - C_{002}) - \frac{\omega_2}{2\rho}(C_{200} + C_{020} + C_{002} - \kappa_{000}), \tag{58}$$

$$D_y v = D_x u + \frac{3\omega_1}{2\rho}(C_{200} - C_{020}), \tag{59}$$

$$D_z w = D_x u + \frac{3\omega_1}{2\rho}(C_{200} - C_{002}). \tag{60}$$

The following cumulants are now modified in their equilibrium:

$$C_{200}^* - C_{020}^* = (1-\omega_1)(C_{200} - C_{020}) - 3\rho\left(1 - \frac{\omega_1}{2}\right)(u^2 D_x u - v^2 D_y v), \tag{61}$$

$$C_{200}^* - C_{002}^* = (1-\omega_1)(C_{200} - C_{002}) - 3\rho\left(1 - \frac{\omega_1}{2}\right)(u^2 D_x u - w^2 D_z w), \tag{62}$$

$$C_{200}^* + C_{020}^* + C_{002}^* = \kappa_{000}\omega_2 + (1-\omega_2)(C_{200} + C_{020} + C_{002}) - 3\rho\left(1 - \frac{\omega_2}{2}\right)(u^2 D_x u + v^2 D_y v + w^2 D_z w). \tag{63}$$

The equilibria for all remaining cumulants are zero.

$$C_{120}^* + C_{102}^* = (1-\omega_3)(C_{120} + C_{102}), \tag{64}$$

$$C_{210}^* + C_{012}^* = (1-\omega_3)(C_{210} + C_{012}), \tag{65}$$

$$C_{201}^* + C_{021}^* = (1-\omega_3)(C_{201} + C_{021}), \tag{66}$$

$$C_{120}^* - C_{102}^* = (1-\omega_4)(C_{120} - C_{102}), \tag{67}$$

$$C_{210}^* - C_{012}^* = (1-\omega_4)(C_{210} - C_{012}), \tag{68}$$

$$C_{201}^* - C_{021}^* = (1-\omega_4)(C_{201} - C_{021}), \tag{69}$$

$$C_{111}^* = (1-\omega_5)C_{111}, \tag{70}$$

$$C_{220}^* - 2C_{202}^* + C_{022}^* = (1-\omega_6)(C_{220} - 2C_{202} + C_{022}), \tag{71}$$

$$C_{220}^* + C_{202}^* - 2C_{022}^* = (1-\omega_6)(C_{220} + C_{202} - 2C_{022}), \tag{72}$$

$$C_{220}^* + C_{202}^* + C_{022}^* = (1-\omega_7)(C_{220} + C_{202} + C_{022}), \tag{73}$$

$$C_{211}^* = (1-\omega_8)C_{211}, \tag{74}$$

$$C_{121}^* = (1-\omega_8)C_{121}, \tag{75}$$

$$C_{112}^* = (1-\omega_8)C_{112}, \tag{76}$$

$$C_{221}^* = (1-\omega_9)C_{221}, \tag{77}$$

$$C^*_{212} = (1-\omega_9)C_{212}, \tag{78}$$
$$C^*_{122} = (1-\omega_9)C_{122}, \tag{79}$$
$$C^*_{222} = (1-\omega_{10})C_{222}. \tag{80}$$

The only relaxation parameter that has a leading order influence on the results is the relaxation rate ω_1. The other parameters are free and can be chosen in the range $\{0\cdots 2\}$. Their value has a varying influence on the result which is not discussed in this paper. In most cases it is save to set all relaxation rates except ω_1 to one.

4.4. Backward cumulant transformation

After the collision the cumulants have to be transformed back into central moments:

$$\kappa^*_{211} = C^*_{211} + (\kappa^*_{200}\kappa^*_{011} + 2\kappa^*_{110}\kappa^*_{101})/\rho, \tag{81}$$
$$\kappa^*_{220} = C^*_{220} + (\kappa^*_{200}\kappa^*_{020} + 2\kappa^{*2}_{110})/\rho, \tag{82}$$
$$\kappa^*_{122} = C^*_{122} + (\kappa^*_{002}\kappa^*_{120} + \kappa^*_{020}\kappa^*_{102} + 4\kappa^*_{011}\kappa^*_{111} + 2(\kappa^*_{101}\kappa^*_{021} + \kappa^*_{110}\kappa^*_{012}))/\rho, \tag{83}$$
$$\begin{aligned}\kappa^*_{222} = {} & C^*_{222} + (4\kappa^{*2}_{111} + \kappa^*_{200}\kappa^*_{022} + \kappa^*_{020}\kappa^*_{202} + \kappa^*_{002}\kappa^*_{220} + 4(\kappa^*_{011}\kappa^*_{211} + \kappa^*_{101}\kappa^*_{121} + \kappa^*_{110}\kappa^*_{112}) \\ & + 2(\kappa^*_{120}\kappa^*_{102} + \kappa^*_{210}\kappa^*_{012} + \kappa^*_{201}\kappa^*_{021}))/\rho \\ & - (16\kappa^*_{110}\kappa^*_{101}\kappa^*_{011} + 4(\kappa^{*2}_{101}\kappa^*_{020} + \kappa^{*2}_{011}\kappa^*_{200} + \kappa^{*2}_{110}\kappa^*_{002}) + 2\kappa^*_{200}\kappa^*_{020}\kappa^*_{002})/\rho^2.\end{aligned} \tag{84}$$

The remaining central moments are obtained by permuting the corresponding indices. Second and third order central moments are directly obtained from the cumulants according to Eqs. (47)–(50). In order for the forcing to take effect the first central moments have to change sign:

$$\kappa^*_{100} = -\kappa_{100}, \tag{85}$$
$$\kappa^*_{010} = -\kappa_{010}, \tag{86}$$
$$\kappa^*_{001} = -\kappa_{001}. \tag{87}$$

This is done because half the force was applied to the definition of the frame of reference prior to the central moment transformation. Applying half the force before and half the force after collision is symmetric in time. Since all quantities have been transformed into the moving frame of reference no contribution of the force to other than first order moments has to be considered. The symmetry in time implies that this method is second order accurate in time. The simplicity of the forcing term in this formalism is noteworthy.

4.5. Backward central moment transformation

The back transformation to distributions reads in its split up version, which is again three times faster than a direct inversion:

$$\kappa^*_{0|\beta\gamma} = \kappa^*_{0\beta\gamma}(1-(u/c)^2) - 2(u/c)\kappa^*_{1\beta\gamma} - \kappa^*_{2\beta\gamma}, \tag{88}$$
$$\kappa^*_{\bar{1}|\beta\gamma} = (\kappa^*_{0\beta\gamma}((u/c)^2 - u/c) + \kappa^*_{1\beta\gamma}(2u/c-1) + \kappa^*_{2\beta\gamma})/2, \tag{89}$$
$$\kappa^*_{1|\beta\gamma} = (\kappa^*_{0\beta\gamma}((u/c)^2 + u/c) + \kappa^*_{1\beta\gamma}(2u/c+1) + \kappa^*_{2\beta\gamma})/2, \tag{90}$$
$$\kappa^*_{i0|\gamma} = \kappa^*_{i|0\gamma}(1-(v/c)^2) - 2(v/c)\kappa^*_{i|1\gamma} - \kappa^*_{i|2\gamma}, \tag{91}$$
$$\kappa^*_{i\bar{1}|\gamma} = (\kappa^*_{i|0\gamma}((v/c)^2 - v/c) + \kappa^*_{i|1\gamma}(2v/c-1) + \kappa^*_{i|2\gamma})/2, \tag{92}$$
$$\kappa^*_{i1|\gamma} = (\kappa^*_{i|0\gamma}((v/c)^2 + v/c) + \kappa^*_{i|1\gamma}(2v/c+1) + \kappa^*_{i|2\gamma})/2, \tag{93}$$
$$f^*_{ij0} = \kappa^*_{ij|0}(1-(w/c)^2) - 2(w/c)\kappa^*_{ij|1} - \kappa^*_{ij|2}, \tag{94}$$
$$f^*_{ij\bar{1}} = (\kappa^*_{ij|0}((w/c)^2 - w/c) + \kappa^*_{ij|1}(2w/c-1) + \kappa^*_{ij|2})/2, \tag{95}$$
$$f^*_{ij1} = (\kappa^*_{ij|0}((w/c)^2 + w/c) + \kappa^*_{ij|1}(2w/c+1) + \kappa^*_{ij|2})/2. \tag{96}$$

This concludes the collision step which is followed by the usual streaming step. Eqs. (43)–(96) list the entire collision operator for direct implementation.

5. Numerical tests

In this section we compare the accuracy of the cumulant method to that of the MRT and cascaded method by simple tests that focus on specific defects of the moment approach. Since our aim here is to investigate the influence of the basis transformation (raw moments, central moments, and cumulants) we have to make some non-standard decisions to exclude the influence of other aspects of the schemes under consideration. For the raw moment MRT method we compare two variants: one uses the non-orthogonal raw moments (RM) where the combinations of countable raw moments correspond exactly to the combinations of the countable cumulants in the cumulant method (see Appendix C). This MRT method is not considered classical since the moments are not orthogonal. A classical orthogonal MRT method is also used (see Appendix B). The cascaded lattice Boltzmann model is defined in Appendix D. We compare models that all share the same velocity set, the same equilibrium function, and the same set of relaxation rates. Our aim is to show that the violation of Galilean invariance in the MRT method is not (only) caused by an insufficient equilibrium function but also by an incorrect basis for the observable quantities. Therefore the considered models differ only in the choice of the basis transformation. For comparison, a single relaxation time (BGK) kernel is also used. In order to provide a fair comparison to the other methods the BGK model here differs from the standard BGK model by using a product equilibrium of higher then second order in velocity and the Galilean correction for the non-existing moments m_{300} and so on (see Appendix A). This improved BGK model is empirically observed to have significantly better stability properties than the standard BGK. It is also more accurate since its viscosity is isotropically Galilean invariant to at least $\mathcal{O}(Ma^4)$.

In order to reduce the influence of round-off errors all models were hand optimized for better conditioning. This leads to more complicated expressions as discussed in Appendix J. We do not expect a significant influence of the conditioning on the results presented in this section since all calculations were done in double precision unless stated otherwise.

The error in the RM, MRT, cascaded, and cumulant methods are functions of the relaxation rates $\omega_2 \cdots \omega_{10}$. Even though there is a superficial correspondence between raw moments, central moments, and cumulants the different rates arguable act on different quantities in the different models. Therefore we chose all relaxation rates except of those acting on shear viscosity (ω_1) to be unity in all models. The rate ω_1 (or s_ν for the classical MRT) acts on second order moments in exactly the same way in all models. Setting all other rates to unity means that the remainder of the distribution is put to equilibrium in each time step. The post-collision distribution hence depends only on the conserved quantities and the shear stress from the second moment in all models. Or, putting it another way, except for the moments m_{000}, m_{100}, m_{010}, m_{001}, m_{110}, m_{101}, m_{011}, $m_{200} - m_{020}$, and $m_{200} - m_{002}$, which are the same in all models, all remaining degrees of freedom are set to equilibrium. It should be noted that this choice is not necessarily a good choice with respect to the stability and the accuracy of the methods but it is the only choice that allows for a fair comparison.

For the following test cases we use diffusive scaling meaning that the time step scales proportional to grid spacing square ($\Delta t \propto \Delta x^2 \to 0$) or that Mach number scales proportional to Knudsen number ($Ma \propto Kn \to 0$). The Reynolds number is constant $Re = MaKn^{-1} = \text{const}$. This is the limit in which the LBE converges to the incompressible Navier–Stokes equation. From an engineering point of view this is the most relevant scaling for the LBE. Note that the LBE is only valid for very small Knudsen numbers $Kn \ll 1$ such that $Re \gg Ma$. The reason why it is often admissible to scale the Mach number while it is never admissible to scale the Reynolds number is exactly that the Mach number is always significantly smaller then the Reynolds number. In particular, for the model under consideration, the Mach number is always smaller than one.

5.1. Shear wave test

The first test is meant to assess the accuracy of the transport coefficient (viscosity) and its Galilean invariance for waves along the lattice axes in the different models. We simulate the decay of a shear wave given the following initial conditions in a periodic domain of size $L \times 3\Delta x \times 3/2L$ of the form:

$$u(t=0) = u_0 L_0/L, \tag{97}$$

$$v(t=0) = v_0 L_0/L \sin(2\pi x/L)\cos(4\pi z/(3L)), \tag{98}$$

$$w(t=0) = 0. \tag{99}$$

The analytical solution for this problem is:

$$u(t) = u_0 L_0/L, \tag{100}$$

$$v(t) = v_0 L_0/L \sin(2\pi(x+u_0 t)/L)\cos(4\pi z/(3L)) e^{-\nu t\left(\left(\frac{2\pi}{L}\right)^2+\left(\frac{4\pi}{3L}\right)^2\right)}, \tag{101}$$

$$w(t) = 0. \tag{102}$$

We assess the asymptotic behavior of the viscosity under diffusive scaling by varying L from $32\Delta x$ to $512\Delta x$ with $L_0 = 32\Delta x$, $u_0 = 0.096\Delta x/\Delta t$, and $v_0 = 0.1\Delta x/\Delta t$. The simulation is run for $20000(L/L_0)^2$ time steps and a spatial Fourier transform of $v(t)$ is performed every $1000(L/L_0)^2$ time steps starting after $11000(L/L_0)^2\Delta t$. This long delay before the measurement is used to allow any inconsistency of the initial condition with the asymptotic behavior to die out. To this end only the decay rate of the amplitude at later times is measured without considering the initial amplitude. The decay of

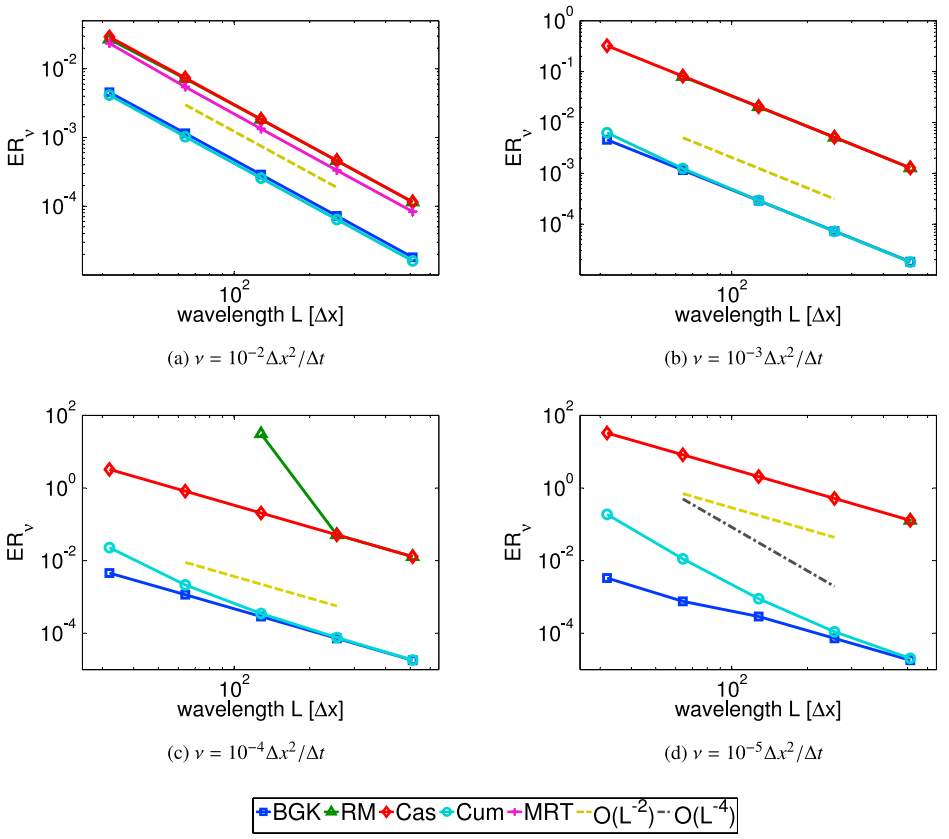

Fig. 1. Normalized error in viscosity measured with two crossing shear waves (Eqs. (97)–(99)) for different nominal viscosities. All models (BGK, RM (raw moments, non-orthogonal MRT), MRT, cascaded, and cumulants) are correct to second order in diffusive scaling, as expected. The non-orthogonal moment methods RM and cascaded LBE have a second order error that is inversely proportional to viscosity. The cumulant method has a fourth order error in diffusive scaling inversely proportional to viscosity. It is only visible if the viscosity is small enough ((c) and (d)). The classical orthogonal MRT method shows poor stability. What is not seen in the figures is that while the error in viscosity is positive in the BGK, RM, cumulant, and cascaded methods, it is negative in the MRT method (i.e. the viscosity is too low). The negative hyper-viscosity, theoretically predicted in Appendix I, is of the same magnitude as the positive hyper-viscosity in the RM and cascaded simulation. It easily dominates the physical viscosity and renders the method unstable once the combination of viscosity and hyper-viscosity becomes negative. Only one simulation in (b) gave a stable result with an error exceeding 300% (point is outside the figure), while all simulations in (c) and (d) failed for the classical MRT method.

the logarithm of the amplitude of the wave is fitted to a linear function to determine the viscosity coefficient. The viscosity was set to:

$$\nu = \frac{1}{3}\left(\frac{1}{\omega_1} - \frac{1}{2}\right)\frac{\Delta x^2}{\Delta t} = 0.01\frac{\Delta x^2}{\Delta t}. \tag{103}$$

We determine the error of the measured viscosity ν_m as $ER_\nu = |\nu_m - \nu|/\nu$, as a function of the resolution L, to assess the asymptotic behavior of the numerical viscosity. In addition we also measure the phase error of the wave. The length of the measurement intervals was chosen such that the wave returned to its original position. The phase ϕ of the wave should hence always be zero for a Galilean invariant method. We fit the phase change to a linear function for each resolution and plot the coefficient of the fit (the phase error) over the resolution L.

As shown in Fig. 1 we observe the following: The amplitude of the viscosity is second order accurate in diffusive scaling for all models. The non-orthogonal raw moment (RM) and the cascaded model suffer from a hyper-viscosity which noticeably increases the absolute magnitude of the error when compared with the BGK and the cumulant LBE. This behavior was predicted from asymptotic analysis in Eqs. (26) and (27) and is further elaborated on in Appendix I. Since the BGK can be obtained from the RM by setting all relaxation rates to be equal to ω_1 it is evident that the RM suffers from the hyper-viscosity due to differences in the relaxation rates. The cumulant LBE does not show this defect even though it uses the same set of relaxation rates as the MR, MRT, and cascaded models. The absence of this error in the cumulant LBE was predicted from asymptotic analysis in Eq. (32). Further explanations are given in Appendix I. The normalized error in the viscosity is independent of viscosity only for the BGK model as seen from the same simulation at different values of viscosity. The cumulant LBE has a higher order error in the viscosity that vanishes under grid refinement. In contrast the error in viscosity is inversely proportional to the value of viscosity in the RM and cascaded model. In the low viscosity regime ($\nu = 10^{-5}\Delta x^2/\Delta t$)

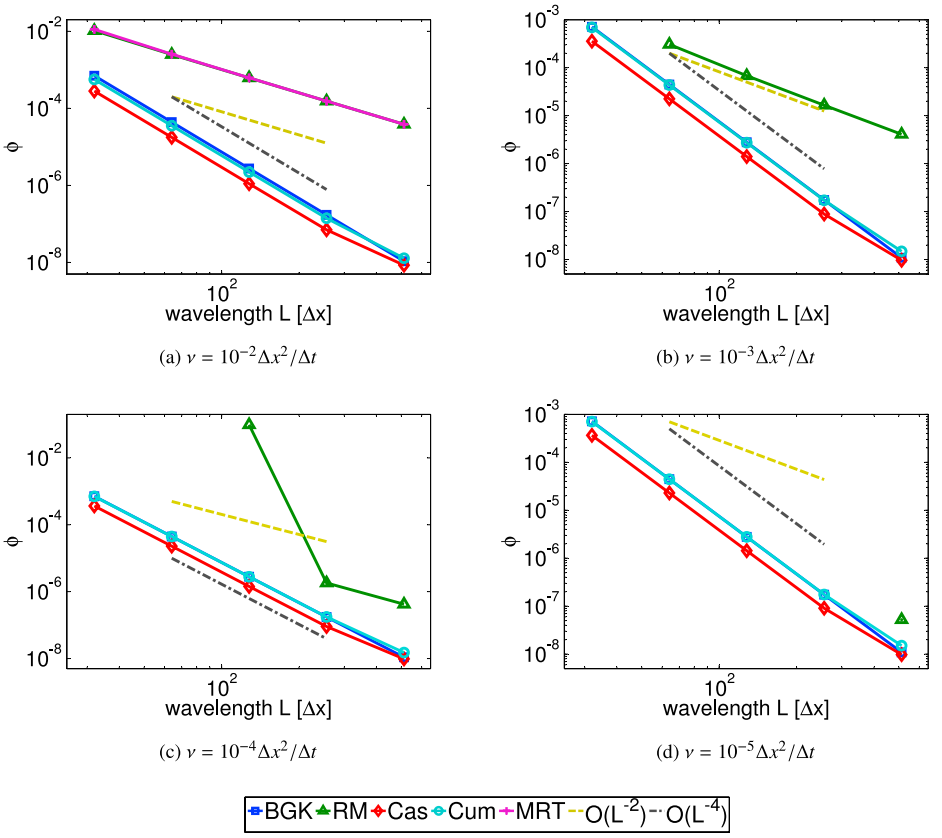

Fig. 2. The cumulative error in phase due to lack of Galilean invariance measured from the same simulations as in Fig. 1. BGK, cascaded, and cumulant models have fourth order errors in diffusive scaling. These errors are independent of viscosity. The RM and MRT models have errors of second order. These errors seem to decrease with viscosity. However, due to the instability of the RM and MRT it is never observed that the errors in RM and MRT are smaller than those in the other models.

at short wave length ($32\Delta x$) the error exceeds 1000% which is clearly unacceptable. Another interesting aspect is that the classical orthogonal MRT model is the most inferior of the models in terms of stability for the given configuration of relaxation rates. It is so unstable that we obtain reliable results only for $\nu = 10^{-2}\Delta x^2/\Delta t$. In the analysis of Appendix I it is shown that the orthogonalization changes the sign of the hyper-viscosity present in the moment methods. While the error is of dissipative nature in the non-orthogonal methods RM and cascaded LBE, it becomes amplifying for the orthogonal MRT model. This unfortunate behavior of the MRT method is a direct consequence of the orthogonalization which, on the other hand, offers no perceivable benefit. Since the hyper-viscosity in the non-orthogonal raw moment method is dissipative in nature the reason for the poor stability of the RM method must be due to its violation of Galilean invariance.

In the considered parameter range the classical MRT method is only stable for $\nu = 10^{-2}\Delta x^2/\Delta t$ and for a single exception at $L = 64\Delta x$ at viscosity $\nu = 10^{-3}\Delta x^2/\Delta t$. The non-orthogonal RM methods is unstable at wave lengths $L \leq 32\Delta x$ for $\nu = 10^{-3}\Delta x^2/\Delta t$, $L \leq 128\Delta x$ for $\nu = 10^{-4}\Delta x^2/\Delta t$, and at $L \leq 256\Delta x$ for $\nu = 10^{-5}\Delta x^2/\Delta t$. All other models including BGK remain stable in the entire parameter space considered. For the phase the asymptotic behavior is different (Fig. 2). Here the cumulant LBE has fourth order accuracy just like the cascaded LBE and the BGK. The RM and MRT models have an inferior phase behavior compared to the other models. The phase error decays only with second order in L for RM and MRT. This defect of the RM (and equivalently for the MRT) is evident from asymptotic analysis in Eq. (22). The absence of this error in the cascaded and cumulant LBE and consequently in the BGK was predicted with asymptotic analysis by Eq. (25). The phase error is not sensitive to viscosity for BGK, cumulants, and the cascaded method. In the case of RM and MRT the error in phase is significantly smaller for lower viscosities but the error remains strictly larger than for the other models.

The analysis in Appendix I implies that the hyper-viscosity in the RM, MRT, and the cascaded model can be canceled by the appropriate choice of the relaxation rates. In particular we can eliminate the errors by coupling all odd and all even relaxation rates. For the RM, cascaded, and cumulant models this means $\omega_1 = \omega_2 = \omega_6 = \omega_7 = \omega_8 = \omega_{10}$ (even moments) and $\omega_3 = \omega_4 = \omega_5 = \omega_9$ (odd moments). For the classical MRT method of Appendix B it means $s_4 = \cdots = s_9 = s_{16} = \cdots = s_{22}$ (even moments) and $s_{10} = \cdots = s_{15} = s_{23} = \cdots = s_{26}$ (odd moments). There are hence only two remaining relaxation parameters and we call this configuration Two Relaxation Times (TRT) [29,37]. One relaxation rate is for the even moments and is defined by viscosity (ω_1) and the other one is for the odd moments and is a free parameter. In the following test we

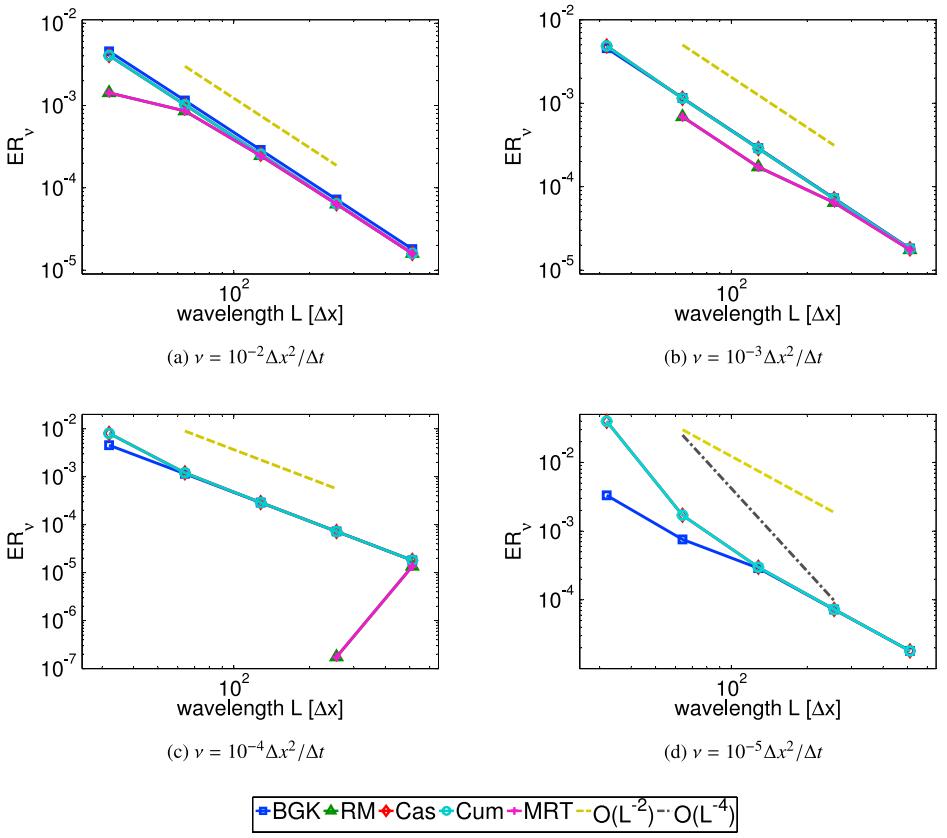

(a) $\nu = 10^{-2}\Delta x^2/\Delta t$ (b) $\nu = 10^{-3}\Delta x^2/\Delta t$

(c) $\nu = 10^{-4}\Delta x^2/\Delta t$ (d) $\nu = 10^{-5}\Delta x^2/\Delta t$

Fig. 3. The same setup as in Fig. 1 with the relaxation rates set to TRT values. The rate for odd moments is one and the rate for even moments is taken from the viscosity. Since orthogonalization has no effect between odd and even moments the RM and MRT kernels give both identical results. The hyper-viscosity has been eliminated but the stability has been reduced for the RM method compared to Fig. 1. The stability is better than for the MRT method in Fig. 1. No results for RM/MRT were obtained at $\nu = 10^{-5}\Delta x^2/\Delta t$. With the TRT parameters cumulants and central moments give the same results in this case. Both methods improve compared to Fig. 1. The improvement of the cumulant method is the least significant as it was already very good in Fig. 1.

set the relaxation rate for the odd moments to unity. This is not necessarily a good choice, but optimizing this parameter is not our goal here. The results are presented in Figs. 3 and 4. The first observation is that the non-orthogonal RM and the orthogonal MRT method give identical results. This is expected since orthogonalization between odd and even moments plays no role (odd and even moments are always orthogonal to each other). The second observation is that, in accordance with the analysis of Appendix I, the hyper-viscosity has been eliminated from the RM, MRT, and cascaded models. However, the MRT/RM method is even slightly less stable than the RM method without TRT parameters (albeit it is considerably more stable than the MRT method without TRT parameters). Cascaded and cumulant models are again stable in the complete parameter range and behave identically. We should note that while the RM and MRT methods are algebraically identical for TRT parameters, the cascaded and cumulant models are only identical in their results for these experiments. They are not algebraically equivalent. The accuracy of the cumulant model benefits from the TRT parameters albeit not to the same extend as the cascaded model. Fig. 4 confirms that the TRT parameters are ineffective with regard to the phase error.

We hence see that, expect for the cumulant model, all moment models have a strong dependence on the relaxation rates of their non-hydrodynamic or ghost moments. The cumulant method can benefit from an optimization of these rates at higher asymptotic order but its errors are largely independent of the relaxation rates of ghost moments and are systematically smaller than the errors in the other methods using multiple relaxation rates.

5.2. Taylor Green vortex test

In the previous example the velocity was always perpendicular to the wave vector and the wave vector was aligned with the lattice directions. In the next example we consider a two dimensional Taylor Green vortex [38] with non-unity aspect ratio. The initial conditions are defined as:

$$u(t=0) = u_0 L_0/L + U L_0/L \sin(2\pi x/L)\cos(4\pi z/(3L)), \tag{104}$$

$$v(t=0) = 0, \tag{105}$$

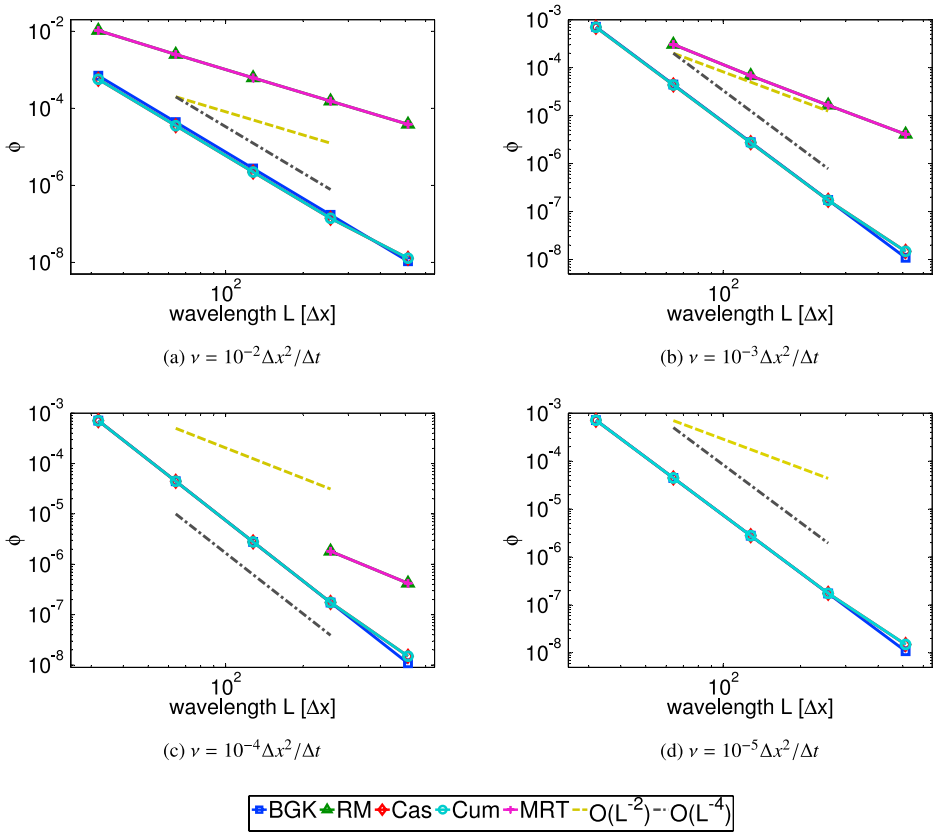

Fig. 4. The same setup as in Fig. 2 with TRT relaxation parameters. The TRT parameters have no influence on the phase error and all methods behave in the same way as in Fig. 2. The only difference is in the stability of the RM/MRT methods.

$$w(t=0) = -3U/2L_0/L\cos(2\pi x/L)\sin(4\pi z/(3L)), \tag{106}$$

$$\rho(t=0) = \rho_0\left(1 + \frac{3U^2L_0^2}{2L^2\Delta x^2/\Delta t^2}(\cos(4\pi x/L) + \cos(8\pi z/(3L)))\right). \tag{107}$$

Here again $L_0 = 32\Delta x$ and $u_0 = 0.096\Delta x/\Delta t$. The amplitude of the wave is $U = 0.001\Delta x/\Delta t$. The grid L is varied from $32\Delta x$ to $512\Delta x$ for different viscosities. As in the previous example we measure the exponential decay of the amplitude every $1000(L/L_0)^2$ time steps from time step $11000(L/L_0)^2$ through time step $20000(L/L_0)^2$ and fit the logarithm of the result to a linear function to recover the actual viscosity. The error in viscosity and phase are recovered in the same way as in the previous example. Since we consider vortices in the current example we also have velocity components that are not aligned with the lattice and errors in isotropy are probed. In diffusive scaling all models are second order accurate as expected. We can distinguish between two different error modes in the magnitude of the viscosity (see Fig. 5). There appears to be an error of second order which is independent of viscosity and an error of fourth order that is proportional to ν^{-1}. In the case of $\nu = 10^{-2}\Delta x^2/\Delta t$ only the second order error is seen. In this case all models have similar accuracy. For viscosities $\nu = 10^{-3}\Delta x^2/\Delta t$ and $\nu = 10^{-4}\Delta x^2/\Delta t$ we observe a transition between the dominance of the second order and the fourth order errors. Finally, in the $\nu = 10^{-5}\Delta x^2/\Delta t$ case only the fourth order error is visible but it is to be expected that the second order error would take the lead at higher resolutions. Note in particular that while the error for low resolutions increases with decreasing viscosity the error for $L = 512\Delta x$ is the same until we reach the lowest viscosity under consideration. While the second order viscosity independent error appears to be the same for all models we observe that the fourth order error in the cumulant and BGK method are one order of magnitude smaller than in the cascaded model. The raw moment methods are again unstable. Orthogonalization reduces the poor stability further and no results are obtained for viscosities $\nu < 10^{-4}\Delta x^2/\Delta t$. In the high viscosity regime the error of the RM behaves similar to the error of the cascaded method. The error in the MRT method is essentially non-convergent for $\nu \leq 10^{-3}\Delta x^2/\Delta t$.

The phase error for the Taylor Green vortex (Fig. 6) is very different from the phase error in the shear wave example (Fig. 2). In fact, all models at all viscosities show the same second order error in diffusive scaling. Since in the current example $u\partial_x u$ is non-zero we have additional violations of Galilean invariance that originate from the third term in Eq. (H.12) as explained in Appendix H. This term cannot be canceled without introducing more speeds to the lattice or additional finite differences. This is in essence a defect of the 27 speed velocity set and it is independent of the collision model. In order

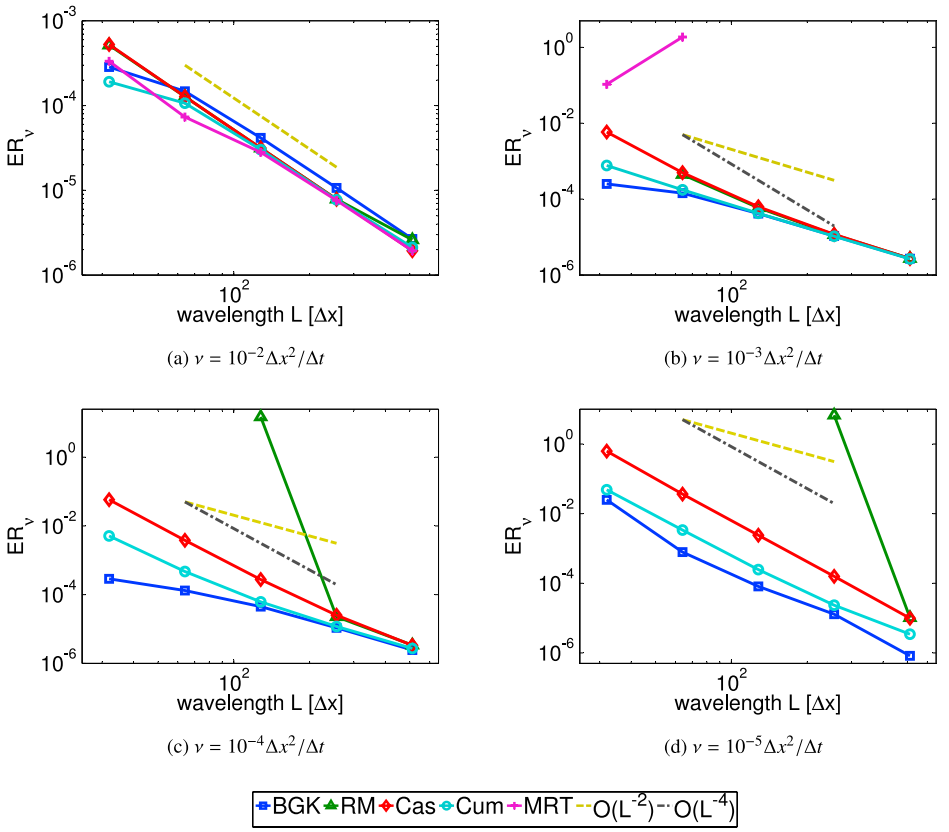

(a) $\nu = 10^{-2}\Delta x^2/\Delta t$ (b) $\nu = 10^{-3}\Delta x^2/\Delta t$

(c) $\nu = 10^{-4}\Delta x^2/\Delta t$ (d) $\nu = 10^{-5}\Delta x^2/\Delta t$

Fig. 5. Error in viscosity measured with the decay of a Taylor Green vortex (Eqs. (104)–(107)) for different viscosities. This measurement is more sensitive to isotropy errors than the one depicted in Fig. 1. However, it is less sensitive to the error analyzed in Eqs. (26) and (27). We again observe second order errors in diffusive scaling that are independent of viscosity and fourth order errors in diffusive scaling that increase with decreasing viscosity. In this measurement the different models stay closer together than in previous example. However, for low viscosities the error in the cumulant model is almost one order of magnitude smaller than the error in the cascaded model. The BGK model shows surprisingly good results in particular with respect to stability. BGK is stable and accurate in the entire measurement domain while RM breaks down already at $\nu = 10^{-3}\Delta x^2/\Delta t$ and $L = 32\Delta x$. The classical MRT method does not even converge for $\nu = 10^3\Delta x^2/\Delta t$.

to verify that at least the amplitude error could be corrected by the method described in Appendix H we run the Taylor Green simulations again with the correction turned off. That is we set $D_x u = D_y v = D_z w = 0$ in Eqs. (61)–(63). We obtain inferior results for the viscosity as compared to the case with correction, as expected (Fig. 7). The RM model is unstable for $\nu = 10^{-3}\Delta x^2/\Delta t$ and $L = 32\Delta x$. It survives for $\nu = 10^{-4}\Delta x^2/\Delta t$ until $L = 128\Delta x$. The classical MRT method is again observed to be unstable and reliable results are only obtained for $\nu = 10^{-2}\Delta x^2/\Delta t$. The phase error is in all cases independent of the correction and second order in diffusive scaling (Fig. 8).

The results of the phase error encourage us to investigate the same problem in a different scaling. We now scale only the Mach number at fixed Reynolds number and fixed grid spacing:

$$u(t=0) = u_0 U/U_0 + U^2/U_0 \sin(2\pi x/L)\cos(4\pi z/(3L)), \tag{108}$$

$$v(t=0) = 0, \tag{109}$$

$$w(t=0) = -3U^2/(2U_0)\cos(2\pi x/L)\sin(4\pi z/(3L)), \tag{110}$$

$$\rho(t=0) = \rho_0\left(1 + \frac{3U^4}{2U_0^2\Delta x^2/\Delta t^2}(\cos(4\pi x/L) + \cos(8\pi z/(3L)))\right). \tag{111}$$

With $U_0 = 0.001\Delta x/\Delta t$. The simulations were run for $20000U_0/U\Delta t$ and measurement started from $11000U_0/U\Delta t$. The other parameters have been chosen as before. In order to keep the Reynolds number fixed we have to scale the viscosity proportional to the Mach number. The observation is that the phase error is completely independent from the Mach number (see Fig. 9). This is in so far surprising as the existence of the phase lack can only be explained by the motion of the wave. For a wave at rest no phase shift could occur. This is clearly a violation of Galilean invariance. The reason why this error is independent of the Mach number and second order in Knudsen number is explained in Appendix H. The fact the Galilean correction leaves an error in Galilean invariance that is independent from the Mach number (i.e. an error that cannot be

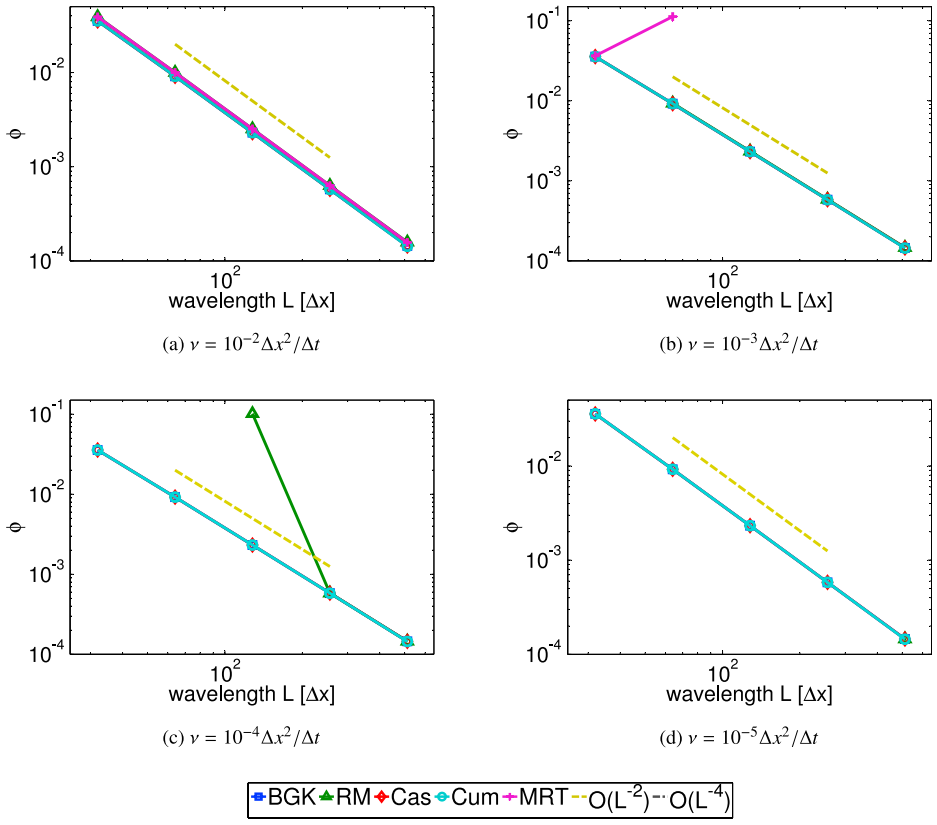

Fig. 6. The phase error from the Taylor Green vortex simulations shown in Fig. 5. Except of a single runaway value in the RM model and one in the MRT model, were they are close to instability, all models show the same second order error that is independent of viscosity.

reduced by lowering the Mach number) is disappointing. In order to remove this error a lattice with more velocities has to be used.

6. Flow around a sphere

The problems considered in the previous section were all linear and only of academic interest. In this section we consider a more serious benchmark example, the flow around a sphere at different Reynolds numbers. The simulation uses 5 different grid levels connected by compact second order interpolation and nested time stepping [39,40]. The grid is depicted in Fig. 10. The boundary conditions used for this simulation are interpolated bounce back (zero velocity) boundary conditions at the surface of the sphere (see Appendix E), constant velocity at front, both sides, top, and bottom and non-reflective extrapolation outflow at the outlet (see Appendix F). The grids are enumerated from the coarsest to the finest from 0 to 4. Grid 0 contains 5 567 553 nodes, grid 1 429 726 nodes, grid 2 1 340 822 nodes, grid 3 16 296 729 nodes, and grid 4 4 015 545 nodes, respectively. The total number of 27 650 375 nodes in single precision were close to the maximum number of nodes that fitted into the 6 GB of one Nvidia Tesla K20X GPU (the connectivity of the unstructured mesh, logistic data for the interpolation between grids, macroscopic quantities for post-processing, and boundary data also had to be stored in the memory of the GPU). Both the cumulant LBE and the BGK operated at about 180 million lattice node updates per second including the interpolation between grids, the application of boundary conditions, and the computation of the drag force. Further details on the code and its performance will be published elsewhere. The lattice Boltzmann velocity at the inlet and at the side walls was kept at $u_0 = 0.07\Delta x/\Delta t$ for all simulations. The sphere had a diameter of $d = 16\Delta x_0$ (on the coarsest grid) or $d = 256\Delta x_4$ on the finest grid level. The Reynolds number was varied solely by adjusting the lattice Boltzmann viscosity via ω_1. All other relaxation rates were kept at unity to have a comparable setup to the one used in the last section. We reiterate here that this is not necessarily a good choice concerning accuracy and stability. The nested time stepping uses acoustic scaling between the grid levels such that $\Delta x_0 = 2\Delta x_1 = 4\Delta x_2 = 8\Delta x_3 = 16\Delta x_4$ and $\Delta t_0 = 2\Delta t_1 = 4\Delta t_2 = 8\Delta t_3 = 16\Delta t_4$. The viscosity was adjusted accordingly for each level to be $\nu = u_0 d/Re$. The drag coefficient of the sphere is defined as:

$$c_D = \frac{8F_D}{\rho u_0^2 \pi d^2}. \tag{112}$$

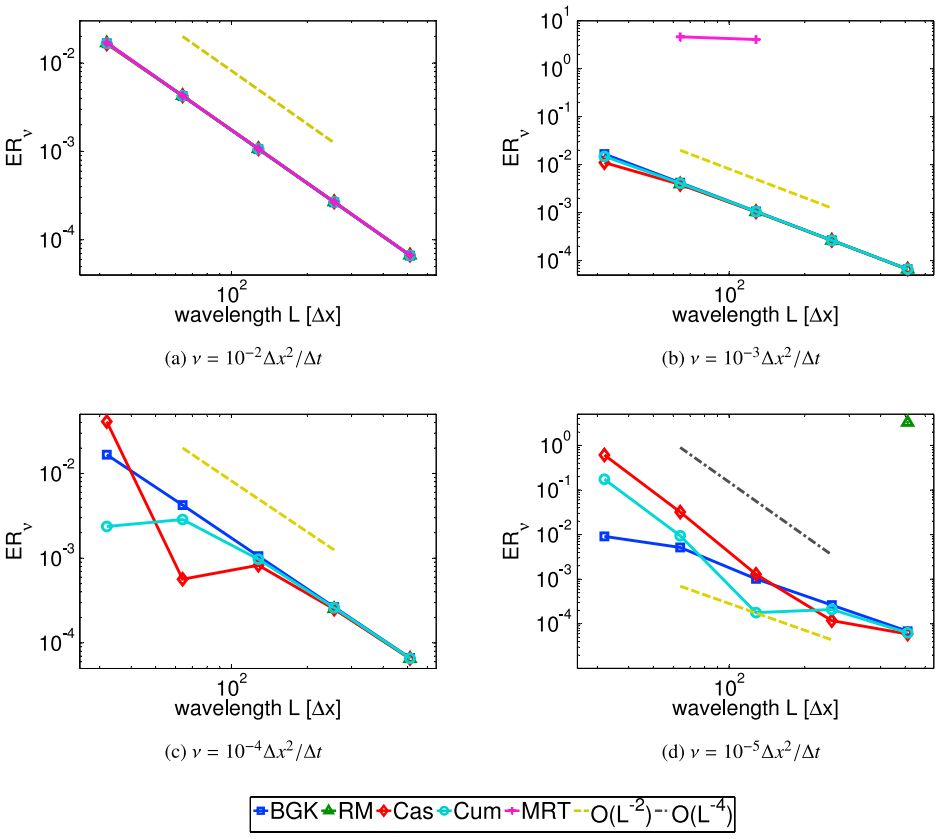

Fig. 7. To demonstrate the importance of the Galilean correction the Taylor Green vortex simulation from Fig. 5 is repeated with the Galilean correction being turned off in all models. In the high viscosity range (a) the errors are several orders of magnitude larger than in the case with correction. The classical MRT model is again the most unstable. Reliable results are only obtained for $\nu = 10^{-2}\Delta x^2/\Delta t$.

Table 1
Drag coefficient c_D of a sphere for Reynolds number 1000 computed with three different resolutions. The viscosity was adjusted to keep the Reynolds number constant. The reference data from Appendix K predicts a drag coefficient in the range $\{0.451349 \cdots 0.533949\}$. All results obtained with the cumulant method fall into this range. For the BGK method only the result for a sphere diameter of $128\Delta x_4$ is in that range.

Diameter	Cumulant	BGK
$64\Delta x_4$	0.476630543	Unstable
$128\Delta x_4$	0.503109089	0.531094037
$256\Delta x_4$	0.516351500	0.580771327

The force acting on the sphere was measured by the momentum exchange method [41,42].

The dependence of the drag coefficient on the grid resolution was investigated by comparing to results from two coarser grids with the same grid levels as the base grid shown in Fig. 10 but the sphere being resolved with $64\Delta x_4$ and $128\Delta x_4$, respectively. This test was done for a Reynolds number of $Re = 1000$. The results are summarized in Table 1 for the cumulant and the BGK method.

The drag coefficient was studied in the range of Reynolds numbers 200 to 10^5 using the improved BGK and the cumulant method. For the BGK model no stable solutions were found for $Re > 8000$. No stability limit for the cumulant method was detected but simulations were stopped at $Re = 10^5$ because above this the viscosity on the finest level would drop below $\nu = 0.0001792\Delta x_4^2/\Delta t_4$. At this resolution the flow in the shear layer on the surface of the sphere is already considerably under-resolved. Since no turbulence model and no wall model was applied in this study we cannot trust simulations at higher Reynolds number unless we use a finer grid which was not feasible within the present hardware constraints.

The drag coefficients were obtained by averaging the flow over the time window $25000\Delta t_0$ to $30000\Delta t_0$. The obtained values are compared in Fig. 11 to the values obtained by Stiebler et al. [43] using MRT-LES simulations and to five different regression equations obtained from experimental data by various authors (see Appendix K for details). A similar study using almost the same resolution was recently presented by Eitel-Amor et al. [44]. Note that the Smagorinsky model was used

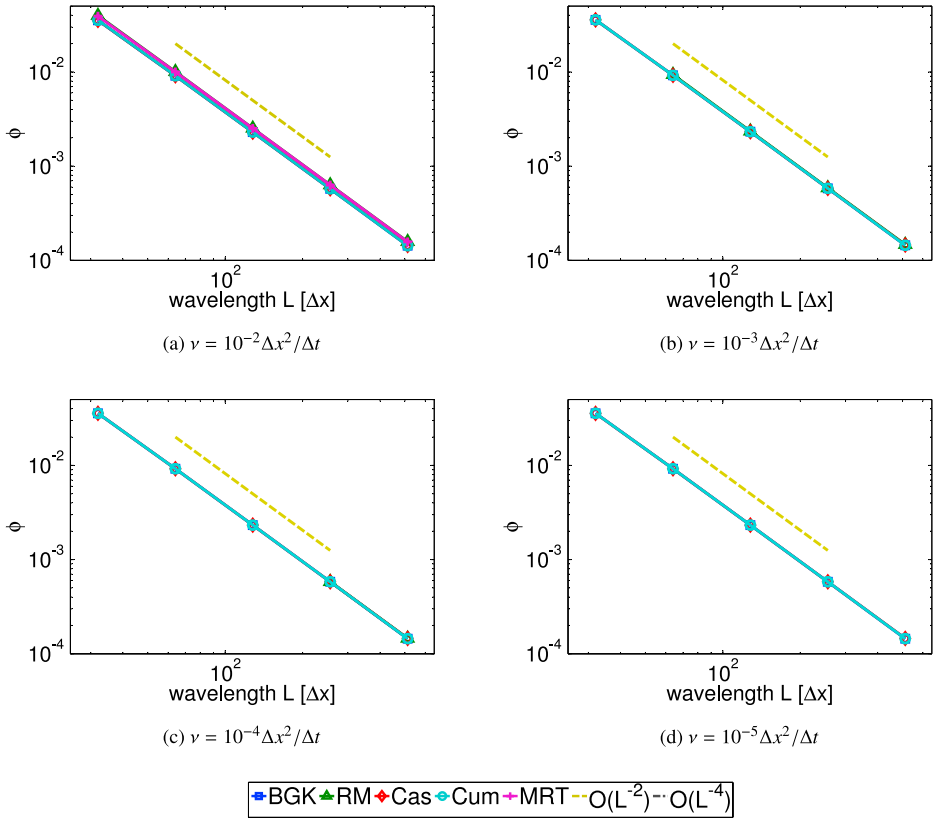

Fig. 8. The phase error in the Taylor Green example without Galilean correction. All plots here are almost identical to those depicted in Fig. 6. The Galilean correction is seen to have no effect on the phase error.

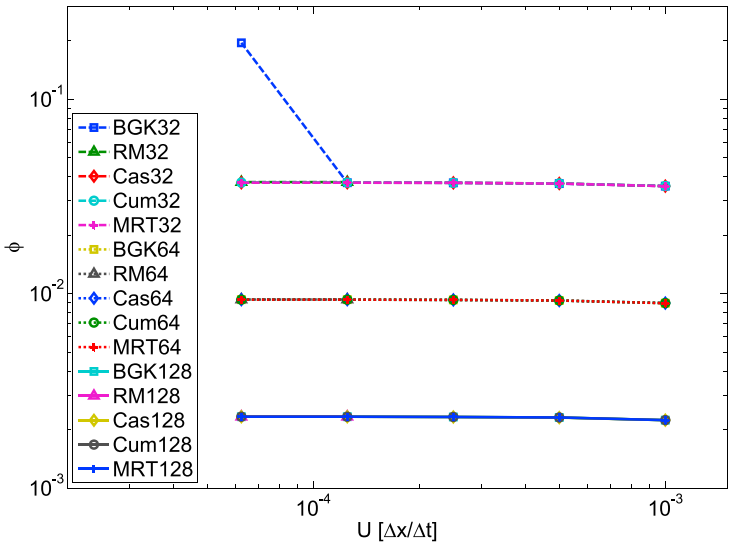

Fig. 9. The phase error in the Taylor Green example with Galilean correction measured against the Mach number at constant Reynolds number at three different resolutions ($L = 32\Delta x$, $L = 64\Delta x$ and $L = 128\Delta x$). The number of time steps were increased proportional to U^{-1} in order to simulate for the same physical time in each case. The results are seen to be independent of Mach number and the model.

in [43,44] while the current study applies no modifications to the collision operator other than setting the appropriate viscosity by ω_1.

To understand why the BGK model appears to be less stable than the cumulant method we look at the velocity fields (see Fig. 12). The apparent superior accuracy of the BGK model observed in the last section was only related to the value of

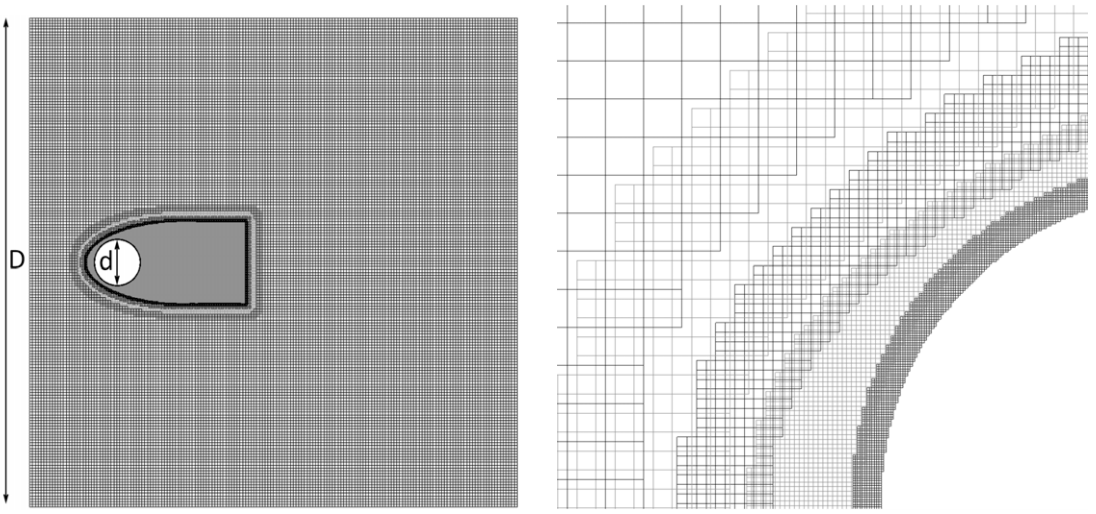

(a) Overview. (b) Detail.

Fig. 10. Cut through the grid used in the simulation of the sphere. The left picture shows the complete setup and the right a zoom into the better resolved regions. Overlap regions for interpolation between the five different grids are visible. The blockage ratio of the grid is $\lambda = d/D = 1/11$.

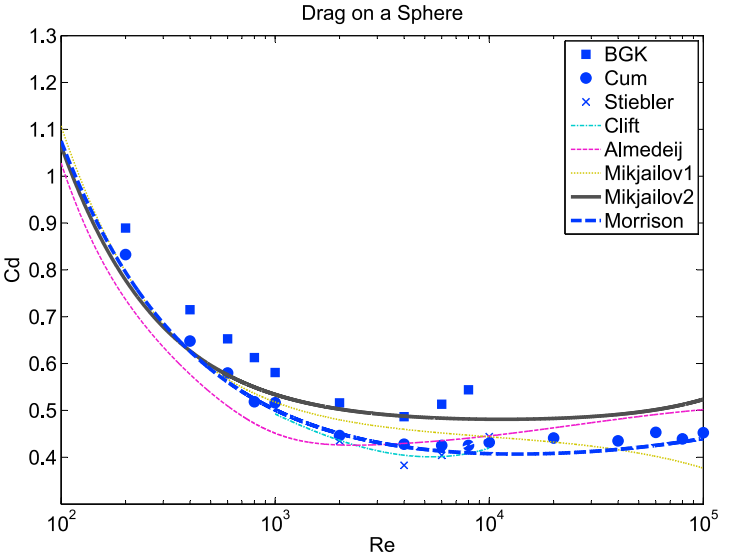

Fig. 11. Comparison of our results to the one by Stiebler (only Reynolds number 2000–10 000) and to regressions to experimental data by different authors. The definitions are given in Appendix K. Clift in Eq. (K.1), Almedeij in Eq. (K.8), Mikhailov 1 and 2 in Eqs. (K.2) and (K.3), and Morrison in Eq. (K.9). A correction for finite blockage ratio (Eq. (K.10)) was applied to all curves.

the viscosity in very simple academic test cases. In this more serious benchmark the BGK model is seen to develop spurious waves if the Reynolds number is too large. These waves increase in magnitude with Reynolds number and deteriorate the solution even before the onset of instabilities. We conjecture that the usage of a Smagorinsky model, as done for the same test case in [44], would have eliminated these spurious oscillations in the BGK solution at higher Reynolds numbers. However, in our opinion, using a turbulence model to cancel numerical artifacts in order to stabilize an otherwise unstable model is incompatible with the physical interpretation or justification for the usage of such a model.

In order to have a detailed look at the flow we follow Hunt et al. [45] and detect vortices with the Q criterion where $Q > 0$ with Q being defined as:

$$Q = \frac{1}{2}(\nabla \times \vec{u}) \cdot (\nabla \times \vec{u}) - \frac{1}{4}\left(\frac{\partial u_i}{\partial x_j} + \frac{\partial u_j}{\partial x_i}\right)^2, \tag{113}$$

with $\vec{u} = \{u_1, u_2, u_3\} = \{u, v, w\}$ and $\{x_1, x_2, x_3\} = \{x, y, z\}$. Summation over i and j is implied. Contours of the Q criterion for different Reynolds numbers are shown in Fig. 13. For Reynolds number 200 we observe a single stationary vortex ring

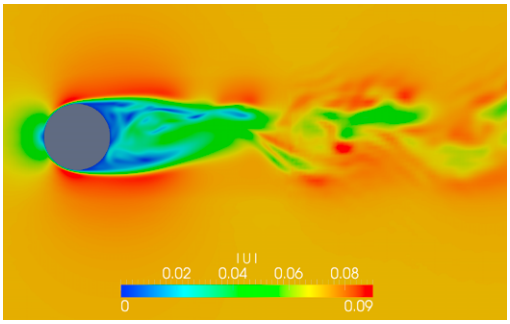

(a) BGK, $Re = 1000$.

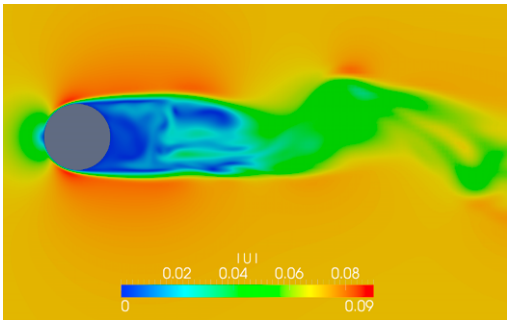

(b) Cumulant, $Re = 1000$.

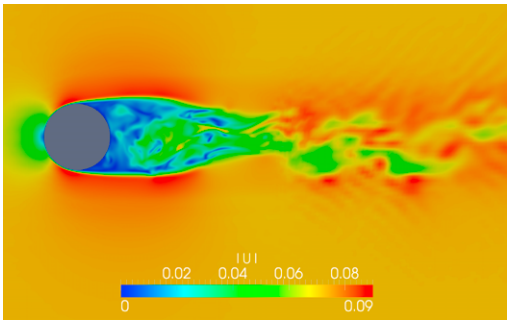

(c) BGK, $Re = 2000$.

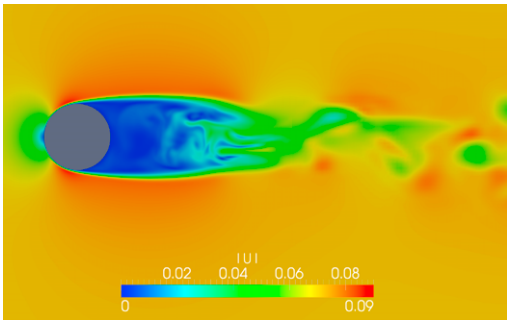

(d) Cumulant, $Re = 2000$.

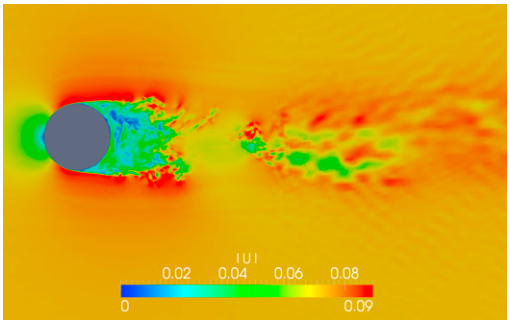

(e) BGK, $Re = 8000$.

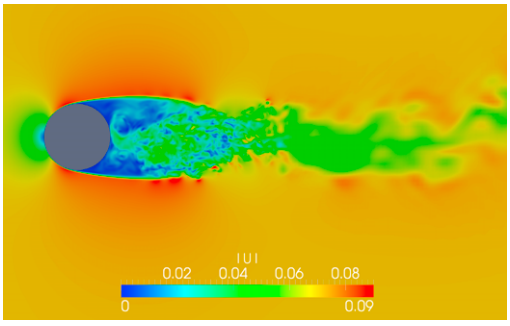

(f) Cumulant, $Re = 8000$.

Fig. 12. Instantaneous velocity magnitudes in the center plane around the sphere in units $\Delta x_0/\Delta t_0$. The solution of the improved BGK model is compared to the solution of the cumulant model. At $Re = 2000$ spurious velocity waves are visible in the BGK simulation. They increase with Re. Above $Re = 8000$ no stable result was obtained from the BGK method. The cumulant method is free from such artifacts.

in the wake of the sphere. At Reynolds number 400 vortex shedding has started and the vortex ring has broken up. With further increasing the Reynolds number the vortices decrease in size and the toroidal structure of the vortices, still visible at Reynolds number 4000, disappears.

7. Conclusions

We proposed to relax cumulants instead of moments in the LBE with multiple relaxation rates. This proposition is supported in this paper in three different ways.

1. *A priori*: Cumulants are statistically independent and Galilean invariant variables. They share the property of Galilean invariance with central moments (used in the cascaded LBE). Raw moments, orthogonal and non-orthogonal, are not Galilean invariant. Both raw and central moments are not statistically independent. Orthogonalization of the base moments, as commonly done in the MRT method, has no effect on the statistical independence of the degrees of freedom. It is hence *a priori* implausible that different moments could relax with independent rates.
2. *Analytically*: Asymptotic analysis shows that the usage of cumulants instead of moments eliminates errors in Galilean invariance and hyper-viscosity.

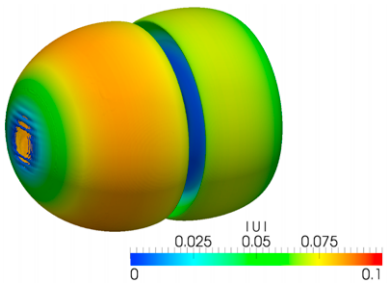

(a) $Re = 200$.

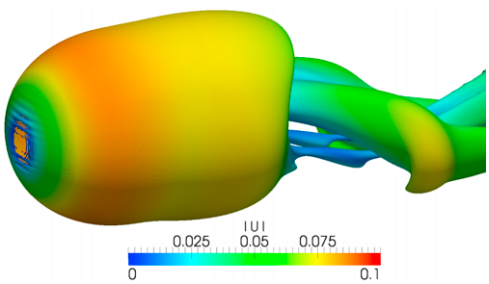

(b) $Re = 400$.

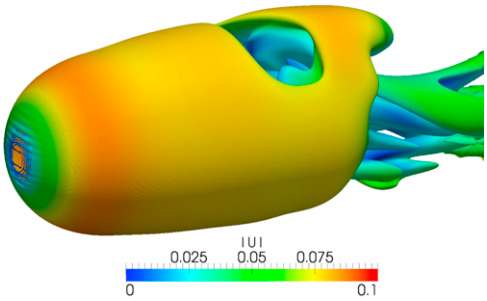

(c) $Re = 1000$.

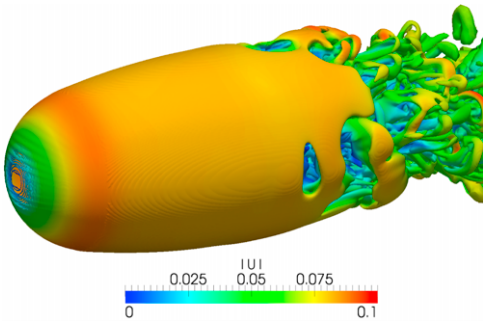

(d) $Re = 4000$.

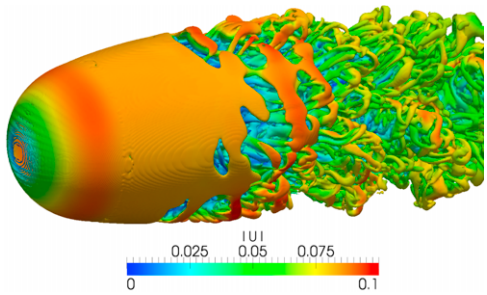

(e) $Re = 10\,000$.

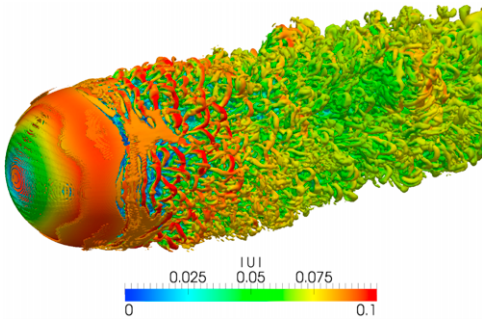

(f) $Re = 100\,000$.

Fig. 13. Contour plots on the Q criterion at time $30000\Delta t_0$ computed with the cumulant LBE. The contour was set at $Q = 10^{-5}\Delta t_0^{-2}$. The color shows the magnitude of the velocity in units $\Delta x_0/\Delta t_0$. All plots were obtained with the same setup. Only ω_1 was varied to change the viscosity. The surface of the sphere was not included in the finite difference stencil for the computation of Q which is why the contour is broken directly on the sphere. (For interpretation of the references to color in this figure legend, the reader is referred to the web version of this article.)

3. *Numerically*: Numerical tests validate the predictions of the asymptotic analysis. The cumulant method is found to be systematically more accurate than the moment methods. It is also found to be more stable than the raw moment method and the classical MRT and at least as stable as the central moment method (cascaded method).

The cumulant LBE combines the two main advantages of the most established lattice Boltzmann models, the BGK model and the MRT model. The advantage of the BGK model is its ease of use since no parameters have to be chosen. Somewhat contradictory to this, the MRT model is often argued to be superior due to the many parameters that can be chosen in order to optimize the model for specific tasks. We have seen in this paper that MRT deteriorates if the rates are not optimally chosen. Arguable, most practitioners searching for appropriate numerical methods to solve engineering problems will not agree that a large number of undetermined free parameters with strong effects on accuracy and stability is an advantage of the method. The cumulant method suits both positions. Unlike the MRT method, the cumulant method does not deteriorate for the simple choice of setting all relaxation rates save ω_1 to unity. It can be used with the same ease, similar accuracy and superior stability as the BGK method. On the other hand it offers the same number of free relaxation rates as the MRT method and can be optimized accordingly. In contrast to the MRT model the relaxation rates of the cumulant method are really free in the sense that they are not already determined by requirements to delete Galilean invariance errors or to eliminating hyper-viscosity. In this paper we deliberately abstained from parameter optimization and demonstrated that the cumulant method produced reliable and stable results for the flow around a sphere across three orders of magnitude

in Reynolds number by only changing viscosity and nothing else. In particular we did not apply any sub-grid-scale models, entropic functionals, or any other kind of limiters. Compared to all other tested models the cumulant LBE offers the widest range of Reynolds numbers, adjusted by a single parameter, in which accurate and stable results can be obtained.

Acknowledgments

The funding of the Coordinated Research Center SFB 880 (Fundamentals of High-Lift for Future Commercial Aircraft) TP A5, the Research Training Group FOR 1083 (MUSIS) grand number KR 1747/13-2, and the Research Training Group 856 (mikroPart) grand number GE 1990/3-1 all by the German Research Foundation (DFG) is gratefully acknowledged. We thank Professor François Dubois for publishing the orthogonal transformation matrix for the D3Q27 MRT model upon our request. Ehsan Goraki Fard helped with his detailed comments to improve the manuscript. Part of the work on the Galilean correction was done on the Isaac Newton Institute in the context of the program Partial Differential Equations in Kinetic Theories. In this context we also acknowledge useful discussions with Dr. Paul John Dellar. Professor Pierre Lallemand helped to detect a mistake in the formulation of the Galilean correction. To our regret, following our discussion, Dr. Dellar preferred that we seek independent publications as his approach to put the correction into the relaxation rates is not self-evidently equivalent to our original suggestion to put the correction into the equilibrium function.

Appendix A. Improved BGK model

The lattice BGK model is usually implemented directly in distribution space. The post-collision distribution is computed from:

$$f^{*}_{ijk} = f_{ijk}(1-\omega_1) + \omega_1 f^{eq}_{ijk}. \tag{A.1}$$

The only difference to the standard BGK model on the D3Q27 lattice is in the definition of the equilibrium which is conveniently stated in product form:

$$\begin{aligned} f^{eq}_{ijk} = {} & \frac{-\rho(-1)^{|i|+|j|+|k|}}{(|i|+1)(|j|+1)(|k|+1)}(|i|-1+\theta+iu+u^2+G_x) \\ & \times (|j|-1+\theta+jv+v^2+G_y)(|k|-1+\theta+kw+w^2+G_z). \end{aligned} \tag{A.2}$$

The equilibrium and all other quantities are given here in dimensionless form for direct implementation. The square of the speed of sound is $\theta = 1/3$. The indices i, j, and k vary in the range $\{-1, 0, 1\}$. The equilibrium depends on the density ρ and the velocities u, v, and w given by:

$$\rho = \sum_{i=-1}^{1}\sum_{j=-1}^{1}\sum_{k=-1}^{1} f_{ijk} \tag{A.3}$$

$$u = \rho^{-1}\sum_{i=-1}^{1}\sum_{j=-1}^{1}\sum_{k=-1}^{1} i f_{ijk} \tag{A.4}$$

$$v = \rho^{-1}\sum_{i=-1}^{1}\sum_{j=-1}^{1}\sum_{k=-1}^{1} j f_{ijk} \tag{A.5}$$

$$w = \rho^{-1}\sum_{i=-1}^{1}\sum_{j=-1}^{1}\sum_{k=-1}^{1} k f_{ijk}. \tag{A.6}$$

The Galilean correction terms G_x, G_y, and G_z are computed in a similar way to Eqs. (58)–(60) by first computing the velocity gradients from the second moments:

$$m_{200} = \sum_{i=-1}^{1}\sum_{j=-1}^{1}\sum_{k=-1}^{1} i^2 f_{ijk} \tag{A.7}$$

$$m_{020} = \sum_{i=-1}^{1}\sum_{j=-1}^{1}\sum_{k=-1}^{1} j^2 f_{ijk} \tag{A.8}$$

$$m_{002} = \sum_{i=-1}^{1}\sum_{j=-1}^{1}\sum_{k=-1}^{1} k^2 f_{ijk} \tag{A.9}$$

$$D_x u = -\frac{\omega_1}{2}(3m_{200}/\rho - 1 - 3u^2) \tag{A.10}$$

$$D_y v = -\frac{\omega_1}{2}(3m_{020}/\rho - 1 - 3v^2) \tag{A.11}$$

$$D_z w = -\frac{\omega_1}{2}(3m_{002}/\rho - 1 - 3w^2) \tag{A.12}$$

$$G_x = -3u^2 D_x u\left(\frac{1}{\omega_1} - \frac{1}{2}\right) \tag{A.13}$$

$$G_y = -3v^2 D_y v\left(\frac{1}{\omega_1} - \frac{1}{2}\right) \tag{A.14}$$

$$G_z = -3w^2 D_y w\left(\frac{1}{\omega_1} - \frac{1}{2}\right). \tag{A.15}$$

An efficient implementation of the improved BGK model is obtained by pre-computing the common sub-expressions. We define:

$$X_i = \frac{(-1)^{|i|}}{|i|+1}(|i| - 1 + \theta + iu + u^2 + G_x) \tag{A.16}$$

$$Y_j = \frac{(-1)^{|j|}}{|j|+1}(|j| - 1 + \theta + jv + v^2 + G_y) \tag{A.17}$$

$$Z_k = \frac{(-1)^{|k|}}{|k|+1}(|k| - 1 + \theta + kw + w^2 + G_z). \tag{A.18}$$

This can be further simplified to:

$$X_0 = \theta - 1 + u^2 + G_x \tag{A.19}$$

$$X_1 = -\frac{X_0 + 1 + u}{2} \tag{A.20}$$

$$X_{\bar{1}} = X_1 + u \tag{A.21}$$

and so on for Y_j and Z_k. The equilibrium (A.2) can then be rewritten as:

$$f^{eq}_{ijk} = -\rho X_i Y_j Z_k. \tag{A.22}$$

This product form can (up to the sign) also be used to write the equilibrium of an improved BGK model for the two dimensional D2Q9 lattice:

$$f^{eq}_{ij} = \rho X_i Y_j. \tag{A.23}$$

Appendix B. D3Q27 MRT model

Countable raw moments for the D3Q27 lattice can be computed by the fast moment transform:

$$m_{ij|\gamma} = \sum_k f_{ijk} k^\gamma \tag{B.1}$$

$$m_{i|\beta\gamma} = \sum_j m_{ij|\gamma} j^\beta \tag{B.2}$$

$$m_{\alpha\beta\gamma} = \sum_i m_{i|\beta\gamma} i^\alpha. \tag{B.3}$$

The D3Q27 lattice is not usually applied together with the MRT collision operator. The only resource in literature that gives a procedure to determine the transformation matrix to our knowledge is [16]. The matrix is given in non-orthogonal form and it is stated that it must be transformed with the Gram–Schmidt procedure. The unweighted orthogonal matrix has also been published online [46]. Using an unweighted orthogonal matrix rather than a weighted orthogonal matrix is in the tradition of the MRT method as it was first introduced for the D2Q9 lattice [15] and for the D3Q15 and D3Q19 lattices [12]. The results of this paper indicate that a weighted orthogonalization would produce a superior method but here we are obliged to give the version that correctly follows the classical MRT philosophy. To generate the matrix starting from the non-orthogonal base vectors in [16] we apply the Gram–Schmidt procedure in the software Mathematica and multiply each

row of the matrix by its largest denominator in order to obtain an integer matrix. The resulting moments M are written here in terms of countable moments:

$$M_0 = m_{000} \tag{B.4}$$
$$M_1 = m_{100} \tag{B.5}$$
$$M_2 = m_{010} \tag{B.6}$$
$$M_3 = m_{001} \tag{B.7}$$
$$M_4 = -2m_{000} + m_{002} + m_{020} + m_{200} \tag{B.8}$$
$$M_5 = -m_{002} - m_{020} + 2m_{200} \tag{B.9}$$
$$M_6 = -m_{002} + m_{020} \tag{B.10}$$
$$M_7 = m_{110} \tag{B.11}$$
$$M_8 = m_{011} \tag{B.12}$$
$$M_9 = m_{101} \tag{B.13}$$
$$M_{10} = -4m_{100} + 3(m_{102} + m_{120}) \tag{B.14}$$
$$M_{11} = -4m_{010} + 3(m_{012} + m_{210}) \tag{B.15}$$
$$M_{12} = -4m_{001} + 3(m_{021} + m_{201}) \tag{B.16}$$
$$M_{13} = 4m_{100} - 6(m_{102} + m_{120}) + 9m_{122} \tag{B.17}$$
$$M_{14} = 4m_{010} - 6(m_{012} + m_{210}) + 9m_{212} \tag{B.18}$$
$$M_{15} = 4m_{001} - 6(m_{021} + m_{201}) + 9m_{221} \tag{B.19}$$
$$M_{16} = 4(m_{000} - m_{002} - m_{020} - m_{200}) + 3(m_{022} + m_{202} + m_{220}) \tag{B.20}$$
$$M_{17} = -8m_{000} + 12(m_{002} + m_{020} + m_{200}) - 18(m_{022} + m_{202} + m_{220}) + 27m_{222} \tag{B.21}$$
$$M_{18} = 2(m_{002} + m_{020}) + 3(m_{202} + m_{220}) - 4m_{200} - 6m_{022} \tag{B.22}$$
$$M_{19} = 2(m_{002} - m_{020}) + 3(m_{220} - m_{202}) \tag{B.23}$$
$$M_{20} = -2m_{110} + 3m_{112} \tag{B.24}$$
$$M_{21} = -2m_{011} + 3m_{211} \tag{B.25}$$
$$M_{22} = -2m_{101} + 3m_{121} \tag{B.26}$$
$$M_{23} = m_{120} - m_{102} \tag{B.27}$$
$$M_{24} = m_{012} - m_{210} \tag{B.28}$$
$$M_{25} = m_{201} - m_{021} \tag{B.29}$$
$$M_{26} = m_{111}. \tag{B.30}$$

The corresponding equilibrium moments are taken from a direct transformation of the equilibrium cumulants to moment space and by adding the Galilean correction to the second order moments:

$$M_0^{eq} = \rho \tag{B.31}$$
$$M_1^{eq} = \rho u \tag{B.32}$$
$$M_2^{eq} = \rho v \tag{B.33}$$
$$M_3^{eq} = \rho w \tag{B.34}$$
$$M_4^{eq} = \rho\left(-1 + u^2 + v^2 + w^2 - 3\left(\frac{1}{s_4} - \frac{1}{2}\right)(u^2 D_x u + v^2 D_y v + w^2 D_z w)\right) \tag{B.35}$$
$$M_5^{eq} = \rho\left(-w^2 - v^2 + 2u^2 - 3\left(\frac{1}{s_\nu} - \frac{1}{2}\right)(2u^2 D_x u - v^2 D_y v - w^2 D_z w)\right) \tag{B.36}$$
$$M_6^{eq} = \rho\left(-w^2 + v^2 - 3\left(\frac{1}{s_\nu} - \frac{1}{2}\right)(v^2 D_y v - w^2 D_z w)\right) \tag{B.37}$$
$$M_7^{eq} = \rho u v \tag{B.38}$$
$$M_8^{eq} = \rho v w \tag{B.39}$$
$$M_9^{eq} = \rho u w \tag{B.40}$$
$$M_{10}^{eq} = \rho(-4u + u(2 + 3(w^2 + v^2))) \tag{B.41}$$

$$M_{11}^{eq} = \rho(-4v + v(2 + 3(w^2 + u^2))) \tag{B.42}$$
$$M_{12}^{eq} = \rho(-4w + w(2 + 3(v^2 + u^2))) \tag{B.43}$$
$$M_{13}^{eq} = \rho(4u - 2u(2 + 3(w^2 + v^2)) + 9u(v^2 + 1/3)(w^2 + 1/3)) \tag{B.44}$$
$$M_{14}^{eq} = \rho(4v - 2v(2 + 3(w^2 + u^2)) + 9(u^2 + 1/3)v(w^2 + 1/3)) \tag{B.45}$$
$$M_{15}^{eq} = \rho(4w - 2w(2 + 3(v^2 + u^2)) + 9(u^2 + 1/3)(v^2 + 1/3)w) \tag{B.46}$$
$$M_{16}^{eq} = \rho(-4(u^2 + v^2 + w^2) + 3((v^2 + 1/3)(w^2 + 1/3) + (u^2 + 1/3)(w^2 + 1/3) + (u^2 + 1/3)(v^2 + 1/3))) \tag{B.47}$$
$$\begin{aligned} M_{17}^{eq} = {} & \rho(4 + 12(w^2 + v^2 + u^2) - 18((v^2 + 1/3)(w^2 + 1/3) + (u^2 + 1/3)(w^2 + 1/3) + (u^2 + 1/3)(v^2 + 1/3)) \\ & + 27(u^2 + 1/3)(v^2 + 1/3)(w^2 + 1/3)) \end{aligned} \tag{B.48}$$
$$M_{18}^{eq} = \rho(2(v^2 + w^2 - 2u^2) + 3((u^2 + 1/3)(w^2 + 1/3) + (u^2 + 1/3)(v^2 + 1/3)) - 6(v^2 + 1/3)(w^2 + 1/3)) \tag{B.49}$$
$$M_{19}^{eq} = \rho(2(w^2 - v^2) + 3((u^2 + 1/3)(v^2 + 1/3) - (u^2 + 1/3)(w^2 + 1/3))) \tag{B.50}$$
$$M_{20}^{eq} = \rho(-2uv + 3uv(w^2 + 1/3)) \tag{B.51}$$
$$M_{21}^{eq} = \rho(-2vw + 3vw(u^2 + 1/3)) \tag{B.52}$$
$$M_{22}^{eq} = \rho(-2uw + 3uw(v^2 + 1/3)) \tag{B.53}$$
$$M_{23}^{eq} = \rho(u(v^2 + 1/3) - u(w^2 + 1/3)) \tag{B.54}$$
$$M_{24}^{eq} = \rho(v(w^2 + 1/3) - v(u^2 + 1/3)) \tag{B.55}$$
$$M_{25}^{eq} = \rho(w(u^2 + 1/3) - w(v^2 + 1/3)) \tag{B.56}$$
$$M_{26}^{eq} = \rho uvw. \tag{B.57}$$

The collision becomes:

$$M_n^* = M^{eq} s_n + (1 - s_n) M_n. \tag{B.58}$$

Here s_n is the relaxation rate for the n-th moment. They correspond to ω in the other methods but we distinguish explicitly between relaxation rates for countable moments and orthogonal moments since there is no correspondence between the ordering of the two. The kinematic viscosity is adjusted by $s_\nu = s_5 = s_6 = s_7 = s_8 = s_9 = \omega_1$. The conserved quantities are computed by (A.3)–(A.6). The spatial derivatives of the velocity for the Galilean correction are determined from

$$\begin{aligned} D_x u = {} & -\frac{s_\nu}{2\rho}(2m_{200} - m_{020} - m_{002} - \rho(2u^2 - v^2 - w^2)) \\ & - \frac{s_4}{2\rho}(m_{200} + m_{020} + m_{002} - \rho(1 + u^2 + v^2 + w^2)) \end{aligned} \tag{B.59}$$
$$D_y v = D_x u + \frac{3s_\nu}{2\rho}(m_{200} - m_{020} - \rho u^2 + \rho v^2) \tag{B.60}$$
$$D_z w = D_x u + \frac{3s_\nu}{2\rho}(m_{200} - m_{002} - \rho u^2 + \rho w^2). \tag{B.61}$$

After collision the orthogonal moments can be transformed to countable moments:

$$m_{000}^* = M_0^* \tag{B.62}$$
$$m_{100}^* = M_1^* \tag{B.63}$$
$$m_{010}^* = M_2^* \tag{B.64}$$
$$m_{001}^* = M_3^* \tag{B.65}$$
$$m_{200}^* = (2M_0^* + M_4^* + M_5^*)/3 \tag{B.66}$$
$$m_{020}^* = (4M_0^* + 2M_4^* - M_5^* + 3M_6^*)/6 \tag{B.67}$$
$$m_{002}^* = (4M_0^* + 2M_4^* - M_5^* - 3M_6^*)/6 \tag{B.68}$$
$$m_{110}^* = M_7^* \tag{B.69}$$
$$m_{011}^* = M_8^* \tag{B.70}$$
$$m_{101}^* = M_9^* \tag{B.71}$$

$$m^*_{120} = (M^*_{10} + 4M^*_1 + 3M^*_{23})/6 \tag{B.72}$$
$$m^*_{102} = (M^*_{10} + 4M^*_1 - 3M^*_{23})/6 \tag{B.73}$$
$$m^*_{012} = (4M^*_2 + M^*_{11} + 3M^*_{24})/6 \tag{B.74}$$
$$m^*_{210} = (4M^*_2 + M^*_{11} - 3M^*_{24})/6 \tag{B.75}$$
$$m^*_{021} = (4M^*_3 + M^*_{12} - 3M^*_{25})/6 \tag{B.76}$$
$$m^*_{201} = (4M^*_3 + M^*_{12} + 3M^*_{25})/6 \tag{B.77}$$
$$m^*_{112} = (2M^*_7 + M^*_{20})/3 \tag{B.78}$$
$$m^*_{121} = (2M^*_9 + M^*_{22})/3 \tag{B.79}$$
$$m^*_{211} = (2M^*_8 + M^*_{21})/3 \tag{B.80}$$
$$m^*_{022} = (4M^*_0 + M^*_{16} - M^*_{18} + 4M^*_4 - 2M^*_5)/9 \tag{B.81}$$
$$m^*_{202} = (8M^*_0 + 2M^*_{16} + M^*_{18} - 3M^*_{19} + 8M^*_4 + 2M^*_5 - 6M^*_6)/18 \tag{B.82}$$
$$m^*_{220} = (8M^*_0 + 2M^*_{16} + M^*_{18} + 3M^*_{19} + 8M^*_4 + 2M^*_5 + 6M^*_6)/18 \tag{B.83}$$
$$m^*_{122} = (2M^*_{10} + 4M^*_1 + M^*_{13})/9 \tag{B.84}$$
$$m^*_{212} = (4M^*_2 + 2M^*_{11} + M^*_{14})/9 \tag{B.85}$$
$$m^*_{221} = (4M^*_3 + 2M^*_{12} + M^*_{15})/9 \tag{B.86}$$
$$m^*_{222} = (8M^*_0 + 6M^*_{16} + M^*_{17} + 12M^*_4)/27 \tag{B.87}$$
$$m^*_{111} = M^*_{26}. \tag{B.88}$$

The post-collision distributions can be obtained by the inverse fast moment transform:

$$m^*_{0|\beta\gamma} = m^*_{0\beta\gamma} - m^*_{2\beta\gamma} \tag{B.89}$$
$$m^*_{\bar{1}|\beta\gamma} = (-m^*_{1\beta\gamma} + m^*_{2\beta\gamma})/2 \tag{B.90}$$
$$m^*_{1|\beta\gamma} = (m^*_{1\beta\gamma} + m^*_{2\beta\gamma})/2 \tag{B.91}$$
$$m^*_{i0|\gamma} = m^*_{i|0\gamma} - m^*_{i|2\gamma} \tag{B.92}$$
$$m^*_{i\bar{1}|\gamma} = (-m^*_{i|1\gamma} + m^*_{i|2\gamma})/2 \tag{B.93}$$
$$m^*_{i1|\gamma} = (m^*_{i|1\gamma} + m^*_{i|2\gamma})/2 \tag{B.94}$$
$$f^*_{ij0} = m^*_{ij|0} - m^*_{ij|2} \tag{B.95}$$
$$f^*_{ij\bar{1}} = (-m^*_{ij|1} + m^*_{ij|2})/2 \tag{B.96}$$
$$f^*_{ij1} = (m^*_{ij|1} + m^*_{ij|2})/2. \tag{B.97}$$

Appendix C. Non-orthogonal MRT model

The non-orthogonal raw moment MRT model or simply the raw moment (RM) model used in this paper is implemented as follows: The raw moments are obtained from Eqs. (B.1)–(B.3). The approximate spatial derivatives of velocity for the Galilean correction are obtained from Eqs. (B.59)–(B.61) with $s_\nu = \omega_1$ and $s_4 = \omega_2$. The collision follows the nomenclature we used in the cumulant model:

$$m^*_{200} - m^*_{020} = (1-\omega_1)(m_{200} - m_{020}) - 3\rho\left(1 - \frac{\omega_1}{2}\right)(u^2 D_x u - v^2 D_y v) + \omega_1(u^2 - v^2)\rho \tag{C.1}$$
$$m^*_{200} - m^*_{002} = (1-\omega_1)(m_{200} - m_{002}) - 3\rho\left(1 - \frac{\omega_1}{2}\right)(u^2 D_x u - w^2 D_z w) + \omega_1(u^2 - w^2)\rho \tag{C.2}$$
$$\begin{aligned} m^*_{200} + m^*_{020} + m^*_{002} \;=\; & (1-\omega_2)(m_{200} + m_{020} + m_{002}) - 3\rho\left(1 - \frac{\omega_2}{2}\right)(u^2 D_x u + v^2 D_y v + w^2 D_z w) \\ & + \omega_2(1 + u^2 + v^2 + w^2)\rho \end{aligned} \tag{C.3}$$
$$m^*_{120} + m^*_{102} = (1-\omega_3)(m_{120} + m_{102}) + \omega_3 u(v^2 + w^2 + 2/3)\rho \tag{C.4}$$
$$m^*_{210} + m^*_{012} = (1-\omega_3)(m_{210} + m_{012}) + \omega_3 v(u^2 + w^2 + 2/3)\rho \tag{C.5}$$

$$m^*_{201} + m^*_{021} = (1-\omega_3)(m_{201} + m_{021}) + \omega_3 w(u^2 + v^2 + 2/3)\rho \tag{C.6}$$
$$m^*_{120} - m^*_{102} = (1-\omega_4)(m_{120} - m_{102}) + \omega_4 u(v^2 - w^2)\rho \tag{C.7}$$
$$m^*_{210} - m^*_{012} = (1-\omega_4)(m_{210} - m_{012}) + \omega_4 v(u^2 - w^2)\rho \tag{C.8}$$
$$m^*_{201} - m^*_{021} = (1-\omega_4)(m_{201} - m_{021}) + \omega_4 w(u^2 - v^2)\rho \tag{C.9}$$
$$m^*_{111} = (1-\omega_5)m_{111} + \omega_5 uvw\rho \tag{C.10}$$
$$\begin{aligned} m^*_{220} - 2m^*_{202} + m^*_{022} &= (1-\omega_6)(m_{220} - 2m_{202} + m_{022}) \\ &\quad + \omega_6(((u^2 + 1/3) + (w^2 + 1/3))(v^2 + 1/3) - 2(u^2 + 1/3)(w^2 + 1/3))\rho \end{aligned} \tag{C.11}$$
$$\begin{aligned} m^*_{220} + m^*_{202} - 2m^*_{022} &= (1-\omega_6)(m_{220} + m_{202} - 2m_{022}) \\ &\quad + \omega_6(((v^2 + 1/3) + (w^2 + 1/3))(u^2 + 1/3) - 2(v^2 + 1/3)(w^2 + 1/3))\rho \end{aligned} \tag{C.12}$$
$$\begin{aligned} m^*_{220} + m^*_{202} + m^*_{022} &= (1-\omega_7)(m_{220} + m_{202} + m_{022}) \\ &\quad + \omega_7((u^2 + 1/3)(v^2 + 1/3) + (v^2 + 1/3)(w^2 + 1/3) + (u^2 + 1/3)(w^2 + 1/3))\rho \end{aligned} \tag{C.13}$$
$$m^*_{211} = (1-\omega_8)m_{211} + \omega_8 vw(u^2 + 1/3)\rho \tag{C.14}$$
$$m^*_{121} = (1-\omega_8)m_{121} + \omega_8 uw(v^2 + 1/3)\rho \tag{C.15}$$
$$m^*_{112} = (1-\omega_8)m_{112} + \omega_8 uv(w^2 + 1/3)\rho \tag{C.16}$$
$$m^*_{221} = (1-\omega_9)m_{221} + \omega_9 w(u^2 + 1/3)(v^2 + 1/3)\rho \tag{C.17}$$
$$m^*_{212} = (1-\omega_9)m_{212} + \omega_9 v(u^2 + 1/3)(w^2 + 1/3)\rho \tag{C.18}$$
$$m^*_{122} = (1-\omega_9)m_{122} + \omega_9 u(v^2 + 1/3)(w^2 + 1/3)\rho \tag{C.19}$$
$$m^*_{222} = (1-\omega_{10})m_{222} + \omega_{10}(u^2 + 1/3)(v^2 + 1/3)(w^2 + 1/3)\rho. \tag{C.20}$$

The transform to post-collision distributions is done by Eqs. (B.89)–(B.97).

Appendix D. Cascaded lattice Boltzmann model

For the cascaded lattice Boltzmann simulations in this paper we use a slightly improved code as compared to the one presented in [8]. First we apply the fast central moment transform to the distributions (Eqs. (43)–(45)). The approximate spatial derivatives of the velocities used in the Galilean correction are computed from:

$$D_x u = -\frac{\omega_1}{2\rho}(2\kappa_{200} - \kappa_{020} - \kappa_{002}) - \frac{\omega_2}{2\rho}(\kappa_{200} + \kappa_{020} + \kappa_{002} - \rho) \tag{D.1}$$
$$D_y v = D_x u + \frac{3\omega_1}{2\rho}(\kappa_{200} - \kappa_{020}) \tag{D.2}$$
$$D_z w = D_x u + \frac{3\omega_1}{2\rho}(\kappa_{200} - \kappa_{002}). \tag{D.3}$$

The collision reads:

$$\kappa^*_{200} - \kappa^*_{020} = (1-\omega_1)(\kappa_{200} - \kappa_{020}) - 3\rho\left(1 - \frac{\omega_1}{2}\right)(u^2 D_x u - v^2 D_y v) \tag{D.4}$$
$$\kappa^*_{200} - \kappa^*_{002} = (1-\omega_1)(\kappa_{200} - \kappa_{002}) - 3\rho\left(1 - \frac{\omega_1}{2}\right)(u^2 D_x u - w^2 D_z w) \tag{D.5}$$
$$\kappa^*_{200} + \kappa^*_{020} + \kappa^*_{002} = \rho\omega_2 + (1-\omega_2)(\kappa_{200} + \kappa_{020} + \kappa_{002}) - 3\rho\left(1 - \frac{\omega_2}{2}\right)(u^2 D_x u + v^2 D_y v + w^2 D_z w) \tag{D.6}$$
$$\kappa^*_{120} + \kappa^*_{102} = (1-\omega_3)(\kappa_{120} + \kappa_{102}) \tag{D.7}$$
$$\kappa^*_{210} + \kappa^*_{012} = (1-\omega_3)(\kappa_{210} + \kappa_{012}) \tag{D.8}$$
$$\kappa^*_{201} + \kappa^*_{021} = (1-\omega_3)(\kappa_{201} + \kappa_{021}) \tag{D.9}$$
$$\kappa^*_{120} - \kappa^*_{102} = (1-\omega_4)(\kappa_{120} - \kappa_{102}) \tag{D.10}$$
$$\kappa^*_{210} - \kappa^*_{012} = (1-\omega_4)(\kappa_{210} - \kappa_{012}) \tag{D.11}$$
$$\kappa^*_{201} - \kappa^*_{021} = (1-\omega_4)(\kappa_{201} - \kappa_{021}) \tag{D.12}$$
$$\kappa^*_{111} = (1-\omega_5)\kappa_{111} \tag{D.13}$$

$$\kappa^*_{220} - 2\kappa^*_{202} + \kappa^*_{022} = (1-\omega_6)(\kappa_{220} - 2\kappa_{202} + \kappa_{022}) \tag{D.14}$$
$$\kappa^*_{220} + \kappa^*_{202} - 2\kappa^*_{022} = (1-\omega_6)(\kappa_{220} + \kappa_{202} - 2\kappa_{022}) \tag{D.15}$$
$$\kappa^*_{220} + \kappa^*_{202} + \kappa^*_{022} = (1-\omega_7)(\kappa_{220} + \kappa_{202} + \kappa_{022}) + \omega_7\rho/3 \tag{D.16}$$
$$\kappa^*_{211} = (1-\omega_8)\kappa_{211} \tag{D.17}$$
$$\kappa^*_{121} = (1-\omega_8)\kappa_{121} \tag{D.18}$$
$$\kappa^*_{112} = (1-\omega_8)\kappa_{112} \tag{D.19}$$
$$\kappa^*_{221} = (1-\omega_9)\kappa_{221} \tag{D.20}$$
$$\kappa^*_{212} = (1-\omega_9)\kappa_{212} \tag{D.21}$$
$$\kappa^*_{122} = (1-\omega_9)\kappa_{122} \tag{D.22}$$
$$\kappa^*_{222} = (1-\omega_{10})\kappa_{222} + \omega_{10}\rho/27. \tag{D.23}$$

After the collision the central moments are transformed back to distributions by Eqs. (88)–(96).

Appendix E. Boundary conditions: velocity

The simulation of a sphere requires off-lattice boundary conditions for velocity. We adopt here a simple single node interpolation scheme for the simple bounce back boundary condition. The scheme is similar in concept and accuracy to the one first proposed by Bouzidi et al. [47]. It differs from that scheme in that it does not distinguish between different cases and it does not require access to a neighboring node or the existence of two arrays for pre- and post-collision distributions. The details of this method are published here for the first time.

We consider a lattice link for the distribution $f_{ijkxyzt}$ that cuts the wall at a distance $q\sqrt{i^2+j^2+k^2}\Delta x$ from the node at location $\{x, y, z\}$. The distribution $f_{\bar{i}\bar{j}\bar{k}xyz(t+\Delta t)}$ moving in opposite direction is missing. It is computed from linear interpolation between the pre- and post-collision distribution:

$$f_{\bar{i}\bar{j}\bar{k}xyz(t+\Delta t)} = \frac{1}{q+1} f^{wall}_{\bar{i}\bar{j}\bar{k}t} + \frac{q}{q+1} f^{*}_{\bar{i}\bar{j}\bar{k}xyzt}. \tag{E.1}$$

For the distribution $f^{wall}_{\bar{i}\bar{j}\bar{k}t}$ we assume the bounce back condition at a wall with velocity $\{u_{wall}, v_{wall}, w_{wall}\}$ and w_{ijk} being the weight of the corresponding link ($w_{000} = 8/27$, $w_{100} = 2/27$, $w_{110} = 1/54$, $w_{111} = 1/216$ and so on by permuting the indices):

$$f^{wall}_{\bar{i}\bar{j}\bar{k}t} = f^{wall}_{ijkt} - 6w_{ijk}(iu_{wall} + jv_{wall} + kw_{wall}). \tag{E.2}$$

This can be computed by a linear interpolation between the pre- and the post-collision distribution:

$$f^{wall}_{ijkt} = (1-q) f_{ijkxyzt} + q f^{*}_{ijkxyzt}. \tag{E.3}$$

Since our code saves only the post-collision distribution we have to recover the pre-collision distribution from the post-collision distribution. For this we use an approximate rule based on the single relaxation time collision operator:

$$f_{ijkxyzt} \approx \frac{f^{*}_{ijkxyzt} - f^{*}_{\bar{i}\bar{j}\bar{k}xyzt}}{2} + \frac{f^{*}_{ijkxyzt} + f^{*}_{\bar{i}\bar{j}\bar{k}xyzt} - \omega_1(f^{eq}_{ijkxyzt} + f^{eq}_{\bar{i}\bar{j}\bar{k}xyzt})}{2-2\omega_1}. \tag{E.4}$$

The equilibrium distribution $f^{eq}_{ijkxyzt}$ is the standard equilibrium of the node at $\{x, y, z\}$ used in the single relaxation time operator (i.e. Eq. (A.2) with the Galilean correction being neglected). This method is also applicable if the collision model in the bulk is not the single relaxation time collision. It is not applicable for $\omega_1 = 1$. For modeling a wall at rest we choose $u_{wall} = 0$, $v_{wall} = 0$, and $w_{wall} = 0$. The unknown boundary value is obtained by inserting (E.4) into (E.3), (E.3) into (E.2), and (E.2) into (E.1).

Appendix F. Boundary conditions: outflow

At the outlet a simple extrapolation boundary condition can be applied by copying the distributions entering the domain from the last node before the outlet. To fix ideas we assume the outflow to be located in positive x-direction seen from the domain and the distributions $f_{\bar{1}jkxyzt}$ missing for all j and k. A simple method to close the domain is by copying the missing distributions from the next node inside the domain:

$$f_{\bar{1}jkxyzt} = f_{\bar{1}jk(x-\Delta x)yzt}. \tag{F.1}$$

The disadvantage of this method is that it causes strong acoustic reflections. In order to reduce them we should copy the distribution from the location in space and time where the pressure wave at $\{x, y, z, t\}$ came from. Here we restrict ourselves to waves normal to the boundary and use linear interpolation in space:

$$f_{\bar{1}jkxyzt} = f_{\bar{1}jk(x-\Delta x)yz(t-\Delta t)}(c\theta^{1/2} - u)\frac{\Delta t}{\Delta x} + \left(1 - (c\theta^{1/2} - u)\frac{\Delta t}{\Delta x}\right) f_{\bar{1}jkxyz(t-\Delta t)}. \tag{F.2}$$

Here $c\theta^{1/2} = \sqrt{1/3}\Delta x/\Delta t$ is the speed of sound and u is the velocity at the outlet which can be taken from the grid node at $\{x, y, z, t - \Delta t\}$. Since $u \ll \theta^{1/2}$ it is also possible to neglect u altogether without inducing strong reflections. The latter strategy was used in the presented study.

Appendix G. Asymptotic analysis

To obtain the equivalent partial differential equations for the lattice Boltzmann equation we apply a combination of Taylor expansion [48] and asymptotic expansion [49]. The starting point is the lattice Boltzmann equation in the following form:

$$f_{ijkxyz(t+\Delta t)} = f^*_{ijk(x-ic\Delta t)(y-jc\Delta t)(z-kc\Delta t)t}. \tag{G.1}$$

The *lhs* of this equation can be Taylor expanded in time, the *rhs* can be Taylor expanded in space:

$$\sum_{o=0}^{\infty} \frac{\Delta t^o}{o!}\partial_{t^o} f_{ijkxyzt} = \sum_{m,n,l=0}^{\infty} \frac{(i^m j^n k^l)(-c\Delta t)^{m+n+l}}{m!n!l!}\partial_{x^m y^n z^l} f^*_{ijkxyzt}. \tag{G.2}$$

The indices for space and time will from now on be dropped. Rewriting the previous definition of countable raw moments gives:

$$m_{\alpha\beta\gamma} = c^{-\alpha-\beta-\gamma}\frac{\partial^\alpha \partial^\beta \partial^\gamma}{\partial \Xi^\alpha \partial \Upsilon^\beta \partial Z^\gamma} F(\Xi, \Upsilon, Z)\Big|_{\Xi=\Upsilon=Z=0} = \sum_{i,j,k} i^\alpha j^\beta k^\gamma f_{ijk}. \tag{G.3}$$

We can apply this definition of countable raw moments to Eq. (G.2) to obtain a Taylor expansion of the moments in space and time:

$$\sum_{o=0}^{\infty} \frac{\Delta t^o}{o!}\partial_{t^o} m_{\alpha\beta\gamma} = \sum_{m,n,l=0}^{\infty} \frac{(-c\Delta t)^{m+n+l}}{m!n!l!}\partial_{x^m y^n z^l} m^*_{(\alpha+m)(\beta+n)(\gamma+l)}. \tag{G.4}$$

We note that $c\Delta t = \Delta x$. At this point it is necessary to decide on a scaling of space and time variables. We adopt here the diffusive scaling where the grid velocity c scales proportional to the inverse of the grid spacing such that $\Delta x = L\epsilon$ and $\Delta t = \tau\epsilon^2$. It is inconvenient that the observable quantities are dimensionless in order to be scalable while the derivatives in space and time have physical dimensions. In the following we substitute the space and time variables by dimensionless ones: $\{x, y, z\} \to \{x/L, y/L, z/L\}$ and $t \to t/\tau$. This leads to the equation:

$$\sum_{o=0}^{\infty} \frac{\epsilon^{2o}}{o!}\partial_{t^o} m_{\alpha\beta\gamma} = \sum_{m,n,l=0}^{\infty} \frac{(-\epsilon)^{m+n+l}}{m!n!l!}\partial_{x^m y^n z^l} m^*_{(\alpha+m)(\beta+n)(\gamma+l)}. \tag{G.5}$$

The observable quantities or moments are expanded asymptotically in the scaling parameter ϵ:

$$m_{\alpha\beta\gamma} = \sum_{q=0}^{\infty} \epsilon^q m^{(q)}_{\alpha\beta\gamma}, \tag{G.6}$$

$$m^*_{\alpha\beta\gamma} = \sum_{q=0}^{\infty} \epsilon^q m^{*(q)}_{\alpha\beta\gamma}. \tag{G.7}$$

The parameters of this expansion are not allowed to depend on ϵ. The next step is to enter the expansion into Eq. (G.5) to obtain:

$$\sum_{o=0}^{\infty} \frac{\epsilon^{2o}}{o!}\partial_{t^o} \sum_{q=0}^{\infty} \epsilon^q m^{(q)}_{\alpha\beta\gamma} = \sum_{m,n,l=0}^{\infty} \frac{(-\epsilon)^{m+n+l}}{m!n!l!}\partial_{x^m y^n z^l} \sum_{q=0}^{\infty} \epsilon^q m^{*(q)}_{(\alpha+m)(\beta+n)(\gamma+l)}. \tag{G.8}$$

Since ϵ is an arbitrary parameter the equation holds for all ϵ only if it holds for all powers of ϵ separately. It is hence possible to extract equivalent partial differential equations for each order of a moment by ordering (G.8) according to the power of ϵ. In order to extract specific equations we have to make some assumptions on the velocity set and the collision

operator. As a velocity set we consider only the D3Q27 lattice. On this lattice there are only 27 independent raw countable moments. For higher order moments we have to consider the following aliasing conditions:

$$m_{300} = m_{100}, \tag{G.9}$$
$$m_{400} = m_{200}, \tag{G.10}$$
$$m_{500} = m_{100}, \tag{G.11}$$
$$m_{310} = m_{110} \tag{G.12}$$

and so on. The expansion in raw countable moments can be used together with raw moments, central moments, and cumulant collision operators since all these quantities can be transformed into raw countable moments. Extracting the zeroth order from (G.8) proofs that all observable quantities are collision invariant at zeroth order (ϵ^0):

$$m^{(0)}_{\alpha\beta\gamma} = m^{*(0)}_{\alpha\beta\gamma}. \tag{G.13}$$

The same still holds at first order (ϵ^1; no proof):

$$m^{(1)}_{\alpha\beta\gamma} = m^{*(1)}_{\alpha\beta\gamma}. \tag{G.14}$$

The divergence free condition follows from the diffusive scaling and is obtained in two steps. From the first order in momentum we obtain the time derivative of the zeroth order of density ($\epsilon^2, \alpha = 0, \beta = 0, \gamma = 0$):

$$\partial_t m^{(0)}_{000} = \partial_x m^{*(1)}_{100} + \partial_y m^{*(1)}_{010} + \partial_z m^{*(1)}_{001}. \tag{G.15}$$

The mass m_{000} appears in the equilibrium for the second order moments. Let us consider the equation for m_{100} at first order to see ($\epsilon^1, \alpha = 1, \beta = 0, \gamma = 0$):

$$m^{(1)}_{100} = m^{*(1)}_{100} - \partial_x m^{*(0)}_{200} - \partial_y m^{*(0)}_{110} - \partial_z m^{*(0)}_{101}. \tag{G.16}$$

Due to (G.13) we know that $m^{*(0)}_{200}$, $m^{*(0)}_{110}$, and $m^{*(0)}_{101}$ are equal to their equilibrium value which is under our control. Only the equilibrium of $m^{*(0)}_{200}$ has a non-zero part:

$$m^{eq(0)}_{200} = m^{(0)}_{000}\theta. \tag{G.17}$$

Combining this with (G.16) gives:

$$0 = \partial_x \theta m^{(0)}_{000}. \tag{G.18}$$

From the equations in y and z-direction we obtain the same way that $\partial_y m^{(0)}_{000} = 0$ and $\partial_z m^{(0)}_{000} = 0$. Since these equations hold everywhere the zero order part of the density can only depend on time and it can only depend on time if its boundary conditions depend on time. By choosing constant boundary conditions for $m^{(0)}_{000}$ we eliminate $\partial_t m^{(0)}_{000}$ from (G.15) and the first order velocity becomes divergence free.

The Navier–Stokes momentum equation is obtained at third order in ϵ: ($\epsilon^3, \alpha = 1, \beta = 0, \gamma = 0$):

$$\begin{aligned}\partial_t m^{(1)}_{100} = {} & m^{*(3)}_{100} - m^{(3)}_{100} - (\partial_x m^{*(2)}_{200} + \partial_y m^{*(2)}_{110} + \partial_z m^{*(2)}_{101}), \\ & + (\partial_{xx} m^{*(1)}_{100} + \partial_{yy} m^{*(1)}_{120} + \partial_{zz} m^{*(1)}_{103})/2 + \partial_{xy} m^{*(1)}_{210} + \partial_{xz} m^{*(1)}_{101} + \partial_{yz} m^{*(1)}_{111}.\end{aligned} \tag{G.19}$$

The term $m^{*(3)}_{100} - m^{(3)}_{100}$ is non-conservative and describes a force term that has to be applied at third order. For the unknown moments $m^{*(2)}_{110}$, $m^{*(1)}_{210}$ and so on we have to derive further equivalent partial differential equations. Fortunately, since at first order all moments are collision invariants they also have to be equal to their equilibrium to first order and we can replace $m^{*(1)}_{\alpha\beta\gamma} = m^{eq(1)}_{\alpha\beta\gamma}$. For the second moments we get ($\epsilon^2, \alpha = 2, \beta = 0, \gamma = 0$):

$$m^{(2)}_{200} = m^{*(2)}_{200} - (\partial_x m^{eq(1)}_{100} + \partial_y m^{eq(1)}_{210} + \partial_z m^{eq(1)}_{201}), \tag{G.20}$$

($\epsilon^2, \alpha = 1, \beta = 1, \gamma = 0$):

$$m^{(2)}_{110} = m^{*(2)}_{110} - (\partial_x m^{eq(1)}_{210} + \partial_y m^{eq(1)}_{120} + \partial_z m^{eq(1)}_{111}), \tag{G.21}$$

and ($\epsilon^2, \alpha = 1, \beta = 0, \gamma = 1$):

$$m^{(2)}_{101} = m^{*(2)}_{101} - (\partial_x m^{eq(1)}_{201} + \partial_y m^{eq(1)}_{111} + \partial_z m^{eq(1)}_{102}). \tag{G.22}$$

From here on we have to consider the specific collision rule. To leading order there is no difference between the moment and the cumulant method. Starting from the relaxation of cumulants we have to use:

$$C^{*(2)}_{110} = (1-\omega_1)C^{(2)}_{110}, \tag{G.23}$$
$$C^{*(2)}_{101} = (1-\omega_1)C^{(2)}_{101}, \tag{G.24}$$
$$C^{*(2)}_{011} = (1-\omega_1)C^{(2)}_{011}, \tag{G.25}$$
$$(C^{*(2)}_{200} - C^{*(2)}_{020}) = (1-\omega_1)(C^{(2)}_{200} - C^{(2)}_{020}), \tag{G.26}$$
$$(C^{*(2)}_{200} - C^{*(2)}_{002}) = (1-\omega_1)(C^{(2)}_{200} - C^{(2)}_{002}), \tag{G.27}$$
$$(C^{*(2)}_{200} + C^{*(2)}_{020} + C^{*(2)}_{002}) = 3\theta\rho^{(2)}\omega_2 + (1-\omega_2)(C^{(2)}_{200} + C^{(2)}_{020} + C^{(2)}_{002}). \tag{G.28}$$

All required cumulants have to be expressed in terms of moments. The required rules are obtained from comparing the definition of cumulants and moments:

$$C^{(2)}_{110} = m^{(2)}_{110} - m^{(1)}_{100}m^{(1)}_{010}/m^{(0)}_{000}, \tag{G.29}$$
$$C^{(2)}_{101} = m^{(2)}_{101} - m^{(1)}_{100}m^{(1)}_{001}/m^{(0)}_{000}, \tag{G.30}$$
$$C^{(2)}_{011} = m^{(2)}_{011} - m^{(1)}_{010}m^{(1)}_{001}/m^{(0)}_{000}, \tag{G.31}$$
$$C^{(2)}_{200} = m^{(2)}_{200} - m^{(1)2}_{100}/m^{(0)}_{000}, \tag{G.32}$$
$$C^{(2)}_{020} = m^{(2)}_{020} - m^{(1)2}_{010}/m^{(0)}_{000}, \tag{G.33}$$
$$C^{(2)}_{002} = m^{(2)}_{002} - m^{(1)2}_{001}/m^{(0)}_{000}, \tag{G.34}$$
$$C^{(1)}_{120} = 0 = m^{(1)}_{120} - m^{(1)}_{100}\theta, \tag{G.35}$$
$$C^{(1)}_{102} = 0 = m^{(1)}_{102} - m^{(1)}_{100}\theta, \tag{G.36}$$
$$C^{(1)}_{210} = 0 = m^{(1)}_{210} - m^{(1)}_{010}\theta, \tag{G.37}$$
$$C^{(1)}_{012} = 0 = m^{(1)}_{012} - m^{(1)}_{010}\theta, \tag{G.38}$$
$$C^{(1)}_{201} = 0 = m^{(1)}_{201} - m^{(1)}_{001}\theta, \tag{G.39}$$
$$C^{(1)}_{021} = 0 = m^{(1)}_{021} - m^{(1)}_{001}\theta, \tag{G.40}$$
$$C^{(1)}_{111} = 0 = m^{(1)}_{111}. \tag{G.41}$$

Inserting the above into the relaxation processes and then into Eq. (G.19), also considering the incompressibility (G.15), defining the forcing term $F^{(3)}_x = m^{*(3)}_{100} - m^{*(3)}_{100}$, assuming ω_1 to be constant, and $\theta = 1/3$ gives rise to:

$$\begin{aligned}\partial_t m^{(1)}_{100} = &-\partial_x \frac{m^{(2)}_{000}}{3} - (m^{(1)}_{100}\partial_x m^{(1)}_{100} + m^{(1)}_{010}\partial_y m^{(1)}_{100} + m^{(1)}_{001}\partial_z m^{(1)}_{100})/m^{(0)}_{000} \\ &+ \frac{1}{3}\left(\frac{1}{\omega_1} - \frac{1}{2}\right)(\partial_{xx}m^{(1)}_{100} + \partial_{xx}m^{(1)}_{100} + \partial_{zz}m^{(1)}_{100}) + F^{(3)}_x.\end{aligned} \tag{G.42}$$

By replacing the moments by the velocities and considering that $m^{(0)}_{000}$ is constant we can write the incompressible Navier–Stokes equation in more conventional form:

$$\begin{aligned}\partial_t u^{(1)} = &-\partial_x \frac{\rho^{(2)}}{3\rho^{(0)}} - (u^{(1)}\partial_x u^{(1)} + v^{(1)}\partial_y u^{(1)} + w^{(1)}\partial_z u^{(1)}) \\ &+ \frac{1}{3}\left(\frac{1}{\omega_1} - \frac{1}{2}\right)(\partial_{xx}u^{(1)} + \partial_{xx}u^{(1)} + \partial_{zz}u^{(1)}) + \frac{F^{(3)}_x}{\rho^{(0)}}.\end{aligned} \tag{G.43}$$

In order to establish that the lattice Boltzmann equation is at least second order accurate in space and at least first order accurate in time with respect to the solution (G.43) we have to prove that all odd orders of velocity and all even orders of density vanish. For this we recall that the lattice Boltzmann equation is symmetric and that the solution does not depend on the chirality of the coordinate system. Moreover we made no assumptions on ϵ other than that it is non-zero. Suppose we consider two different but arbitrary non-zero scaling parameters $\epsilon_1 = -\epsilon_2$. The expansion of the lattice Boltzmann equation in ϵ_1 and ϵ_2 leads to the same result just with opposite chirality. Say the equivalent partial differential equations

for ϵ_1 are the left-handed equations and those for ϵ_2 are the right-handed equations. Since nothing in the lattice Boltzmann equation depends on chirality these two sets of equations are identical and hence their numerical solution must be identical up to the change in sign for the velocities. However, the asymptotic expansion of the solution is not identical. Considering $u^{(l)} = -u^{(r)}$ gives:

$$\sum_{i=0}^{\infty} \epsilon_1^i u^{(i)} = -\sum_{j=0}^{\infty} \epsilon_2^j u^{(j)}, \tag{G.44}$$

$$\sum_{i=0}^{\infty} \epsilon_1^i u^{(i)} = \sum_{j=0}^{\infty} -(-\epsilon_1)^j u^{(j)}. \tag{G.45}$$

This can only be true in general if all even orders of u vanish. Similar we obtain for the density which is not sensitive to chirality $\rho^{(l)} = \rho^{(r)}$:

$$\sum_{i=0}^{\infty} \epsilon_1^i \rho^{(i)} = \sum_{j=0}^{\infty} \epsilon_2^j \rho^{(j)}, \tag{G.46}$$

$$\sum_{i=0}^{\infty} \epsilon_1^i \rho^{(i)} = \sum_{j=0}^{\infty} (-\epsilon_1)^j \rho^{(j)}. \tag{G.47}$$

This can only be true if all odd orders in ρ vanish and it concludes the proof that the lattice Boltzmann equation is second order accurate for velocity and pressure. Boundary conditions have to be analyzed independently and are not covered by the proof.

Appendix H. Galilean correction

A finite lattice supports only a finite number of independent moments. Moments and cumulants beyond a certain order are functions of moments of lower order. The first moment that does not exist independently on the D3Q27 lattice is the moment m_{300}. In fact we have the aliasing $m_{300} = m_{100}$. This is an undesired property of the finite lattice and we seek measures to minimize its effect. The first measure is classical [36] and is based on choosing the temperature or a reference speed of sound. We see this by taking the cumulant c_{300} and express it in terms of moments:

$$\bar{c}_{300} = 2\frac{m_{100}^3}{m_{000}^3} - 3\frac{m_{100}\bar{m}_{200}}{m_{000}^2} + \frac{\bar{m}_{300}}{m_{000}}. \tag{H.1}$$

The overbar is not written for the conserved quantities since $\bar{m}_{100} = m_{100} = m_{100}^*$ and $\bar{m}_{000} = m_{000} = m_{000}^*$. Taking $\bar{m}_{300} = m_{100}$ into consideration this gives:

$$\bar{c}_{300} = 2\frac{m_{100}^3}{m_{000}^3} + \frac{m_{100}(m_{000} - 3\bar{m}_{200})}{m_{000}^2}. \tag{H.2}$$

The second moment is:

$$\bar{m}_{200} = \theta m_{000} + \frac{m_{100}^2}{m_{000}} + m_{200}^{neq}. \tag{H.3}$$

We include here a non-equilibrium part of the moment m_{200} which requires further information and cannot be deduced from the previous equation. Inserting (H.3) into Eq. (H.2) gives:

$$\bar{c}_{300} = \frac{m_{100}(m_{000} - 3\theta m_{000})}{m_{000}^2} - 3\frac{m_{100}m_{200}^{neq}}{m_{000}^2} - \frac{m_{100}^3}{m_{000}^3}. \tag{H.4}$$

Since we are not solving an independent equation for c_{300} the best we can do is to put it as close to equilibrium as possible. As for other cumulants the equilibrium is zero and so we eliminate the leading error by choosing $\theta = 1/3$. The remainder of the error contains two terms of identical order of which one is easily eliminated and the other is not. The error that can be removed is the term m_{100}^3/m_{000}^3. For this to see we have to perform an asymptotic expansion and recover the equivalent partial differential equation for the evolution of the moments. Since the moments of second order are not relaxed on their own (except in the BGK model) the equivalent partial differential equations on the order of the leading error are written as:

$$\bar{m}_{200-020}^{(4)} = m_{200-020}^{eq(4)} - \left(\frac{1}{\omega_1} - \frac{1}{2}\right)\left(\partial_t \bar{m}_{200-020}^{(2)} + \partial_x(\bar{m}_{300}^{(3)} - \bar{m}_{120}^{(3)}) + \partial_y(\bar{m}_{210}^{(3)} - \bar{m}_{030}^{(3)}) + \partial_z(\bar{m}_{201}^{(3)} - \bar{m}_{021}^{(3)})\right), \tag{H.5}$$

$$\bar{m}_{200-002}^{(4)} = m_{200-002}^{eq(4)} - \left(\frac{1}{\omega_1} - \frac{1}{2}\right)\left(\partial_t \bar{m}_{200-002}^{(2)} + \partial_x(\bar{m}_{300}^{(3)} - \bar{m}_{102}^{(3)}) + \partial_y(\bar{m}_{210}^{(3)} - \bar{m}_{012}^{(3)}) + \partial_z(\bar{m}_{201}^{(3)} - \bar{m}_{003}^{(3)})\right), \tag{H.6}$$

$$\bar{m}_{\mathrm{P}}^{(4)} = m_{\mathrm{P}}^{eq(4)} - \left(\frac{1}{\omega_2} - \frac{1}{2}\right)\left(\partial_t \bar{m}_{\mathrm{P}}^{(2)} + \partial_x(\bar{m}_{300}^{(3)} + \bar{m}_{120}^{(3)} + \bar{m}_{102}^{(3)}) + \partial_y(\bar{m}_{210}^{(3)} + \bar{m}_{030}^{(3)} + \bar{m}_{012}^{(3)}) + \partial_z(\bar{m}_{201}^{(3)} + \bar{m}_{021}^{(3)} + \bar{m}_{003}^{(3)})\right) \tag{H.7}$$

with:

$$m_{200-020} = m_{200} - m_{020}, \tag{H.8}$$

$$m_{200-002} = m_{200} - m_{002}, \tag{H.9}$$

$$m_{\mathrm{P}} = m_{200} + m_{020} + m_{020}. \tag{H.10}$$

We see that the moment $\bar{m}_{300}$ appears only together with a derivative in x-direction. Let us rearrange Eq. (H.1) with $\bar{c}_{300} = 0$ (assuming equilibrium) and $\theta = 1/3$ to find the correct value for $\bar{m}_{300}$:

$$\bar{m}_{300} = m_{100} + \frac{m_{100}^3}{m_{000}^2} + 3\frac{m_{100}m_{200}^{neq}}{m_{000}} = m_{100} + u^3\rho + 3\frac{m_{100}m_{200}^{neq}}{m_{000}}. \tag{H.11}$$

To the required third order this leads to:

$$\bar{m}_{300}^{(3)} = m_{100}^{(3)} + u^{(1)3}\rho^{(0)} - 2u^{(1)}\rho^{(0)}\left(\frac{1}{\omega_1} - \frac{1}{2}\right)\partial_x u^{(1)}. \tag{H.12}$$

Only the first term in (H.12) actually appears in Eqs. (H.5)–(H.7) in the place of $\bar{m}_{300}$ but we can repair the equivalent partial differential equation by putting the spatial derivative of the remainder into the equilibrium of $m_{200-020}$, $m_{200-002}$, and m_{P}. Note that at leading order we can write:

$$\partial_x u^{(1)3}\rho^{(0)} = 3u^{(1)2}\rho^{(0)}\partial_x u^{(1)}. \tag{H.13}$$

This term is known since at second order in diffusive scaling the asymptotic expansion gives:

$$m_{200-020}^{(2)} = m_{200-020}^{(2)eq} - \frac{2}{3\omega_1}\rho^{(0)}(\partial_x u^{(1)} - \partial_y v^{(1)}), \tag{H.14}$$

$$m_{200-002}^{(2)} = m_{200-002}^{(2)eq} - \frac{2}{3\omega_1}\rho^{(0)}(\partial_x u^{(1)} - \partial_z w^{(1)}), \tag{H.15}$$

$$m_{\mathrm{P}}^{(2)} = m_{\mathrm{P}}^{(2)eq} - \frac{2}{3\omega_2}\rho^{(0)}(\partial_x u^{(1)} + \partial_y v^{(1)} + \partial_z w^{(1)}) = m_{\mathrm{P}}^{(2)eq}. \tag{H.16}$$

To second order in diffusive scaling we can ignore the contribution of Eq. (H.16) which leads to the simpler form:

$$m_{200}^{(2)} = m_{200}^{(2)eq} - \frac{2}{3\omega_1}\rho^{(0)}\partial_x u^{(1)}. \tag{H.17}$$

In this paper we decided not to ignore the contribution from (H.16). That is we do not assume incompressibility. This leads to:

$$\partial_x u^{(1)} = \frac{3\omega_1}{2\rho^{(0)}}(m_{200-020}^{(2)eq} - m_{200-020}^{(2)} + m_{200-002}^{(2)eq} - m_{200-002}^{(2)}) - \frac{3\omega_1}{2\rho^{(0)}}(m_{\mathrm{P}}^{(2)eq} - m_{\mathrm{P}}^{(2)}), \tag{H.18}$$

$$\partial_y v^{(1)} = \frac{3\omega_1}{2\rho^{(0)}}(-2m_{200-020}^{(2)eq} + 2m_{200-020}^{(2)} + m_{200-002}^{(2)eq} - m_{200-002}^{(2)}) - \frac{3\omega_1}{2\rho^{(0)}}(m_{\mathrm{P}}^{(2)eq} - m_{\mathrm{P}}^{(2)}), \tag{H.19}$$

$$\partial_z w^{(1)} = \frac{3\omega_1}{2\rho^{(0)}}(m_{200-020}^{(2)eq} + m_{200-020}^{(2)} - 2m_{200-002}^{(2)eq} + 2m_{200-002}^{(2)}) - \frac{3\omega_1}{2\rho^{(0)}}(m_{\mathrm{P}}^{(2)eq} - m_{\mathrm{P}}^{(2)}). \tag{H.20}$$

Since the velocity gradients are only required to second order accuracy the obvious solution of (H.17) is equivalent to the one from (H.18). In fact, there are several other choices which are also equivalent to the desired order.

We can add the so recovered term to the equilibria of $m_{200-020}$, $m_{200-002}$, and m_{P} to correct for the absence of this term in $\bar{m}_{300}$. It is not required to consider the correction in the equilibrium while computing the derivative of $u^{(1)}$ by Eq. (H.17) or (H.18) because the correction is fourth order while (H.17) and (H.18) are only second order.

The modified equilibria for Eqs. (H.5)–(H.7) are:

$$m_{200-020}^{eqMod} = m_{200-020}^{eq} - 3\rho\left(\frac{1}{\omega_1} - \frac{1}{2}\right)(u^2\partial_x u - v^2\partial_y v), \tag{H.21}$$

$$m_{200-002}^{eqMod} = m_{200-002}^{eq} - 3\rho\left(\frac{1}{\omega_1} - \frac{1}{2}\right)(u^2\partial_x u - w^2\partial_z w), \tag{H.22}$$

$$m_{\mathrm{P}}^{eqMod} = m_{\mathrm{P}}^{eq} - 3\rho\left(\frac{1}{\omega_2} - \frac{1}{2}\right)(u^2\partial_x u + v^2\partial_y v + w^2\partial_z w). \tag{H.23}$$

It must be stressed that this is an incomplete correction and it does not improve the asymptotic order of the method. The reason is that the third term on the left hand side of (H.12) has been neglected and this is actually of the same order as the second term. The incomplete correction is the reason why a phase-lack is observed in the attenuation of a Taylor Green vortex. We could recover the neglected term by introducing a second derivative of $u^{(1)}$ into the equilibrium of $m_{200-020}$, $m_{200-002}$, and m_{P}. It is, however, not possible to compute this second derivative locally, thus additionally finite differences would be required.

In diffusive scaling the error in (H.12) that we can correct and the error that we cannot correct are both of the same order. To understand that the error that we cannot correct is actually more annoying than the one that we can correct we have to use a different scaling. Note that:

$$u^3\rho/Ma = \mathcal{O}(Ma^2), \tag{H.24}$$

$$2u\rho\left(\frac{1}{\omega_1} - \frac{1}{2}\right)\partial_x u/Ma = \mathcal{O}(Re^{-1}KnMa). \tag{H.25}$$

We divide here by the Mach number since the solution is of $\mathcal{O}(Ma)$ and we are interested in the error. Since the Reynolds number is fixed and since it is the ratio between Mach and Knudsen number $Re = MaKn^{-1}$ we also have $\mathcal{O}(Re^{-1}KnMa) = \mathcal{O}(Kn^2)$. So we see that the error that has been canceled by the Galilean correction is $\mathcal{O}(Ma^2)$ while the one that has not been canceled is $\mathcal{O}(Kn^2)$. To understand why this makes a difference we have to take the computational effort into consideration that is required to reduce the respective errors by either grid refinement or time step refinement. Let us measure the computational effort spent by the tuple $\langle\mathcal{O}(\mathcal{N}), \mathcal{O}(\mathcal{U})\rangle$ where $\mathcal{N}$ denotes the number of required lattice nodes and $\mathcal{U}$ denotes the number of lattice node updates, respectively. Errors in Mach number are only sensitive to the resolution in time. They are not effected by the resolution in space. Or put another way, the effort in lattice updates is inversely proportional to the Mach number but the effort in the number of lattice nodes is independent of the Mach number:

$$\mathcal{O}(\mathcal{U}) = \mathcal{O}(Ma^{-1}) \to \mathcal{O}(Ma) = \mathcal{O}(\mathcal{U}^{-1}), \tag{H.26}$$

$$\mathcal{O}(\mathcal{N}) = \mathcal{O}(Ma^0). \tag{H.27}$$

In contrast an error in Knudsen number depends on the resolution in space which is three dimensional. If we want to keep the Mach number constant we also have to scale the time step proportional to the grid spacing (acoustic scaling). This leads to the relationships:

$$\mathcal{O}(\mathcal{U}) = \mathcal{O}(Kn^{-4}) \to \mathcal{O}(Kn) = \mathcal{O}(\mathcal{U}^{-1/4}), \tag{H.28}$$

$$\mathcal{O}(\mathcal{N}) = \mathcal{O}(Kn^{-3}) \to \mathcal{O}(Kn) = \mathcal{O}(\mathcal{N}^{-1/3}). \tag{H.29}$$

From this we see that while both errors in (H.12) are of the same order in diffusive scaling they have quite different consequences for the computational effort that has to be spent in order to reduce them. The error that was removed by the Galilean correction is $\mathcal{O}(Ma^2)$ and it is proportional to the computational effort $\langle\mathcal{O}(0), \mathcal{O}(\mathcal{U}^{-2})\rangle$. The error that could not be removed is $\mathcal{O}(Kn^2)$ and hence proportional to the effort $\langle\mathcal{O}(\mathcal{N}^{-2/3}), \mathcal{O}(\mathcal{U}^{-1/2})\rangle$. The error in Knudsen number is seen to cause much more computational effort than the error in Mach number. Thus, from two errors that are of the same order in diffusive scaling we removed the one that made little trouble and left the one that makes big trouble. The Galilean correction is hence not a significant improvement of the method. However, it still deserves to be implemented since it comes at very little additional cost.

The Galilean correction suggested here is algebraically equivalent to the Taylor expanded correction in [11] that uses the relaxation rates for the correction rather than introducing new terms in the equilibrium. Note that in [11] grids with a very high resolution of 1024×1024 nodes were used for simple shear wave examples to reduce errors in Knudsen number to such an extent that the effect of the correction in Mach number could be appreciated.

Appendix I. Equivalent partial differential equations for leading errors

The equivalent partial differential equations for the leading error for each moment can, in principle, be obtained by asymptotic analysis to the appropriate order. Following the procedure introduced in Appendix G we would choose $\alpha = 1$, $\beta = 0$, and $\gamma = 0$ in Eq. (G.8) and select terms multiplied by ϵ^5 to obtain the equation for the leading error in u. While it is in principle possible to do this the result of this calculation will fill several tens of pages and is therefore difficult to interpret. Since our primary interest is in the difference between raw and central moments and cumulants we will instead look at the much simpler equations for the moments m_{211}, κ_{211}, M_{21}, and C_{211} at the order to which they appear in the leading error and compare their behavior in the different models. All models choose different degrees of freedom but all these degrees of

freedom can be translated into each other to make the models comparable. For the non-orthogonal raw moment method of Appendix C the evolution equations of the different degrees of freedom read:

$$\bar{C}^{(2)RM}_{211} = -\frac{\rho^{(0)}}{9}\left(\frac{1}{\omega_8}-\frac{1}{\omega_1}\right)(\partial_y w^{(1)}+\partial_z v^{(1)}), \tag{I.1}$$

$$\bar{\kappa}^{(2)RM}_{211} = -\frac{\rho^{(0)}}{9}\left(\frac{1}{\omega_8}-\frac{1}{2}\right)(\partial_y w^{(1)}+\partial_z v^{(1)}), \tag{I.2}$$

$$\bar{m}^{(2)RM}_{211} = \frac{\rho^{(0)}}{3}v^{(1)}w^{(1)} - \frac{\rho^{(0)}}{9}\left(\frac{1}{\omega_8}-\frac{1}{2}\right)(\partial_y w^{(1)}+\partial_z v^{(1)}), \tag{I.3}$$

$$\bar{M}^{(2)RM}_{21} = -\rho^{(0)}v^{(1)}w^{(1)} - \frac{\rho^{(0)}}{3}\left(\frac{1}{\omega_8}-\frac{2}{\omega_1}\right)(\partial_y w^{(1)}+\partial_z v^{(1)}). \tag{I.4}$$

For the classical (orthogonal) MRT method according to Appendix B:

$$\bar{C}^{(2)MRT}_{211} = -\frac{\rho^{(0)}}{9}\left(\frac{1}{s_\nu}-\frac{1}{s_{21}}\right)(\partial_y w^{(1)}+\partial_z v^{(1)}), \tag{I.5}$$

$$\bar{\kappa}^{(2)MRT}_{211} = -\frac{\rho^{(0)}}{9}\left(\frac{2}{s_\nu}-\frac{1}{s_{21}}\right)(\partial_y w^{(1)}+\partial_z v^{(1)}), \tag{I.6}$$

$$\bar{m}^{(2)MRT}_{211} = \frac{\rho^{(0)}}{3}v^{(1)}w^{(1)} - \frac{\rho^{(0)}}{9}\left(\frac{2}{s_\nu}-\frac{1}{s_{21}}\right)(\partial_y w^{(1)}+\partial_z v^{(1)}), \tag{I.7}$$

$$\bar{M}^{(2)MRT}_{21} = -\rho^{(0)}v^{(1)}w^{(1)} - \frac{\rho^{(0)}}{3}\left(\frac{1}{2}-\frac{1}{s_{21}}\right)(\partial_y w^{(1)}+\partial_z v^{(1)}). \tag{I.8}$$

Note that $s_\nu = \omega_1$. It is immediately seen that the viscosity parameter s_ν comes with opposite sign in the equation for the cumulant when we compare the non-orthogonal raw moment method (Eq. (I.1)) to the classical MRT method (Eq. (I.5)).

For the cascaded LBE we obtain the following equations:

$$\bar{C}^{(2)Cas}_{211} = -\frac{\rho^{(0)}}{9}\left(\frac{1}{\omega_8}-\frac{1}{\omega_1}\right)(\partial_y w^{(1)}+\partial_z v^{(1)}), \tag{I.9}$$

$$\bar{\kappa}^{(2)Cas}_{211} = -\frac{\rho^{(0)}}{9}\left(\frac{1}{\omega_8}-\frac{1}{2}\right)(\partial_y w^{(1)}+\partial_z v^{(1)}), \tag{I.10}$$

$$\bar{m}^{(2)Cas}_{211} = \frac{\rho^{(0)}}{3}v^{(1)}w^{(1)} - \frac{\rho^{(0)}}{9}\left(\frac{1}{\omega_8}-\frac{1}{2}\right)(\partial_y w^{(1)}+\partial_z v^{(1)}), \tag{I.11}$$

$$\bar{M}^{(2)Cas}_{21} = -\rho^{(0)}v^{(1)}w^{(1)} - \frac{\rho^{(0)}}{3}\left(\frac{1}{\omega_8}-\frac{2}{\omega_1}\right)(\partial_y w^{(1)}+\partial_z v^{(1)}). \tag{I.12}$$

Eqs. (I.1)–(I.4) are identical to (I.9)–(I.12). To leading order non-orthogonal raw and central moments are equivalent for the considered moments.

Finally, the cumulant LBE has the following equivalent partial differential equations:

$$\bar{C}^{(2)Cum}_{211} = 0, \tag{I.13}$$

$$\bar{\kappa}^{(2)Cum}_{211} = -\frac{\rho^{(0)}}{9}\left(\frac{1}{\omega_1}-\frac{1}{2}\right)(\partial_y w^{(1)}+\partial_z v^{(1)}), \tag{I.14}$$

$$\bar{m}^{(2)Cum}_{211} = \frac{\rho^{(0)}}{3}v^{(1)}w^{(1)} - \frac{\rho^{(0)}}{9}\left(\frac{1}{\omega_1}-\frac{1}{2}\right)(\partial_y w^{(1)}+\partial_z v^{(1)}), \tag{I.15}$$

$$\bar{M}^{(2)Cum}_{21} = -\rho^{(0)}v^{(1)}w^{(1)} - \frac{\rho^{(0)}}{3}\left(\frac{1}{2}-\frac{1}{\omega_1}\right)(\partial_y w^{(1)}+\partial_z v^{(1)}). \tag{I.16}$$

The cumulant method is seen to eliminate ω_8 in all cases at the order of the leading error. The leading error is therefore seen to be independent of ω_8.

In the equivalent partial differential equation for the error in the momentum equation at leading order a third derivative of $\bar{C}^{(2)}_{211}$ appears and introduces the spurious hyper-viscosity observed in Fig. 1. This error vanishes unconditionally in the cumulant method since the cumulant in question (Eq. (I.13)) is zero for all combinations of relaxation rates. In all other

methods the error can be eliminated by and only by coupling the relaxation rates $\omega_8 = \omega_1$ (Eqs. (I.1) and (I.13)) or $s_\nu = s_{21}$ (Eq. (I.5)) as demonstrated in Fig. 3. This is the case in the BGK and in the TRT methods where the rates in question are all equal. In all other cases the spurious cumulant can be written in the form:

$$\bar{C}^{(2)}_{211} = -\Lambda(\partial_y w^{(1)} + \partial_z v^{(1)}) \tag{I.17}$$

where Λ is a model specific (hyper)-diffusion coefficient. As is the case with a usual diffusion coefficient, Λ needs to be positive in order for the error to dissipate energy. A negative Λ promotes the growth of spatial velocity oscillations and causes the method to lose stability whenever the physical viscosity is not strong enough to suppress the error. These considerations are important to understand why the classical (orthogonal) MRT method shows significantly inferior stability properties as compared to the non-orthogonal raw moment method. Choosing $\omega_8 = s_{21} = 1$ and considering the usual definition of viscosity ν from Eq. (103) with $s_\nu = \omega_1$ and $\Delta x = \Delta t = 1$ we obtain for the two raw moment methods:

$$\Lambda^{RM} = \frac{\rho^{(0)}}{3}\left(\nu - \frac{1}{6}\right), \tag{I.18}$$

$$\Lambda^{MRT} = -\frac{\rho^{(0)}}{3}\left(\nu - \frac{1}{6}\right). \tag{I.19}$$

Orthogonalization is seen to invert the sign of the hyper-viscosity. Since the lattice Boltzmann method is usually used in over-relaxation mode, it is $\nu < 1/6$ and $\Lambda^{MRT} < 0$. Having a negative transport coefficient for its higher moments reduces the stability of the classical MRT drastically. It is instructive to note that this instability is a direct consequence of the orthogonalization which has, despite its popularity, no known justification.

Appendix J. Well conditioned collision operator

The collision operator for the cumulant method in Eqs. (43)–(96) is not optimized with regard to its susceptibility to round-off errors. This will be a problem when the method is implemented in single precision arithmetic or even in double precision arithmetic when the velocity is too small. The code that was actually used for the simulations was hand-optimized for better conditioning. We presented the unoptimized version first since the optimization adds an additional layer of complexity to the method.

The simplest and most important measure to reduce round-off errors is in the elimination of the constant part of the distribution function. Instead of the variables $f_{ijkxyzt}$ we define modified distributions $\mathrm{f}_{ijkxyzt} = f_{ijkxyzt} - w_{ijk}$. Note that due to the parasitic constant part $f_{ijkxyzt} = \mathcal{O}(1)$ while $\mathrm{f}_{ijkxyzt} = \mathcal{O}(\epsilon)$ in diffusive scaling.

The second measure to improve conditioning is to write all arithmetic operations in an order that avoids summation over variables of different order in ϵ. The distribution function contains the information on all cumulants. Velocity for example is of $\mathcal{O}(\epsilon)$ while stress and pressure are of $\mathcal{O}(\epsilon^2)$. The separation of these cumulants inside the distribution is only $\mathcal{O}(\epsilon)$. It is beneficial for accuracy to group all calculations in such a way that only terms of odd or even order remain. For example $\mathrm{f}_{ijkxyzt} + \mathrm{f}_{\bar{i}\bar{j}kxyzt} = \mathcal{O}(\epsilon^2)$ has only contributions of even order while $\mathrm{f}_{ijkxyzt} - \mathrm{f}_{\bar{i}\bar{j}kxyzt} = \mathcal{O}(\epsilon)$ contains only odd orders in ϵ. When computing density (which is of $\mathcal{O}(\epsilon^2)$ for the well conditioned case) it is beneficial to do it in the following way:

$$\begin{aligned}\delta\rho \;=\; & ((((\mathrm{f}_{111} + \mathrm{f}_{\bar{1}\bar{1}\bar{1}}) + (\mathrm{f}_{1\bar{1}1} + \mathrm{f}_{\bar{1}1\bar{1}})) + ((\mathrm{f}_{11\bar{1}} + \mathrm{f}_{\bar{1}\bar{1}1}) + (\mathrm{f}_{1\bar{1}\bar{1}} + \mathrm{f}_{\bar{1}1\bar{1}})))\\ & + (((\mathrm{f}_{011} + \mathrm{f}_{0\bar{1}\bar{1}}) + (\mathrm{f}_{01\bar{1}} + \mathrm{f}_{0\bar{1}1})) + ((\mathrm{f}_{101} + \mathrm{f}_{\bar{1}0\bar{1}}) + (\mathrm{f}_{10\bar{1}} + \mathrm{f}_{\bar{1}01})) + ((\mathrm{f}_{110} + \mathrm{f}_{\bar{1}\bar{1}0}) + (\mathrm{f}_{1\bar{1}0} + \mathrm{f}_{\bar{1}10})))\\ & + ((\mathrm{f}_{100} + \mathrm{f}_{\bar{1}0}) + (\mathrm{f}_{010} + \mathrm{f}_{0\bar{1}0}) + (\mathrm{f}_{001} + \mathrm{f}_{00\bar{1}}))) + \mathrm{f}_{000},\end{aligned} \tag{J.1}$$

$$\rho = \delta\rho + 1. \tag{J.2}$$

Velocity should be computed like this:

$$\begin{aligned}u \;=\; & ((((\mathrm{f}_{111} - \mathrm{f}_{\bar{1}\bar{1}\bar{1}}) + (\mathrm{f}_{1\bar{1}1} - \mathrm{f}_{\bar{1}1\bar{1}})) + ((\mathrm{f}_{11\bar{1}} - \mathrm{f}_{\bar{1}\bar{1}1}) + (\mathrm{f}_{1\bar{1}\bar{1}} - \mathrm{f}_{\bar{1}11})))\\ & + (((\mathrm{f}_{101} - \mathrm{f}_{\bar{1}0\bar{1}}) + (\mathrm{f}_{10\bar{1}} - \mathrm{f}_{\bar{1}01})) + ((\mathrm{f}_{110} - \mathrm{f}_{\bar{1}\bar{1}0}) + (\mathrm{f}_{1\bar{1}0} - \mathrm{f}_{\bar{1}10}))) + (\mathrm{f}_{100} - \mathrm{f}_{\bar{1}0}))/\rho\end{aligned} \tag{J.3}$$

and so on for v and w.

Applying the same measures to the central moment transformation leads to expressions that are slightly more complicated than Eqs. (43)–(45):

$$\kappa_{ij|0} = (\mathrm{f}_{ij1} + \mathrm{f}_{ij\bar{1}}) + \mathrm{f}_{ij0}, \tag{J.4}$$

$$\kappa_{ij|1} = (\mathrm{f}_{ij1} - \mathrm{f}_{ij\bar{1}}) - w(\kappa_{ij|0} + \mathrm{K}_{ij|0}(1 - \delta\rho)), \tag{J.5}$$

$$\kappa_{ij|2} = (\mathrm{f}_{ij1} + \mathrm{f}_{ij\bar{1}}) - 2w(\mathrm{f}_{ij1} - \mathrm{f}_{ij\bar{1}}) - w^2(\kappa_{ij|0} + \mathrm{K}_{ij|0}(1 - \delta\rho)), \tag{J.6}$$

$$\kappa_{i|0\gamma} = (\kappa_{i|1\gamma} + \kappa_{i|\bar{1}\gamma}) + \kappa_{i|0\gamma}, \tag{J.7}$$

$$\kappa_{i|1\gamma} = (\kappa_{i|1\gamma} - \kappa_{i|\bar{1}\gamma}) - v(\kappa_{i|0\gamma} + \mathrm{K}_{i|0\gamma}(1 - \delta\rho)), \tag{J.8}$$

$$\kappa_{i|2\gamma} = (\kappa_{i|1\gamma} + \kappa_{i|\bar{1}\gamma}) - 2v(\kappa_{i|1\gamma} - \kappa_{i|\bar{1}\gamma}) - v^2(\kappa_{i|0\gamma} + \mathrm{K}_{i|0\gamma}(1-\delta\rho)), \tag{J.9}$$

$$\kappa_{0\beta\gamma} = (\kappa_{1\beta\gamma} + \kappa_{\bar{1}\beta\gamma}) + \kappa_{0\beta\gamma}, \tag{J.10}$$

$$\kappa_{1\beta\gamma} = (\kappa_{1\beta\gamma} - \kappa_{\bar{1}\beta\gamma}) - u(\kappa_{0\beta\gamma} + \mathrm{K}_{0\beta\gamma}(1-\delta\rho)), \tag{J.11}$$

$$\kappa_{2\beta\gamma} = (\kappa_{1\beta\gamma} + \kappa_{\bar{1}\beta\gamma}) - 2u(\kappa_{1\beta\gamma} - \kappa_{\bar{1}\beta\gamma}) - u^2(\kappa_{0\beta\gamma} + \mathrm{K}_{0\beta\gamma}(1-\delta\rho)). \tag{J.12}$$

Since we started from the well conditioned distributions f_{ijk} we have introduced the constant parameters K that can be computed from the weights w_{ijk}:

$$\mathrm{K}_{ij|\gamma} = \sum_k k^\gamma w_{ijk}, \tag{J.13}$$

$$\mathrm{K}_{i|\beta\gamma} = \sum_j j^\beta \mathrm{K}_{ij|\gamma}, \tag{J.14}$$

$$\mathrm{K}_{\alpha\beta\gamma} = \sum_i i^\alpha \mathrm{K}_{i|\beta\gamma}. \tag{J.15}$$

The conditioning also increases the complexity of the transformation from central moments to cumulants. Cumulants up to order three are not affected. From order four onwards we have:

$$C_{211} = \kappa_{211} - ((\kappa_{200} + 1/3)\kappa_{011} + 2\kappa_{110}\kappa_{101})/\rho, \tag{J.16}$$

$$C_{220} = \kappa_{220} - ((\kappa_{200}\kappa_{020} + 2\kappa_{110}^2) + (\kappa_{200} + \kappa_{020})/3)/\rho + (\delta\rho/\rho)/9, \tag{J.17}$$

$$C_{122} = \kappa_{122} - ((\kappa_{002}\kappa_{120} + \kappa_{020}\kappa_{102} + 4\kappa_{011}\kappa_{111} + 2(\kappa_{101}\kappa_{021} + \kappa_{110}\kappa_{012})) + (\kappa_{120} + \kappa_{102})/3)/\rho, \tag{J.18}$$

$$\begin{aligned} C_{222} = {} & \kappa_{222} - (4\kappa_{111}^2 + \kappa_{200}\kappa_{022} + \kappa_{020}\kappa_{202} + \kappa_{002}\kappa_{220} + 4(\kappa_{011}\kappa_{211} + \kappa_{101}\kappa_{121} + \kappa_{110}\kappa_{112}) \\ & + 2(\kappa_{120}\kappa_{102} + \kappa_{210}\kappa_{012} + \kappa_{201}\kappa_{021}))/\rho \\ & + (16\kappa_{110}\kappa_{101}\kappa_{011} + 4(\kappa_{101}^2\kappa_{020} + \kappa_{011}^2\kappa_{200} + \kappa_{110}^2\kappa_{002}) + 2\kappa_{200}\kappa_{020}\kappa_{002})/\rho^2 \\ & - (3(\kappa_{022} + \kappa_{202} + \kappa_{220}) + (\kappa_{200} + \kappa_{020} + \kappa_{002}))/(9\rho) \\ & + 2(2(\kappa_{101}^2 + \kappa_{011}^2 + \kappa_{110}^2) + (\kappa_{002}\kappa_{020} + \kappa_{002}\kappa_{200} + \kappa_{020}\kappa_{200}) + (\kappa_{002} + \kappa_{020} + \kappa_{200})/3)/(3\rho^2) \\ & + (\delta\rho^2 - \delta\rho)/(27\rho^2). \end{aligned} \tag{J.19}$$

The collision itself is not affected by the conditioning. After collision Eqs. (J.16)–(J.19) have to be solved for the post-collision central moments. The post-collision central moments are transformed into well conditioned distributions like this:

$$\kappa^*_{0|\beta\gamma} = \kappa^*_{0\beta\gamma}(1-(u/c)^2) - 2(u/c)\kappa^*_{1\beta\gamma} - \kappa^*_{2\beta\gamma}, \tag{J.20}$$

$$\kappa^*_{\bar{1}|\beta\gamma} = ((\kappa^*_{0\beta\gamma} + \mathrm{K}_{0\beta\gamma}(1-\delta\rho))((u/c)^2 - u/c) + \kappa^*_{1\beta\gamma}(2u/c-1) + \kappa^*_{2\beta\gamma})/2, \tag{J.21}$$

$$\kappa^*_{1|\beta\gamma} = ((\kappa^*_{0\beta\gamma} + \mathrm{K}_{0\beta\gamma}(1-\delta\rho))((u/c)^2 + u/c) + \kappa^*_{1\beta\gamma}(2u/c+1) + \kappa^*_{2\beta\gamma})/2, \tag{J.22}$$

$$\kappa^*_{i0|\gamma} = \kappa^*_{i|0\gamma}(1-(v/c)^2) - 2(v/c)\kappa^*_{i|1\gamma} - \kappa^*_{i|2\gamma}, \tag{J.23}$$

$$\kappa^*_{i\bar{1}|\gamma} = ((\kappa^*_{i|0\gamma} + \mathrm{K}_{i|0\gamma}(1-\delta\rho))((v/c)^2 - v/c) + \kappa^*_{i|1\gamma}(2v/c-1) + \kappa^*_{i|2\gamma})/2, \tag{J.24}$$

$$\kappa^*_{i1|\gamma} = ((\kappa^*_{i|0\gamma} + \mathrm{K}_{i|0\gamma}(1-\delta\rho))((v/c)^2 + v/c) + \kappa^*_{i|1\gamma}(2v/c+1) + \kappa^*_{i|2\gamma})/2, \tag{J.25}$$

$$\mathrm{f}^*_{ij0} = \kappa^*_{ij|0}(1-(w/c)^2) - 2(w/c)\kappa^*_{ij|1} - \kappa^*_{ij|2}, \tag{J.26}$$

$$\mathrm{f}^*_{ij\bar{1}} = ((\kappa^*_{ij|0} + \mathrm{K}_{ij|0}(1-\delta\rho))((w/c)^2 - w/c) + \kappa^*_{ij|1}(2w/c-1) + \kappa^*_{ij|2})/2, \tag{J.27}$$

$$\mathrm{f}^*_{ij1} = ((\kappa^*_{ij|0} + \mathrm{K}_{ij|0}(1-\delta\rho))((w/c)^2 + w/c) + \kappa^*_{ij|1}(2w/c+1) + \kappa^*_{ij|2})/2. \tag{J.28}$$

Appendix K. Drag curve

The drag coefficient of a sphere is a complicated function of the Reynolds number *Re*. Many authors have tried to condense experimentally available data into approximate functions. We can only list a few of them. The book by Clift et al. [50] presents several functions for different ranges. The Reynolds numbers 1000–10 000 are covered by:

$$\log_{10}(c_D^C) = -2.4571 + 2.5558\log_{10}(Re) - 0.9295\log_{10}(Re)^2 + 0.1049\log_{10}(Re)^3. \tag{K.1}$$

For the range below $Re = 118\,300$ Mikhailov et al. [51] presented two formulas fitted to different experimental data:

$$c_D^{M1} = 777\frac{\frac{669806}{875} + \frac{114976}{1155}Re + \frac{707}{1380}Re^2}{646Re\left(\frac{32869}{952} + \frac{924}{643}Re + \frac{1}{385718}Re^2\right)}, \tag{K.2}$$

$$c_D^{M2} = 3808 \frac{\frac{1617933}{2030} + \frac{178861}{1063} Re + \frac{1219}{1084} Re^2}{681 Re \left(\frac{77531}{422} + \frac{13529}{976} Re - \frac{1}{71154} Re^2\right)}. \tag{K.3}$$

Almedeij [52] developed an approximate curve that covers the range from the Stokes flow to $Re = 10^6$:

$$\phi_1 = (24 Re^{-1})^{10} + (21 Re^{-0.67})^{10} + (4 Re^{-0.33})^{10} + (0.4)^{10}, \tag{K.4}$$

$$\phi_2 = \frac{1}{(0.148 Re^{0.11})^{-10} + (0.5)^{-10}}, \tag{K.5}$$

$$\phi_3 = (1.57 \times 10^8 Re^{-1.625})^{10}, \tag{K.6}$$

$$\phi_4 = (1(6 \times 10^{-17} Re^{2.63})^{-10}) + (0.2)^{-10}, \tag{K.7}$$

$$c_D^A = \left(\frac{1}{(\phi_1 + \phi_2)^{-1} + (\phi_3)^{-1}} + \phi_4\right)^{1/10}. \tag{K.8}$$

The same range is covered by an approximate function of Morrison [53]:

$$c_D^{Mor} = \frac{24}{Re} + \frac{\frac{26}{50} Re}{1 + \left(\frac{Re}{5}\right)^{1.52}} + \frac{0.411 \left(\frac{Re}{263000}\right)^{-7.94}}{1 + \left(\frac{Re}{263000}\right)^{-8}} + \frac{Re^{0.8}}{461000}. \tag{K.9}$$

The list presented here is by no means exhaustive as can be seen by the many other possibilities cited in [51]. Unfortunately the functions do not only look differently but they also disagree with each other by up to 20% in the range from $Re = 2000$ to $Re = 100\,000$. To compensate for the finite blockage ratio λ we follow Clift [50] and use the correction:

$$c_{D,corr} = \frac{c_D}{1 - 1.6\lambda^{1.6}}. \tag{K.10}$$

References

[1] R. Benzi, S. Succi, M. Vergassola, The lattice Boltzmann equation: theory and applications, Phys. Rep. 222 (3) (1992) 145–197. http://dx.doi.org/10.1016/0370-1573(92)90090-M.
[2] X. He, L.-S. Luo, Theory of the lattice Boltzmann method: From the Boltzmann equation to the lattice Boltzmann equation, Phys. Rev. E 56 (1997) 6811–6817. http://dx.doi.org/10.1103/PhysRevE.56.6811.
[3] R.A. Fisher, The derivation of the pattern formulae of two-way partitions from those of simpler patterns, Proc. Lond. Math. Soc. 33 (1931) 195–208.
[4] A. White, C. Chong, Rotational invariance in the three-dimensional lattice Boltzmann method is dependent on the choice of lattice, J. Comput. Phys. 230 (16) (2011) 6367–6378.
[5] S.K. Kang, Y.A. Hassan, The effect of lattice models within the lattice Boltzmann method in the simulation of wall-bounded turbulent flows, J. Comput. Phys. 232 (1) (2013) 100–117. http://dx.doi.org/10.1016/j.jcp.2012.07.023.
[6] S. Geller, S. Uphoff, M. Krafczyk, Turbulent jet computations based on MRT and cascaded lattice Boltzmann models, Comput. Math. Appl. 65 (12) (2013) 1956–1966.
[7] G. Silva, V. Semiao, Truncation errors and the rotational invariance of three-dimensional lattice models in the lattice Boltzmann method, J. Comput. Phys. 269 (2014) 259–279. http://dx.doi.org/10.1016/j.jcp.2014.03.027. URL: http://www.sciencedirect.com/science/article/pii/S0021999114002083.
[8] M. Geier, A. Greiner, J.G. Korvink, Cascaded digital lattice Boltzmann automata for high Reynolds number flow, Phys. Rev. E 73 (2006) 066705. http://dx.doi.org/10.1103/PhysRevE.73.066705.
[9] S. Hou, J. Sterling, S. Chen, G. Doolen, A lattice Boltzmann subgrid model for high Reynolds number flows, in: Pattern Formation and Lattice Gas Automata, Vol. 6, 1996, pp. 151–166.
[10] R.A. Brownlee, A.N. Gorban, J. Levesley, Nonequilibrium entropy limiters in lattice Boltzmann methods, 2008.
[11] P.J. Dellar, Lattice Boltzmann algorithms without cubic defects in Galilean invariance on standard lattices, J. Comput. Phys. 259 (2014) 270–283. http://dx.doi.org/10.1016/j.jcp.2013.11.021.
[12] D. d'Humières, I. Ginzburg, M. Krafczyk, P. Lallemand, L.-S. Luo, Multiple-relaxation-time lattice Boltzmann models in three dimensions, Phil. Trans. R. Soc. A 360 (2002) 437–451.
[13] I. Ginzburg, D. d'Humières, Multireflection boundary conditions for lattice Boltzmann models, Phys. Rev. E 68 (2003) 066614. http://dx.doi.org/10.1103/PhysRevE.68.066614. URL: http://link.aps.org/doi/10.1103/PhysRevE.68.066614.
[14] L.-S. Luo, W. Liao, X. Chen, Y. Peng, W. Zhang, Numerics of the lattice Boltzmann method: Effects of collision models on the lattice Boltzmann simulations, Phys. Rev. E 83 (2011) 056710. http://dx.doi.org/10.1103/PhysRevE.83.056710. URL: http://link.aps.org/doi/10.1103/PhysRevE.83.056710.
[15] P. Lallemand, L.-S. Luo, Theory of the lattice Boltzmann method: Dispersion, dissipation, isotropy, Galilean invariance, and stability, Phys. Rev. E 61 (2000) 6546–6562. http://dx.doi.org/10.1103/PhysRevE.61.6546.
[16] F. Dubois, P. Lallemand, Quartic parameters for acoustic applications of lattice Boltzmann scheme, Comput. Math. Appl. 61 (12) (2011) 3404–3416. mesoscopic Methods for Engineering and Science Proceedings of ICMMES-09 Mesoscopic Methods for Engineering and Science. http://dx.doi.org/10.1016/j.camwa.2011.01.011. URL: http://www.sciencedirect.com/science/article/pii/S0898122111000162.
[17] P.J. Dellar, Incompressible limits of lattice Boltzmann equations using multiple relaxation times, J. Comput. Phys. 190 (2) (2003) 351–370. http://dx.doi.org/10.1016/S0021-9991(03)00279-1.
[18] J. Latt, B. Chopard, Lattice Boltzmann method with regularized pre-collision distribution functions, Math. Comput. Simul. 72 (2–6) (2006) 165–168. http://dx.doi.org/10.1016/j.matcom.2006.05.017.
[19] P. Asinari, Generalized local equilibrium in the cascaded lattice Boltzmann method, Phys. Rev. E 78 (2008) 016701. http://dx.doi.org/10.1103/PhysRevE.78.016701. URL: http://link.aps.org/doi/10.1103/PhysRevE.78.016701.
[20] M. Geier, A. Greiner, J.G. Korvink, A factorized central moment lattice Boltzmann method, Eur. Phys. J. Spec. Top. 171 (1) (2009) 55–61. http://dx.doi.org/10.1140/epjst/e2009-01011-1.
[21] K.N. Premnath, S. Banerjee, On the three-dimensional central moment lattice Boltzmann method, J. Stat. Phys. 143 (4) (2011) 747–794. http://dx.doi.org/10.1007/s10955-011-0208-9.

[22] D.M. Holman, R.M. Brionnaud, Z. Abiza, Solution to industry benchmark problems with the lattice-Boltzmann code XFlow, in: 6th European Congress On Computational Methods In Applied Sciences and Engineering, 2013.
[23] M. Geier, A. Greiner, J.G. Korvink, Reference frame independent partioning of the momentum distribution function in lattice Boltzmann methods with multiple relaxation rates, June 2008.
[24] S. Seeger, H. Hoffmann, The cumulant method for computational kinetic theory, Contin. Mech. Thermodyn. 12 (6) (2000) 403–421. http://dx.doi.org/10.1007/s001610050145.
[25] S. Seeger, K. Hoffmann, The cumulant method applied to a mixture of Maxwell gases, Contin. Mech. Thermodyn. 14 (4) (2002) 321–335. http://dx.doi.org/10.1007/s001610100067.
[26] S. Seeger, K. Hoffmann, The cumulant method for the space-homogeneous Boltzmann equation, Contin. Mech. Thermodyn. 17 (1) (2005) 51–60. http://dx.doi.org/10.1007/s00161-004-0187-z.
[27] H. Grad, On the kinetic theory of rarefied gases, Comm. Pure Appl. Math. 2 (4) (1949) 331–407. http://dx.doi.org/10.1002/cpa.3160020403.
[28] Y.H. Qian, D. d'Humières, P. Lallemand, Lattice BGK models for Navier–Stokes equation, Europhys. Lett. 17 (6) (1992) 479.
[29] I. Ginzburg, Equilibrium-type and link-type lattice Boltzmann models for generic advection and anisotropic-dispersion equation, Adv. Water Resour. 28 (11) (2005) 1171–1195. http://dx.doi.org/10.1016/j.advwatres.2005.03.004. URL: http://www.sciencedirect.com/science/article/pii/S0309170805000874.
[30] D. d'Humières, M. Bouzidi, P. Lallemand, Thirteen-velocity three-dimensional lattice Boltzmann model, Phys. Rev. E 63 (2001) 066702. http://dx.doi.org/10.1103/PhysRevE.63.066702. URL: http://link.aps.org/doi/10.1103/PhysRevE.63.066702.
[31] A. Fakhari, T. Lee, Multiple-relaxation-time lattice Boltzmann method for immiscible fluids at high Reynolds numbers, Phys. Rev. E 87 (2013) 023304. http://dx.doi.org/10.1103/PhysRevE.87.023304. URL: http://link.aps.org/doi/10.1103/PhysRevE.87.023304.
[32] X. Guo, C. Zhong, C. Zhuo, J. Cao, Multiple-relaxation-time lattice Boltzmann method for study of two-lid-driven cavity flow solution multiplicity, Theor. Comput. Fluid Dyn. 28 (2) (2014) 215–231. http://dx.doi.org/10.1007/s00162-013-0312-3. URL: http://dx.doi.org/10.1007/s00162-013-0312-3.
[33] P.J. Dellar, Nonhydrodynamic modes and a priori construction of shallow water lattice Boltzmann equations, Phys. Rev. E 65 (2002) 036309. http://dx.doi.org/10.1103/PhysRevE.65.036309. URL: http://link.aps.org/doi/10.1103/PhysRevE.65.036309.
[34] P. Asinari, Asymptotic analysis of multiple-relaxation-time lattice Boltzmann schemes for mixture modeling, Comput. Math. Appl. 55 (7) (2008) 1392–1407. mesoscopic Methods in Engineering and Science. http://dx.doi.org/10.1016/j.camwa.2007.08.006. URL: http://www.sciencedirect.com/science/article/pii/S089812210700630X.
[35] A. Augier, F. Dubois, B. Graille, P. Lallemand, On rotational invariance of lattice Boltzmann schemes, Comput. Math. Appl. 67 (2) (2014) 239–255. mesoscopic Methods for Engineering and Science (Proceedings of ICMMES-2012, Taipei, Taiwan, 23–27 July 2012). http://dx.doi.org/10.1016/j.camwa.2013.06.009. URL: http://www.sciencedirect.com/science/article/pii/S089812211300374X.
[36] M. Geier, Ab initio derivation of the cascaded lattice Boltzmann automaton (Ph.D. thesis), Albert-Ludwigs University Freiburg, 2006.
[37] D. d'Humières, I. Ginzburg, Viscosity independent numerical errors for lattice Boltzmann models: From recurrence equations to "magic" collision numbers, Comput. Math. Appl. 58 (5) (2009) 823–840. mesoscopic Methods in Engineering and Science. http://dx.doi.org/10.1016/j.camwa.2009.02.008. URL: http://www.sciencedirect.com/science/article/pii/S0898122109000893.
[38] G.I. Taylor, A.E. Green, Mechanism of the production of small eddies from large ones, Proc. R. Soc. A 158 (895) (1937) 499–521. arXiv:http://rspa.royalsocietypublishing.org/content/158/895/499.full.pdf+html http://dx.doi.org/10.1098/rspa.1937.0036.
[39] M. Geier, A. Greiner, J.G. Korvink, Bubble functions for the lattice Boltzmann method and their application to grid refinement, Eur. Phys. J. Spec. Top. 171 (1) (2009) 173–179. http://dx.doi.org/10.1140/epjst/e2009-01026-6.
[40] M. Schönherr, K. Kucher, M. Geier, M. Stiebler, S. Freudiger, M. Krafczyk, Multi-thread implementations of the lattice Boltzmann method on non-uniform grids for CPUs and GPUs, Comput. Math. Appl. 61 (12) (2011) 3730–3743. http://dx.doi.org/10.1016/j.camwa.2011.04.012.
[41] A.J.C. Ladd, Numerical simulations of particulate suspensions via a discretized Boltzmann equation. Part 1. Theoretical foundation, J. Fluid Mech. 271 (1994) 285–309.
[42] R. Mei, D. Yu, W. Shyy, L.-S. Luo, Force evaluation in the lattice Boltzmann method involving curved geometry, Phys. Rev. E 65 (2002) 041203.
[43] M. Stiebler, M. Krafczyk, S. Freudiger, M. Geier, Lattice Boltzmann large eddy simulation of subcritical flows around a sphere on non-uniform grids, Comput. Math. Appl. 61 (12) (2011) 3475–3484. http://dx.doi.org/10.1016/j.camwa.2011.03.063.
[44] G. Eitel-Amor, M. Meinke, W. Schröder, A lattice-Boltzmann method with hierarchically refined meshes, Comput. & Fluids 75 (2013) 127–139.
[45] J. Hunt, A. Wray, P. Moin, Eddies, streams, and convergence zones in turbulent flow, in: Center for Turbulence Research Proceedings of the Summer Program 1988, 1988.
[46] F. Dubois, 2014. [link] URL: http://www.math.u-psud.fr/~fdubois/travaux/reseau/reseau.html.
[47] M. Bouzidi, M. Firdaouss, P. Lallemand, Momentum transfer of a Boltzmann-lattice fluid with boundaries, Phys. Fluids (1994-present) 13 (11) (2001) 3452–3459. http://dx.doi.org/10.1063/1.1399290.
[48] F. Dubois, Equivalent partial differential equations of a lattice Boltzmann scheme, Comput. Math. Appl. 55 (7) (2008) 1441–1449.
[49] M. Junk, A. Klar, L.-S. Luo, Asymptotic analysis of the lattice Boltzmann equation, J. Comput. Phys. 210 (2) (2005) 676–704. http://dx.doi.org/10.1016/j.jcp.2005.05.003.
[50] M.E.W.R. Clift, J.R. Grace, Bubbles, Drops and Particles, Academic Press, 1978.
[51] M. Mikhailov, A.S. Freire, The drag coefficient of a sphere: An approximation using shanks transform, Powder Technol. 237 (2013) 432–435. http://dx.doi.org/10.1016/j.powtec.2012.12.033.
[52] J. Almedeij, Drag coefficient of flow around a sphere: Matching asymptotically the wide trend, Powder Technol. 186 (3) (2008) 218–223. http://dx.doi.org/10.1016/j.powtec.2007.12.006.
[53] F.A. Morrison, An Introduction to Fluid Mechanics, Cambridge University Press, 2013.